Doctoral Dissertations   Graduate School

Summer 2010

Elimination of deck joints using a corrosion resistant FRP approach

Ashok Reddy Aleti
Louisiana Tech University

Follow this and additional works at: https://digitalcommons.latech.edu/dissertations

 Part of the Civil Engineering Commons, and the Mechanical Engineering Commons

ELIMINATION OF DECK JOINTS USING A CORROSION RESISTANT FRP APPROACH

by

Ashok Reddy Aleti, M.E, B.E

Ashok Reddy Aleti, M.E, B.E

A Dissertation Presented in Partial Fulfillment
of the Requirements for the Degree
Doctor of Philosophy

COLLEGE OF ENGINEERING AND SCIENCE
LOUISIANA TECH UNIVERSITY

August 2010

UMI Number: 3429512

LOUISIANA TECH UNIVERSITY

THE GRADUATE SCHOOL

04 / 01 / 2010
_____
Date

We hereby recommend that the dissertation prepared under our supervision

by _____ Ashok Reddy Aleti _____

entitled _____

Elimination of Deck Joints Using a Corrosion Resistant FRP Approach
_____

_____

_____

_____

be accepted in partial fulfillment of the requirements for the Degree of
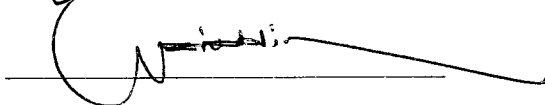
Doctor of Philosophy in Engineering (Civil)
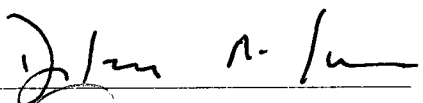_____

_____
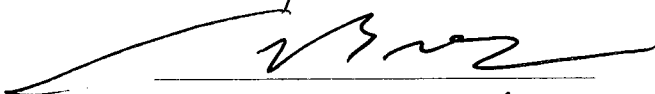Supervisor of Dissertation Research
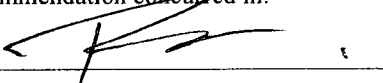
_____
Head of Department
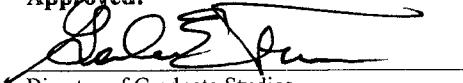
Civil Engineering
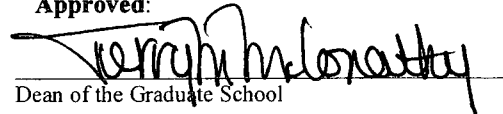_____
Department

Recommendation concurred in:

_____

_____

_____   Advisory Committee

_____

Approved:

_____
Director of Graduate Studies

_____
Dean of the College

Approved:

_____
Dean of the Graduate School

ABSTRACT

The research presented herein describes the development of durable link slabs for jointless bridge decks based on using FRP grid for reinforcement. Specifically, the ductility of the FRP material was utilized to accommodate bridge deck deformations imposed by girder deflection, temperature variations, and concrete shrinkage. It would also provide a solution to a number of deterioration problems associated with bridge deck joints.

The design concept of the link slabs was then examined to form the basis of design for FRP grid link slabs. Improved design of FRP grid link slab/concrete deck slab interface was confirmed in the numerical analysis. The mechanical properties between the FRP grid and concrete were evaluated. The behavior of the link slab was investigated and confirmed for durability.

The results indicated that the technique would allow simultaneous achievement of structural need (lower flexural stiffness of the link slab approaching the behavior of a hinge) and durability need of the link slab. Also, the development length results confirm that the bond between the FRP grid and the concrete was highly improved. The overall investigation supports the contention that durable jointless concrete bridge decks may be designed and constructed with FRP grid link slabs. It is recommended that the link slab technique be used during new construction of the bridge decks and in repair and retrofit of the bridge decks.

APPROVAL FOR SCHOLARLY DISSEMINATION

The author grants to the Prescott Memorial Library of Louisiana Tech University the right to reproduce, by appropriate methods, upon request, any or all portions of this Dissertation. It is understood that "proper request" consists of the agreement, on the part of the requesting party, that said reproduction is for his personal use and that subsequent reproduction will not occur without written approval of the author of this Dissertation. Further, any portions of the Dissertation used in books, papers, and other works must be appropriately referenced to this Dissertation.

Finally, the author of this Dissertation reserves the right to publish freely, in the literature, at any time, any or all portions of this Dissertation.

Author _____

Date _July 19, 2010_

DEDICATION

I dedicate this work to my mother, Mrs. Swarna Latha Aleti, father, Mr. Ram Reddy Aleti, mentor and my father's youngest brother, Mr. Krishna Reddy Aleti, my late grandfather, Mr. Malla Reddy Aleti, and my late brother-in-law, Mr. Ram Krupakar Reddy Yelipeddi.

TABLE OF CONTENTS

LIST OF TABLES

LIST OF FIGURES

ACKNOWLEDGMENTS

I wish to express my sincere gratitude and appreciation to my advisor Dr. Aziz Saber for his valuable guidance and constant supervision throughout my research at Tech. It was really a wonderful and unforgettable experience working with Dr. Saber on a structural research project, and a great opportunity to learn a few things, which extend beyond technical knowledge. It might not be so easy to complete my research in three and a half years if I would have not worked under his guidance.

I would like to express my sincere gratitude and appreciation to Dr. Xingran Wang for teaching me the foundation engineering concepts, Dr. Dileep Sule for staying in his off-campus apartments and being in my advisory committee. I would also like to express my sincere gratitude to the members of my advisory committee, Dr. Wasiuddin Nazimuddin and Dr. Rob McKim, and civil engineering professors Dr. Ray Sterling, Dr. Erez Allouche, and Dr. Mike Baumert.

I am greatly indebted to Louisiana Tech University and Louisiana Transportation Research Center (LTRC) for supporting my doctoral research and Project (No. 06-2ST) with Report No. FHWA/LA.09/443 and providing me grants (State Project No.736-99-1391).

I would like to thank my fellow researchers Ajay Mothukuri, Kanielle Gordon, Neha Verma, Prashanth Arasanagi, Sai Prasad, all my friends and roommates for their

care and valuable discussions; and the people who have helped me in the Labs Mr. Jimmy Cook, Mr. McKinney Ray, Jim Ellingburg, and Christopher Fournerat.

Finally, I am greatly thankful to my family members: father, Mr. Ram Reddy Aleti, mother, Mrs. Swarna Latha Aleti, dearest sisters, Mrs. Jaya Sudha and Mrs. Aruna Jyothi, all my relatives, and especially my cousin, Ms. Swetha, for their care, love, affection and their endless support throughout my life.

CHAPTER I

INTRODUCTION

Many of the thousands of bridges in the United States are constructed as simple spans. The bridges require the use of expansion joints over piers. The joints create short-term and long-term problems including leaks through the joints which deteriorate the supporting girders and the piers, and debris accumulation in the joints prevents them from functioning properly. These problems lead to massive direct and indirect costs (Saber et al. 2005). So, there is a need for reducing or eliminating expansion joints in bridge decks. The objective of this study is to develop a new technique using advancement in materials and current technology. An innovative system is proposed for this study (as first discussed in LTRC Report No. FHWA/LA.09/443 [Li and Saber 2009]). The new system replaces expansion joints by a link slab. The link slab joins decks of adjacent spans without imposing any continuity in the bridge girders. The link slab is subjected to tensile forces and stresses due to the negative moment developed at the joint. FRP reinforcement is used to carry the tension forces (Saber 2001) and its corrosion resistance.

The most common type of reinforcement used in bridge construction is steel rods. The deterioration of steel caused by corrosion has been plaguing these structures across the nation, decreasing their service life and increasing cost of repair and maintenance. Many investigations were conducted to resolve the problems associated with corrosion by such methods as decreasing the porosity of concrete, coating steel bars with a protective

outer layer, and increasing the reinforcement cover. However, these methods only extend the time it takes for corrosion to take place.

For more than three decades, researchers have investigated the use of FRP (fiber reinforced polymers) as an alternate to steel reinforcement in concrete structures. In recent years, the use of FRP rods for structural applications has been gaining acceptance around the world. Recently, FRP grids have been used for reinforcement of concrete beams and slabs (Dutta et al. 1998). A grid is a latticework of rigid, interconnecting ribs in two, three, or four groups and directions. Such grid reinforcement enhances the energy absorption capability and the overall ductility of the structure is improved, leading to an increase in ultimate load carrying capacity of concrete beams and slabs. When the opening of grids is filled with concrete, the combined structure derives its shear rigidity from the concrete filler and the concrete prevents the ribs from buckling. FRP composite grids provide a mechanical anchorage within the concrete due to the interlocking elements (cross-ribs), and thus no bond is necessary for proper load transfer.

Although there have been a number of studies on the use of FRP grid reinforced concrete beams or slabs, there is currently a lack of information on the use of FRP grid reinforced concrete link slabs for the replacement of the expansion joints. Because the link slab will be subjected to a negative bending moment and thermal stress, it is expected that the design and performance will be different from conventional beams or slabs, which is primarily subjected to a positive bending moment and transverse shear force. Therefore, there is a need to conduct experimental testing and theoretical modeling analysis of FRP grid reinforced concrete link slabs for the replacement of the expansion joints.

1.1 Objectives

The main purpose of the research is to reduce, or eliminate, the number of expansion joints over bridge piers. This is achieved by constructing a link slab at the expansion joint. The link slab will be subjected to tensile forces due to the negative moment that is developed at the location of the joint due to continuity. FRP reinforcement will be used to carry the tension forces in the link slab. The following objectives are made to analyze the stresses in the link slabs:

- Evaluate the structural behavior of the bridge with link slabs by finite element modeling.

- Determine the behavior and strength of the jointless bridge decks under static loading by conducting an experimental test program.

- Verify the development length requirements for the FRP grids. Since, there are no equations available for the development of the FRP grid in ACI 440 code.

1.2 Organization

This report has been organized into a few chapters to make it easy to understand. The previous research and on-going research on bridge deck joints, FRP grid reinforced beams and slabs are presented in Chapter II. The methodology to develop the bridge model using finite element analysis, structural testing of FRP grid reinforced decks and test for the development length of FRP grid is presented in Chapter III. The finite element analysis (theoretical) and experimental results are discussed in Chapter IV. Finally, the conclusions and recommendations for this study are presented in Chapter V.

CHAPTER II

LITERATURE REVIEW

Sudden brittle failure and FRP (fiber reinforced polymer) rebar slippage have been a problem for years with FRP rebar reinforced concrete. This motivated the research of using AGS grids/panel to reinforce concrete because of the mechanical interlocking between the concrete and the grid. Early research in the field of composite grid reinforcement of concrete was reported by

"Sugita et al. (1992) of Japan, who worked with a New Fiber Composite Material for Reinforced Concrete (NEFMAC) grid made of either carbon fibers or a hybrid combination of carbon and glass fibers in a polymeric matrix. Its primary use is to reinforce concrete. The applications to date include reinforcement for tunnel lining, shotcrete reinforcement, LPG tanks, fender plates and precast curtain walls (none of which are primary structural components). Other types of commercial FRP grids include IMCO (molded grating), DURADEK (pultruded grating), SAFE-T-GRATE, KORDEK (rectangular grating), KORLOK (pultruded grating), and custom manufactured grids.

The design of a reinforced concrete structure requires that flexural behavior be understood. The flexural behavior of a reinforced concrete beam can be characterized by its ultimate strength, failure mode, stiffness

(or amount of deflection), and predictability. Composite materials generally have a higher ultimate strength than steel, which allows for higher ultimate loads in composite-reinforced concrete. Sugita (1993) and Sugita et al. (1992) indicate that the Japanese have also explored the use of FRP-grid reinforcement for shotcrete applications. The prefabricated nature of the FRP grid lowers construction effort. The flexible nature of the grid that results from its lower stiffness permits easier placement on non-planar surfaces such as those found in tunnels. These researchers have also found that the higher flexibility of the FRP grid results in fewer voids in the shotcrete matrix that later require filling, further reducing construction costs. This may indicate a viable use for FRP reinforcement in constructing concrete elements with curved surfaces (e.g., domes, etc.)" [Dutta et al. 1998]

Banthia et al. (1995) studied the behavior of concrete slabs reinforced with fiber-reinforced plastic grid. The two-dimensional FRP grids were used to reinforce the concrete slabs, as an alternative to the steel grid. The behavior and strength of FRP grid reinforced slab was compared with steel grid reinforced slab. In the experimental program, three-FRP grid reinforced slabs, four-steel grid reinforced slabs, and four beam specimens were cast. The slabs were tested for transverse loading, and the beam specimens were tested for four-point flexure with loading at the third points. The FRP grid reinforced slabs showed an improved overall energy-absorption capacity and the ultimate load carrying capacity when compared to the steel grid reinforced concrete

slabs. Banthia et al. recommended that the codes used for the design of steel reinforcement, can be applied for the design of FRP grid reinforcement also.

Rahman et al. (2000) evaluated the behavior and strength of concrete deck slab reinforced with carbon NEFMAC grid. The purpose of the work was to find the behavior due to service loads, stresses in the FRP grid, failure mode and the ultimate load carrying capacity of the bridge deck slab. In the experimental program, one deck slab of 6 m long, 6 m wide and 185 mm thick was cast. Strain gages were fixed to the FRP grid to measure the strain distribution. Then, monotonic and cyclic loads were applied on the deck slab until failure. Rahman et al. found that the behavior under service load and constructability of the bridge deck using a grid are satisfactory. The deck failed due to punching shear. Also, degradation due to cyclical loading, stress and deflection were found to be small while the ultimate load carrying capacity of the bridge deck was found to be exceptionally high.

Another study was conducted by Yost et al. (2001) investigated the flexural behavior of composite NEFMAC FRP grids. They tested 15 simply supported concrete beams reinforced with two dimensional FRP grids, and varied the FRP grid in each type of beam in a longitudinal direction. The main purpose of the study was to predict the deflection response, strength, and behavior of the beam specimens using ACI 318-95 code. The strain gages were fixed to the FRP bars in the longitudinal direction to measure the strains at different applied loads. The results found that the flexural strength of FRP grid reinforced beams can be estimated using ACI 318-95 code. The study also concluded that two-dimensional FRP grid transfers loads to the concrete effectively. At ultimate loads, there was no shear failure between FRP reinforcement and concrete.

The usage of FRP grids and gratings to reinforce the concrete structures has continued in recent years (Berg et al., 2006, Zhang et al., 2004, Huang et al., 2002, Matthys and Taerwe, 2000, Smart and Jensen, 1997). The grid reinforcement in concrete structures increases the ultimate load and ductile nature. The open or bay area of the FRP grid is filled with concrete and when it cures, the concrete stops the longitudinal and transverse bars from buckling. There is no bond required between the concrete and the grid to transfer the loads effectively in composite FRP grid reinforced concrete because of mechanical anchorage and interlocking between materials. There was no bearing or shear failure found between the concrete and the transverse reinforcement at ultimate tensile stress. In most of the civil applications till now, the commercial grids such as molded, pultruded and rectangular gratings were used.

El-Salakawy et al. (2005) recently tested the GFRP (Glass Fiber Reinforced Polymer) bar reinforced bridge deck constructed in Canada. The usage of fiber-reinforced polymer products has been increasing as bridge deck reinforcement. The main reason for using GFRP bars is because of their corrosion resistance and high strength when compared to the steel reinforcement for bridge decks. Cookshire-Eaton concrete bridge was built with two equal spans of 26.04 m long. Each span had five pre-cast, pre-stressed concrete girders. The thickness of the concrete deck slab was 200 mm. The deck measured over four spans of 2.7 m between bridge girders. The bridge girders were connected to the deck slab by using shear keys. Intermediate diaphragms were placed in each span for improving stability and load distribution during construction. In the project, two bridges were constructed; one bridge was reinforced with steel bars, and another

bridge was reinforced with GFRP bars. According to CHBDC (Canadian Highway Bridge Design Code), both bridges were inspected for service loads.

El-Salakawy et al. (2005) concluded that the measured strains were small in concrete or in GFRP bars due to the truck loads, and comparing these strains with the strains obtained from the flexural design moments showed that the deck behaves differently under concentrated wheel loads. An arching action between girders in the bridge will be developed in the deck because of cracks in the deck. A recently proposed design approach, by the Ministry of Transportation of Quebec (MTQ), finds the required FRP reinforcement ratio from the obtained flexural moments by satisfying maximum stress limits and crack width, instead of strength and stiffness limits, reduces the required FRP reinforcement. The obtained girder distribution factors from the two bridges were well comparable to that of AASHTO (1998), LRFD distributions factors. There were no cracks found either in the GFRP bar's reinforced deck or the galvanized steel reinforced deck in the first year of service. As the truck load moves over the gage, the measured tensile strains were between 4 - 8 micro-strains. The maximum tensile strains in the concrete were very small when the truck was not over the gage. For normal weight concrete with a compressive strength of $30 - 37$ Mpa, the tensile strains were in the range of $100 - 130$ micro-strains. Hence, the obtained tensile strains in the concrete were very low. The measured maximum tensile strain in the GFRP bars was 30 micro-strains. Hence, the obtained maximum tensile strains in GFRP bars were also very small. The deflections obtained in the bridge deck slab were below Canadian Highway Bridge Design Code's allowable limits, and the maximum deflections for the concrete girders and slabs never exceeded the limits.

El-Ghandour et al. (2003) evaluated the punching shear strength of the concrete slabs with FRP reinforcement. The tests were conducted in two phases. The problems associated with the bond slip between the concrete and the FRP, and cracks developed in the concrete were discussed in the first phase. In the next phase of the experimental program, the bond and crack problems were avoided by decreasing the longitudinal FRP bar spacing. The flat slabs in the second phase were designed to fail due to punching shear. In each phase, four flat slabs were designed and tested. The slabs were loaded up to 150 KN until failure. El-Ghandour et al. concluded that slab capacity was not increased because of using CFRP (Carbon Fiber Reinforced Polymer) reinforcement. The proposed and modified strain approach accurately estimated the shear strength of the flat slabs. Also, they proposed a limit for strain and spacing in shear reinforcement.

Karbhari et al. (2003) worked on the gap analysis of FRP composites. Even though research was done on durability and gap analysis of FRP composites in civil applications, the critical gaps in the database were not identified. The research was mainly concentrated on the application of fiber reinforced polymer materials in deck slabs, structural members, and in the repair and retrofit of earthquake affected structures. Karbhari et al. worked on gap analysis for different environmental conditions. They found that the selection of an appropriate database is important to use in Civil Engineering applications. The importance of one environment over another is difficult to identify. They concluded that the database needs to be documented properly for its effective usage. There is a need for developing laboratory conditions that are very close to conditions in the field. It is also necessary to develop the protective coatings to the FRP materials to test under different environments and conditions. They recommended a

method from this study of gap analysis of FRP materials and also based on the previous research in this area. The recommended method is divided into three steps: (1) An integrated knowledge system needs to be developed, (2) Establishing a method for collecting, testing and validating the data, and (3) The data obtained from the laboratory requires implementation in the field.

Tavarez et al. (2003) analyzed the behavior of the concrete beams reinforced with FRP grids by using the finite element analysis software, LS-DYNA. In the analysis, a four-point bending tests were conducted on the beams to predict the failure mode and crack propagation. The shell and beam elements were used to model the composite FRP grid. The load-deflection behavior of the beams and the stresses in the longitudinal bars of the grid at ultimate loads were analyzed. And, they also developed a procedure for the beams reinforced with FRP grids to analyze different failures, particularly due to flexure-shear cracks. Tavarez et al. compared the finite element analysis results with the experimental results and concluded that longitudinal bars in the grid failed due to large flexure-shear cracks. Also, recommended to consider the flexure-shear cracking in the design and analysis of beams reinforced with FRP composite grids. In the models, the failure of the short beam was due to low shear span to depth ratio, whereas the shear span to depth ratio was good enough in long and medium beams. Thus, the stresses in the longitudinal reinforcement of the long and medium beams were not influenced by shear cracks. The shear strength of the long and medium beams never reached the critical shear for these beam lengths. Hence, the beams can be designed with the help of conventional flexural theory. In the design, the numerical simulations can be used to understand the complex behavior and the multiple failures of the composite grid reinforced beams. The

proposed method from finite element analysis will help for a conservative design, even though the method underestimated the strength of the beam with multiple failures. The beam fails due to large flexure-shear cracks followed by concrete crushing, which ensures that the longitudinal FRP reinforcement will not fail suddenly.

Bakis et al. (2002) conducted a survey using FRP materials for various construction applications. They discussed the past, current usage, and future applications of FRP composites in bridge decks and structural components, etc. The application of FRP material in bridge decks has increased in recent years, because of its non-corrosive nature, high strength and stiffness, and less weight as compared to steel reinforcement. The currently available FRP decks can be divided into two categories based on the type of construction. FRP bars are primarily used as internal reinforcement to improve the corrosion resistance of the structure. The beams with FRP reinforcement increases their flexural capacity, deflections and crack widths, and reduces the shear strength. Bakis et al. concluded that the guidelines for using FRP composites in concrete structures are already published or still working on them. In the design of FRP reinforced structures, coefficient of thermal expansion requires to be included.

Matthys and Taerwe (2000) evaluated the performance and behavior of FRP composite grid reinforced concrete slabs under punching shear. The fiber reinforced polymer material is brittle in nature and exhibits a low Young's modulus. Hence, its application in RC structures is not effective than the PSC members. However, the use of FRP composites in concrete structures is feasible by considering serviceability. In the experimental program, seventeen punching tests were done on the concrete slabs. The dimensions of the square slab were 1000 mm long/wide and 120 or 150 mm deep.

Different types of reinforcements such as steel grid, carbon FRP, NEFMAC C and H grids were provided in the concrete slabs. The slabs were positioned vertically, and loads, deflection, cracks and strains were noted while testing the concrete slabs. They concluded that the bond between the FRP grid and concrete affected the development of cracks in the slabs. The punching load and strength of the composite grid reinforced slabs were less than the concrete slabs reinforced with steel, even though both slabs had the same flexural stiffness. The composite grid slabs with higher reinforcement and reference steel slabs had taken the same punching load. The empirical equations underestimated the punching load of the composite grid reinforced slabs with low young's modulus. The Menetrey (1996) mechanical model underestimates the punching load. However, Hallgren's (1996) model estimates fair punching load for composite grid and reference slabs.

Dutta et al. (1998) used FRP grid to reinforce the concrete beams, panels and columns. The advantages of FRP grid reinforcement over typical steel reinforcement were discussed. Both 2-D and 3-D composite grids were used to reinforce the concrete elements. In the experimental program, tests were conducted on concrete slabs and reinforced with two and three-dimensional FRP composite grids. The slab or beam specimens were tested for flexure using a four-point bending configuration. Beams with steel reinforcement were also designed in order to compare with FRP grid reinforced specimens. The dimensions of the beam specimens were 30 in. long, with a 6 in. square cross-section. In the FRP grid reinforced beams, the strength and stiffness of the grid were varied. Columns were also tested by reinforcing the FRP grid in longitudinal and circumferential directions. The concrete columns take higher compressive loads because

of providing reinforcement in two directions. The columns were 18 in. long, and a circular cross-section of 8 in., and reinforced with 0.5 in. thick stacked FRP grids. A total of seventeen columns were cast and tested on the compression testing machine which applies an ultimate load of 300 Kip. From the test specimens found that the FRP grid concrete undergoes continuous deformation before a sudden failure. The ultimate load and strength of the FRP reinforced members were enhanced by increasing the FRP reinforcement in the concrete.

The authors Dutta et al. (1998) from extensive research concluded that the new method to reinforce FRP composite grid in beams and columns found to be economically feasible. The main reason for designing concrete structures with FRP grid was to utilize unique nature of the grid. The FRP grid and steel reinforced beams exhibited similar load-deflection response, but the ultimate load carried by the FRP reinforced beam was higher than the steel reinforced beam. From the column specimens found that initially concrete had taken the load until it reached the yield point, and then the composite grid carried the load. The results obtained from the test specimen's aid in designing the FRP composite grid to reinforce the concrete members. From the experimental results, found that the load-deflection response depends on the mechanical properties of the composite grid and the concrete. The proposed method would make design guidelines easy and reduce costs while placing and pouring concrete in the field.

Harris et al. (1998) discussed a hybrid composite reinforcement for concrete members. The ductile FRP material was manufactured at Drexel University. The modulus of elasticity of FRP reinforcement is low compared to steel reinforcement. The modulus of elasticity of this new hybrid FRP bar is almost the same as that of steel reinforcement.

The in-line braiding and pultrusion methods were followed in the making of the new hybrid FRP bar, and it showed high bond strength and properties. It exhibits ductile properties like steel reinforcement during its usage in concrete members as a main reinforcement and allows using limit state method in the design. It was found that the new hybrid composite bar fails gradually, and it has a higher ultimate capacity compared to its yield strength. The advantages of the new FRP bar compared to steel reinforcement are: light weight, non-corrosive in nature and possess high tensile capacity. This research focuses on the process of making, designing and the experimental verification of new ductile fibrous FRP rebar. The design of RC members using steel bars considers the ductility of the bar, but the design of the FRP reinforced concrete members considers deflections and deformations. The ductile bar reinforced members undergo large deflections. In this study, tensile strength tests were done on the new FRP bars, and monotonic load was applied on the specimens. The dimensions of the tensile specimens were 425 mm long, 5 mm in diameter with 60 mm long GFRP. The FRP bars were manufactured in a tapered aluminum mold. Three beam specimens with ductile FRP bar and a beam reinforced with steel bar were also designed. The dimensions of the beam specimens were 1.2 m long and 50 X 100 mm cross-section. The beams were tested using four-point bending configuration.

Harris et al. (1998) found that the new hybrid FRP bars showed good bond strength, and the tensile specimens reached their maximum flexural strength. From the load-deflection response of FRP and steel reinforced beam specimens found that the pre-cracking and post-cracking behavior of both specimens were similar. They concluded that the new FRP reinforced concrete members can be effectively used in aggressive

environments, and also in new, repaired or retrofitted of concrete members. The beam specimens had taken large deformations. The ductility indexes of beams reinforced with ductile FRP bars were the same as that of the beam reinforced with steel rods or a reference beam.

Kumar et al. (1998) investigated the fatigue response of the FRP bar reinforced concrete bridge deck slabs. The fatigue behavior is important to the durability of the member. The purpose of the study was to evaluate the guidelines for glass fiber reinforced polymer reinforced concrete deck slab for ultimate loads, deflections, cracks and strains. The tests were performed on four concrete deck slab specimens. The decks 1 and 2 were 2.1 m long; decks 3 and 4 were 2.06 m long; and all four decks were 3.66 m wide. The No.13 FRP bars were provided in transverse direction as the main reinforcement and the No.10 long FRP stirrups were provided in the other direction to the decks. In the fatigue test, 2,500,000 cycles were applied on the deck slabs. It was observed that there was no bond failure between the FRP and the concrete in the four deck slabs. The spacing of the fatigue crack was 0.15 m in the deck specimens. For deck 1 and 2, the fatigue cracks were distributed all over the width of the deck. Kumar et al. concluded that the rate of degradation of FRP and steel reinforced bridge decks were similar. The failure due to fatigue in the deck specimens were affected by the crack propagation.

Schmeckpeper and Goodspeed (1994) discussed the use of FRP grids in concrete slabs, pavements and highway bridge decks as a main reinforcement. The performance and behavior of the FRP composite bridge decks and concrete beams were experimentally examined. Also, they concentrated on the splice and the development

length requirements for the FRP composite grids. There are two types of FRP grids: one with carbon fibers and another one with a mixture of carbon and E-Glass fibers were used in the program. The mechanical properties of these two types of FRP composite grids were evaluated. The reinforcement ratios were varied in the flexural testing of the beams specimens. In the experimental program, they have tested five beam specimens until failure occurred for each of the two types of FRP grids. The load-deflection behavior, failure modes and anchorage requirements were monitored and discussed during the beam tests. They have concluded that the formula derived for the splice/development length requirements for the FRP grid was conservative. The beam specimens were tested for flexure with reinforcement ratios from 0.3 to 2.2% which showed that measured deflection response, failure mode and the ultimate loads were consistent with the predicted values.

CHAPTER III

METHODOLOGY

3.1 Theoretical Work - Structural Modeling of FRP Grid Reinforced Bridge Decks

3.1.1 Introduction

In this section, focus was on the structural modeling of FRP grid reinforced concrete bridge decks and link slabs. The structural modeling and testing of FRP grid reinforced bridge decks were also discussed in LTRC Report No. FHWA/LA.09/443 (Li and Saber 2009). Here, two models were considered, one with open joints and the other with the joints closed over the supports. In developing the model, appropriate elements were chosen for modeling concrete and FRP reinforcement in the link slab. Then, required material properties were assigned to the elements. The models were properly meshed and boundary conditions were applied to the models. The truck load was applied on the bridge models to produce maximum negative moments in the link slab. The loads were applied at the same locations for both the bridge models.

The stresses obtained in bridge girders, decks and link slabs from both models were compared. The results were then used to evaluate the structural behavior of the FRP grid reinforced link slab.

3.1.2 Bridge Model Description

A typical three-span bridge was considered for modeling. In each span, four AASHTO type III girders, end and intermediate diaphragms were modeled. A typical AASHTO type III girder is shown in Figure 3.1. The deck was 60 feet long, 30 feet wide and 8 inches thick. The gap between two adjacent decks (open joint) was taken as 1 inch. The gap between two girders in adjacent spans was 6 inches. The open joint and gap between girders in adjacent spans is shown in Figure 3.2. The distance, center-to-center, between adjacent girders in a span was 104 inches (8 ft. 8 in). The four girder model and spacing between the girders is shown in Figure 3.3. The end diaphragms were placed between two adjacent girders, from the bottom of the top flange to the mid-depth of the girder. The intermediate diaphragms were placed from the bottom of the top flange to the top of the bottom flange. The thickness of the end and intermediate diaphragms was 7 inches. At the two adjacent ends of the open joint, the link slab was modeled for a distance of 2 feet. The length of the link slab was based on the theoretical studies which showed that the load-deflection behavior of the structure would not be affected by a debonding length of up to 5% of the span length (Paul et al., 1995). Volumes for the girders, decks and diaphragms were modeled. Then, all the volumes were joined.
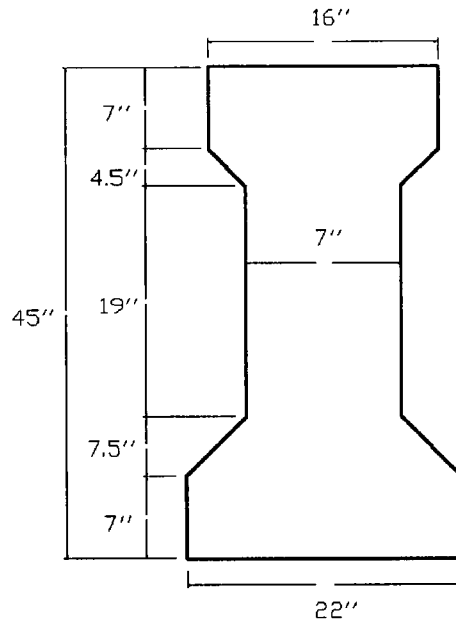
Figure 3.1 A Typical AASHTO Type III Girder.
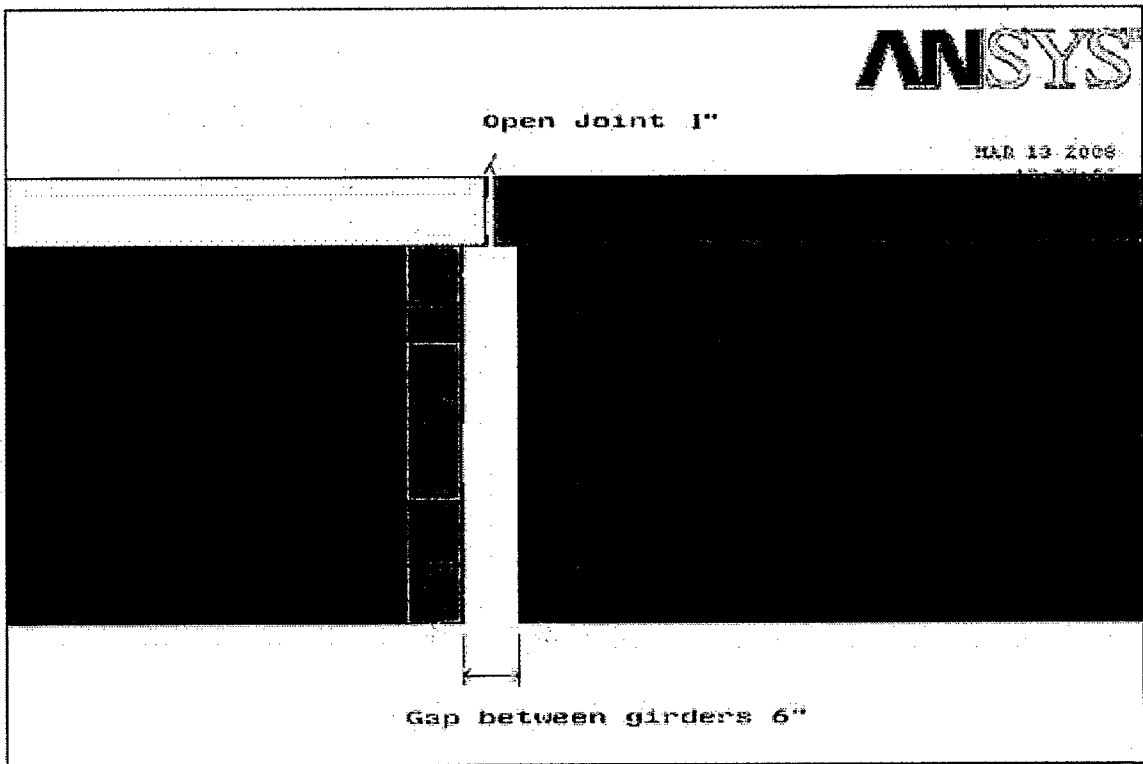
Figure 3.2 Open Joint and Gap between Girders in Adjacent Spans of a Bridge.
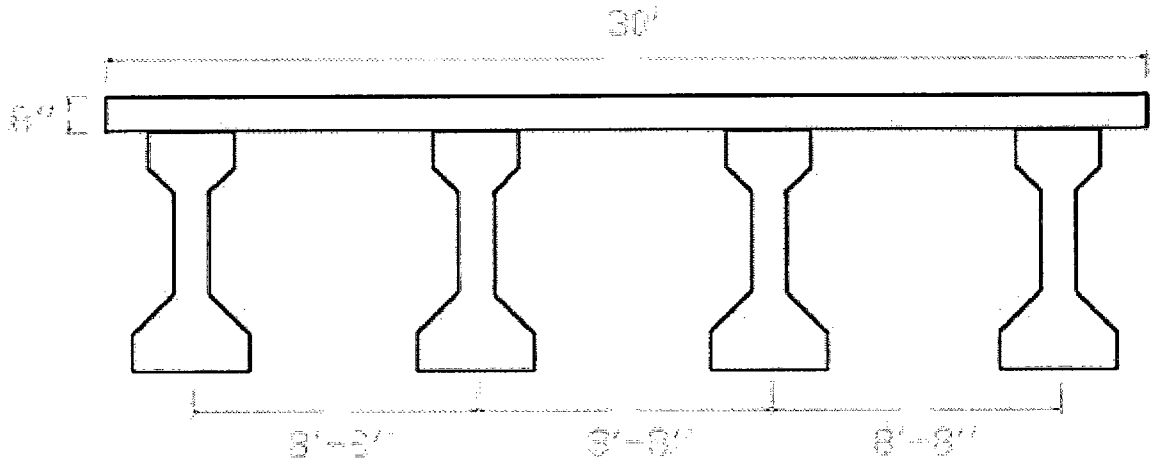
Figure 3.3 Model Used for Bridge Analysis - Four Girders Model.

The X-axis was taken along the transverse direction of the bridge (30 ft.), the Y-axis along the height, and the negative Z-axis in the longitudinal direction (60 ft.). The bridge decks, girders, diaphragms, and FRP blocks were meshed. The girders were restrained at supports and both extreme ends of the decks were restrained in x, y and z directions (translations). A standard truck load (HS20-44) was applied in such a way on the bridge to produce the maximum negative moment and tensile force in the link slab. The three-span bridge model generated in ANSYS is shown in Figure 3.4.
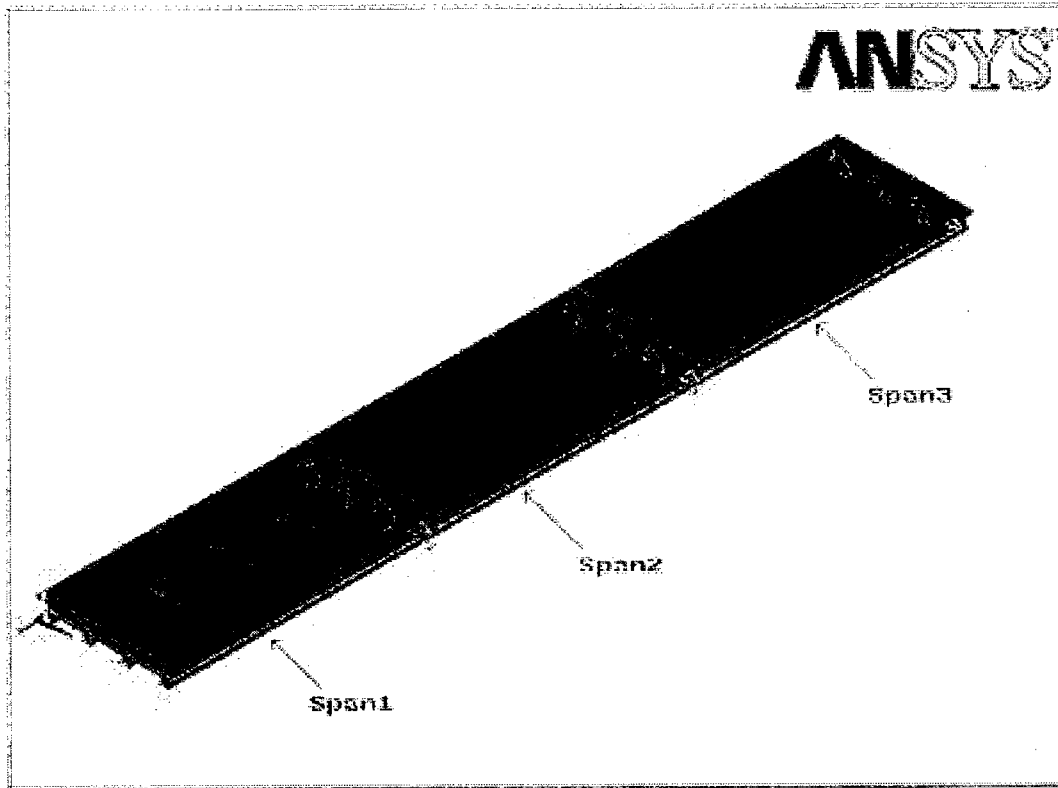
Figure 3.4 The Three-Span Bridge Model.

3.1.3 Elements Used in Modeling

The elements used for modeling the bridge were SOLID65 and SOLID46. For the

modeling of concrete, a 3-D reinforced concrete solid element SOLID65 was used. The

solid was capable of cracking in tension and crushing in compression. The element was

defined by eight nodes having three degrees of freedom at each node with translations in

x, y and z directions. The element had eight nodes and isotropic material properties. The

geometry and coordinate system of the element is shown in Figure 3.5.

The input data required for the SOLID65 element were the modulus of elasticity

and Poisson's ratio. The modulus of elasticity of the concrete was calculated from the

compressive strength of the concrete. The average Poisson's ratio of the concrete used was 0.16.
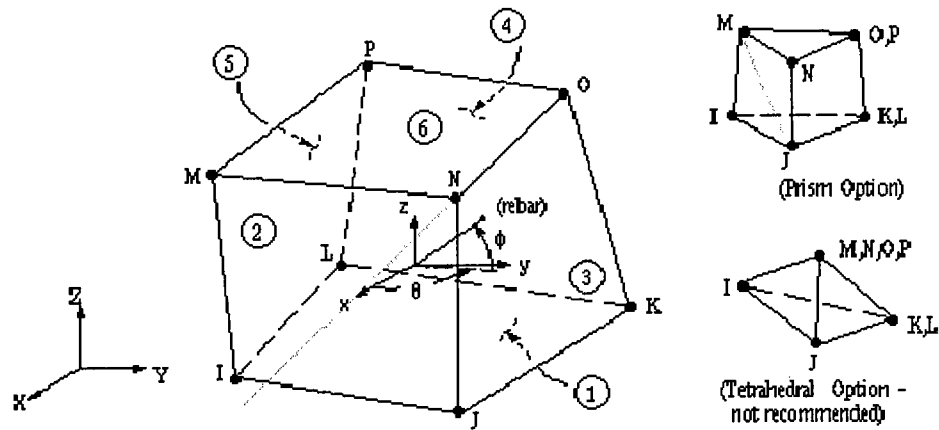
Figure 3.5 SOLID65 Element Geometry and Coordinate System. [ANSYS Tutorials]

A 3-D layered structural element SOLID46 was used to model FRP blocks in the link slab. The element allowed up to 250 layers. The element had three degrees of freedom at each node with translation in x, y and z directions. The element was defined by eight nodes, number of layers, layer thickness, layer material direction, and orthotropic material properties. The geometry and coordinate system is shown in Figure 3.6.
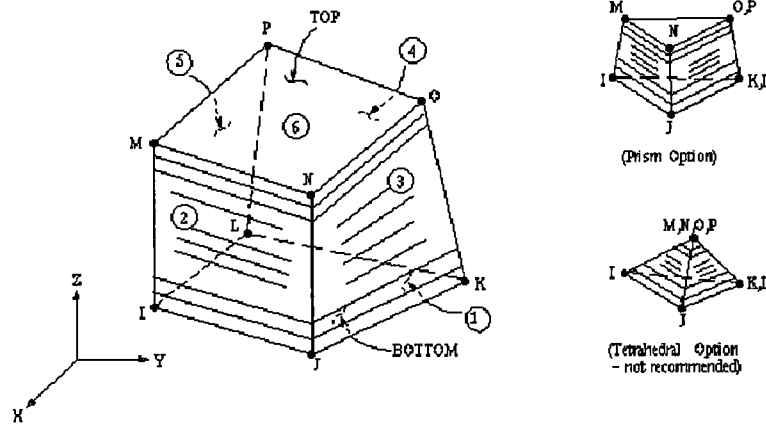
Figure 3.6 SOLID46 Element Geometry and Coordinate System. [ANSYS Tutorials]

3.1.4 Material Properties

In the model, the compressive strength 4000 psi was considered for decks and diaphragms. The compressive strength 6000 psi was considered for girders. The material properties required for SOLID65 element were the modulus of elasticity, Poisson's ratio and density of the concrete. The material properties required for SOLID46 element were the modulus of elasticity, Poisson's ratio and density of FRP grid. A load factor of 1.25 was applied to the dead load of concrete and FRP. The properties of the FRP were obtained from the manufacturer (Fibergrate, composite structures). The material properties used for the bridge model are listed in Table 3.1.

Table 3.1 Material Properties Used for Bridge Model.

Material / Properties	Poisson's Ratio	Modulus of Elasticity , E 10^6 (psi)	Density (lb/ in^3)
Girders	0.16	3.61	0.109
Decks & Diaphragms	0.16	4.42	0.109
FRP Grid	0.22	2.80	0.083

3.1.5 Meshing

The FRP layers were meshed using SOLID46 element. The FRP material properties (Modulus of elasticity, Poisson's ratio and density) were assigned while meshing. The element edge length of FRP was 6 inches. Small size element was chosen because the depth of FRP was just 1 inch. The bridge decks and diaphragms were meshed using SOLID65 element. Girder, deck and diaphragm material properties (Modulus of elasticity, Poisson's ratio and density) were assigned during the meshing processes. The element edge length of the concrete element was 24 inches. Different size elements were considered in meshing to keep the total number of elements within the allowable limit.

The mesh was refined twice at the girder supports to generate a larger number of nodes and to properly restrain girders over piers. Separate volumes were created for tire contact areas in the deck. The element edge length of these volumes was 5 inches. The meshed model of the first span of the bridge is shown in Figure 3.7.
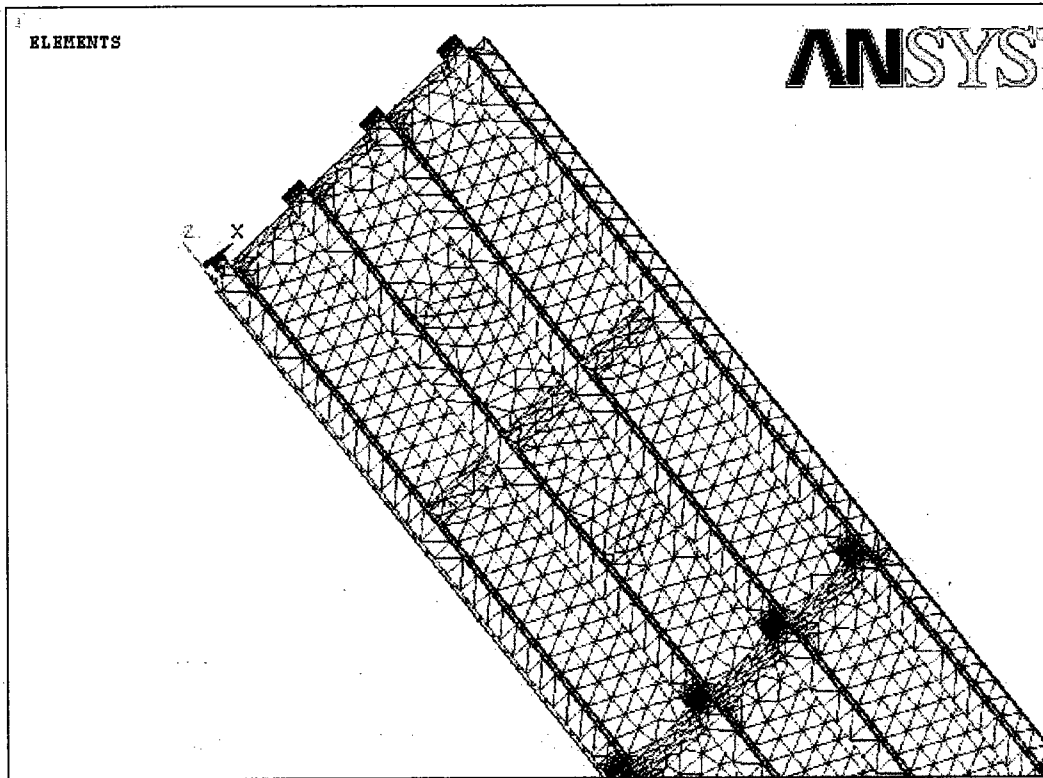
Figure 3.7 Meshed Model Showing the First Span of the Bridge.

3.1.6 Boundary Conditions

The interface area between the girders and sub-structure was restrained in x and y directions (translations). The restrained supports between girders and sub-structure are shown in Figure 3.8. Both the extreme ends of the decks (area along the depth) were restrained in x, y and z directions (translations).
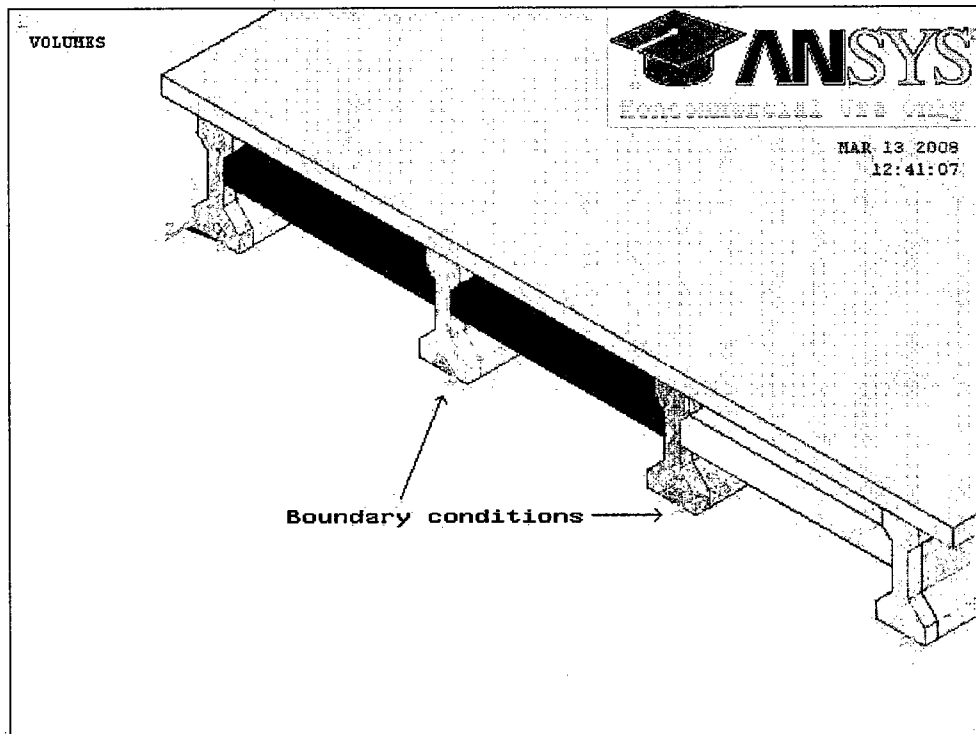
Figure 3.8 Restrained Supports between Girders and Sub-structure.

3.1.7 Modeling of Link Slab

A link slab was modeled at each open joint. The length of the link slab was 2 feet

on either side of the open joint, which was about 3.33% of the span of each girder.

Therefore, the total length of the link slab was 4 feet and 1 inch. The width of the link

slab was 30 feet, which was equal to the width of the bridge. The three FRP layers were

placed in the link slab. The clear vertical spacing between the two layers was 1 inch with

a 1.5 inch cover. The FRP layers were placed throughout the length and width of the link

slab. The link slab (which connects two adjacent decks) with FRP layers is shown in

Figure 3.9.
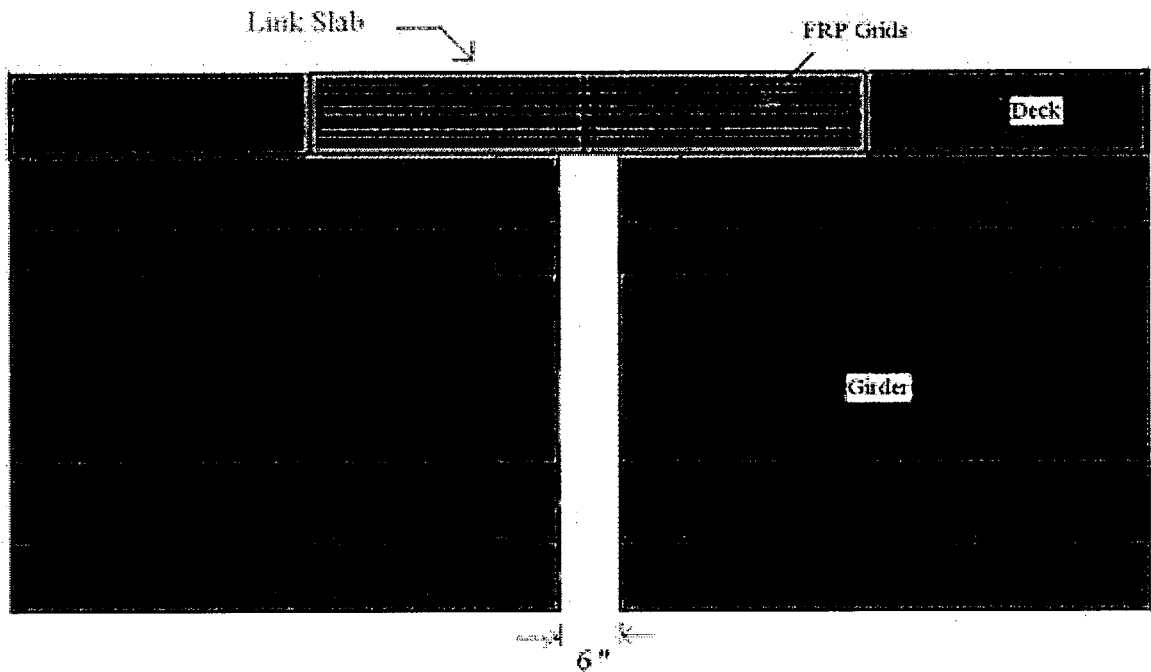
Figure 3.9 Link Slab with FRP Layers.

3.1.8 Loading System

In this study, strength-I (LRFD Bridge Design) load combination was considered, and the corresponding load factors were applied to the model, as shown in Table 3.2. However, LFRD code specified eleven load combinations (strength I- V, extreme event I & II, service I- III, and fatigue). The strength-I load combination was chosen because of its higher load factors. The vehicular live load and live load surcharge were applied to the bridge. The truck load was applied to produce maximum negative moments in the link slab. A single HS20-44 truck was placed on the first span of the bridge. The 8.0 kip axle was placed in the first span at a distance of 15 feet from the left end of the deck (Xiang, 2007). The spacing between the 8.0 kip axle and the adjacent 32.0 kip axle, and the two 32.0 kip axles was 14 feet. The transverse spacing of the wheels was 6 feet. Therefore, the truck load was applied at six locations on the deck.

Table 3.2 AASHTO LFRD Bridge Design Load Combination and Load Factors.

Load Combination	Dead Load (DL)	Vehicular Live Load (LL)	Live Load Surcharge (LS)
Strength I Max	1.25	1.75	1.75

The tire contact area of a wheel was assumed to be a rectangle, whose width was 20 inches and the length was 15 inches. The tire contact area was calculated using LRFD Bridge design Specifications (3.6.1.2.5). Each wheel load was applied as uniform pressure on the tire contact area. The pressure applied on the front two areas was 23.33 psi including the live load factor. The pressure applied on the remaining four areas was 93.33 psi including the live load factor. The applied pressure was taken by the nodes in that area. A live load surcharge (2-inch bituminous wearing surface) was applied as a pressure on the top surface area of the decks. The applied truck load on the bridge is shown in Figure 3.10.
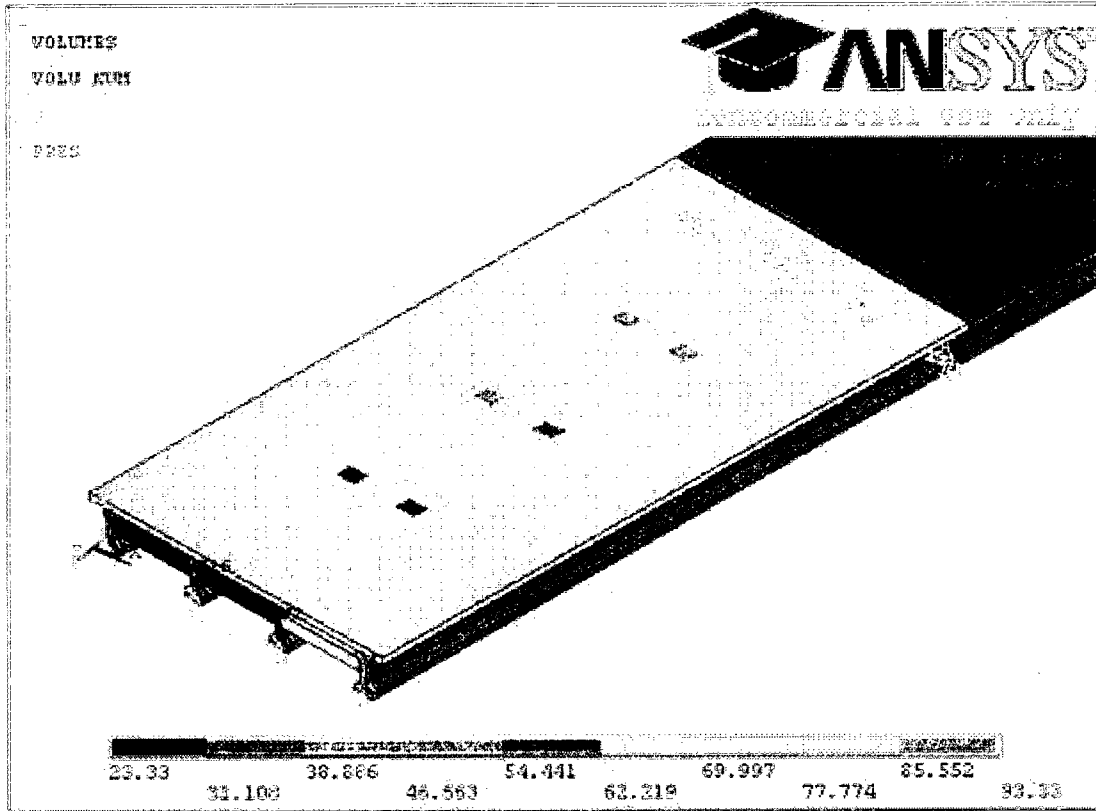
Figure 3.10 The Applied Truck Load.

The ANSYS input data for developing two models, bridge with link slabs (link slab bridge) and bridge with expansion joints (open joint bridge) is presented in APPENDIX A.

3.2 Experimental Work - Structural Testing of FRP Grid
Reinforced Decks

3.2.1 Purpose of the Test

A test program was conducted to determine the behavior and strength of jointless bridge decks under static loading. The jointless decks could be achieved by replacing expansion joints by a link slab that could join bridge decks of adjacent spans without imposing any continuity in the bridge girders. The link slab would be subjected to tensile forces due to negative moment that developed at the location of the joint. The link slab panel was cut into beam specimens to determine the strength of the link slab against tensile forces. The test program included two test specimens: (1) a reinforced concrete beam with two layers of 1.00 inch deep FRP grids; (2) a similar concrete beam with two layers of 1.25 deep FRP grids.

The specimens were tested under the same support conditions. Loads, deflections, strains, and load carrying capacity were measured for each test specimen. Since there were no design equations for FRP grid reinforced concrete beams, the existing design equations in ACI 440 for FRP rebar reinforced concrete beams were modified and used.

3.2.2 Description of Test Specimens

The specimens were designed as per ACI 318-05 and ACI 440 guidelines. The cross section of the specimens was rectangular in shape with a width of 1 ft., 8 in. deep, and 8 ft. long. The beams were reinforced with three # 4 bars. A cover of 1.5 inch was provided to the reinforcing bars. Shear reinforcement was not provided to the beams since depth of the beam was not greater than 10 in. (ACI 318-05, 11.5.5.1).

The first beam contained two layers of 1.00 in. deep FRP grids and the beam was designated as Beam 1. Each grid was 4 ft. long and 9 in. wide. The grids were placed at

30

2 feet from one end of the beam, i.e., in the center 4 feet, along the length of the beam. The clear spacing between the two FRP grids was 1 in. The dimensions and cross-section details of Beam 1 are shown in Figures 3.11 and 3.12, respectively.
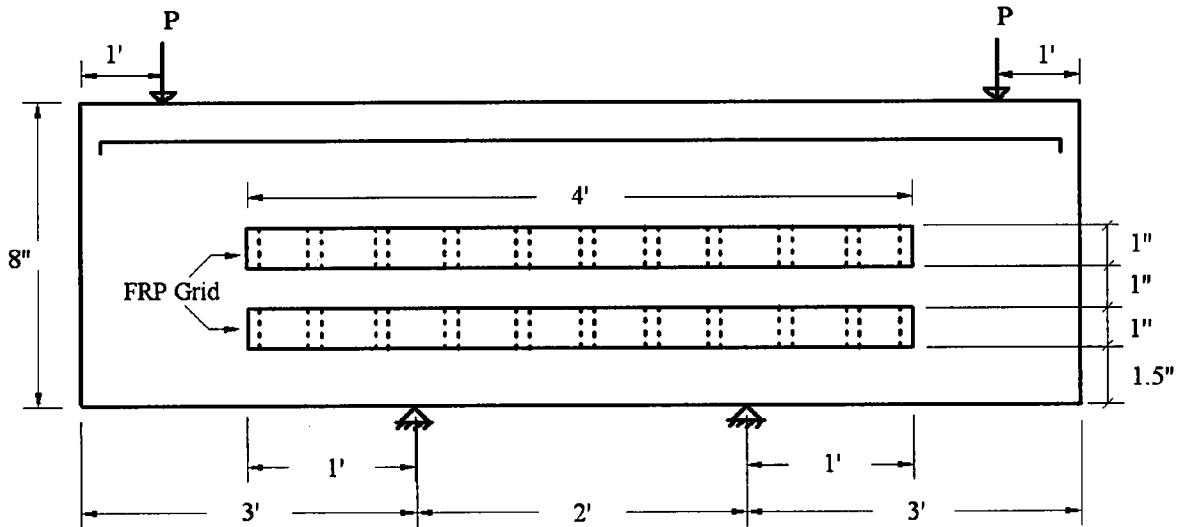
Figure 3.11 Beam 1 Dimensions (not to scale).
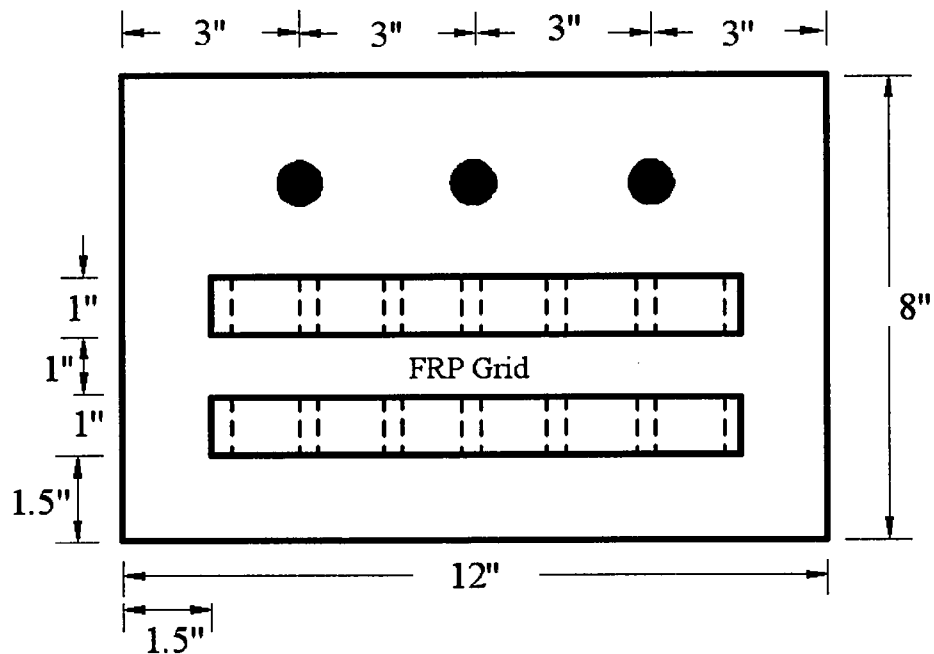
Figure 3.12 Beam 1 Cross-Section Details.

The second beam contained two layers of 1.25 in. deep FRP grids and the beam was designated as Beam 2. Each grid was 4 ft. long and 9 in. wide. The dimensions and cross-section details of Beam 2 were similar to Beam1, except for the depth of the FRP grids, as shown in Figures 3.13 and 3.14, respectively. The two rectangular beams were cast from the batch delivered by a ready mix truck to the Structural and Materials Laboratory at Louisiana Tech University. To simulate field conditions, the beams were cured in dry air conditions for 28 days before they were tested.
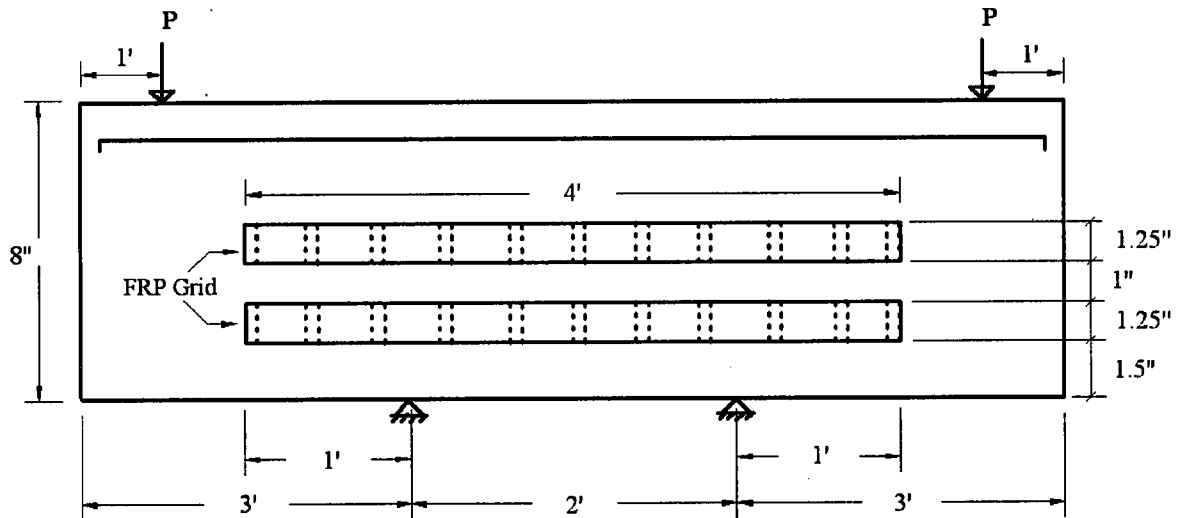
Figure 3.13 Beam 2 Dimensions (not to scale).
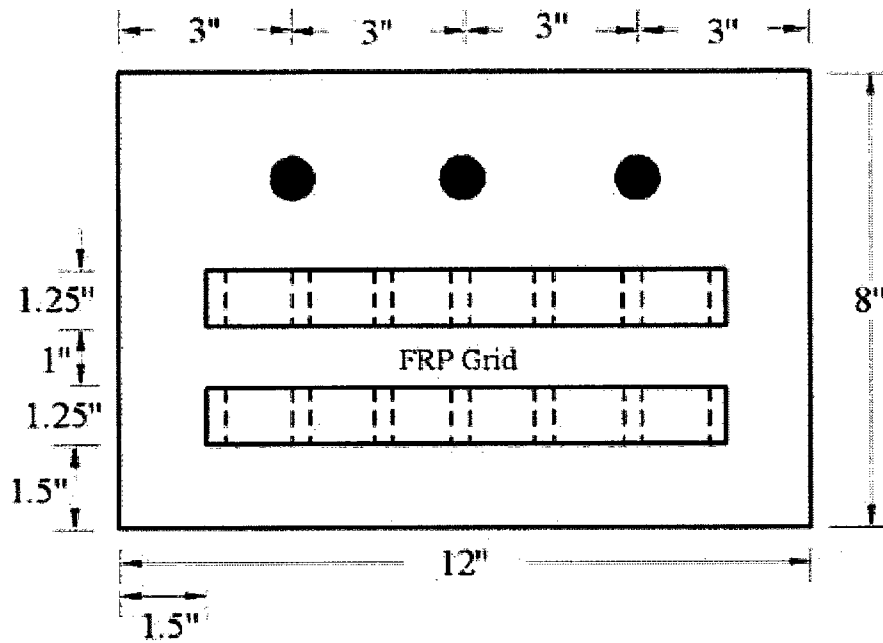
Figure 3.14 Beam 2 Cross-Section Details.

3.2.3 Test Set-Up

The two specimens were tested under the same set-up. The two support and two load locations were shown in Figures 3.11 and 3.13. The applied loads and reactions were symmetrical with respect to the center of the beam. The specimen was placed on a high reaction stands of stiffened steel section. At each reaction point, a roller support was placed between the specimen and the steel section. Load was applied by a MTS hydraulic jack at load points. A steel section was used between the hydraulic jack and beam specimen to apply the load equally at the load locations. At the load points, roller supports were provided to disperse the load from the steel section to the specimen. The jack was activated by a single automatic MTS electric pump.

3.2.4 <u>Instrumentation Plan</u>

The instrumentation used for the testing of each beam included a deflectometer, a twenty-four channel data acquisition system and Micro-Measurements N2A-06-20CBW-120 strain gauges with a 2 in. gage length.

The shear force and bending moment diagrams of the three-span rectangular beam for live loads and dead loads are shown in Figure 3.15. The shear force due to live load was maximum in regions EB and CF. The bending moment due to the live load was maximum in span BC. Therefore, strain gages were placed at locations on the grids where the shear forces and bending moments were high.

For each grid, strain gages were installed on the outer surface along the longitudinal direction. On each layer of the FRP grid in Beam 1, eight strain gages were installed to monitor the strain distribution during the test. The locations of the sixteen strain gages in Beam 1 and Beam 2 are shown in Figure 3.16. The top grid was designated as Layer 1 and the bottom grid was designated as Layer 2. The Layer 1 strain gages were designated as L1G1 through L1G8 from left end to the right end of the grid. Similarly, Layer 2 strain gages were designated as L2G1 through L2G8 from the left end to the right end of the grid.

After connecting DSV cables to the strain gages, environmental/concrete protection coating (MCOAT-J3) was applied on them. The deflection of each beam was measured during the test by a deflectometer placed at the mid-span of the beam.
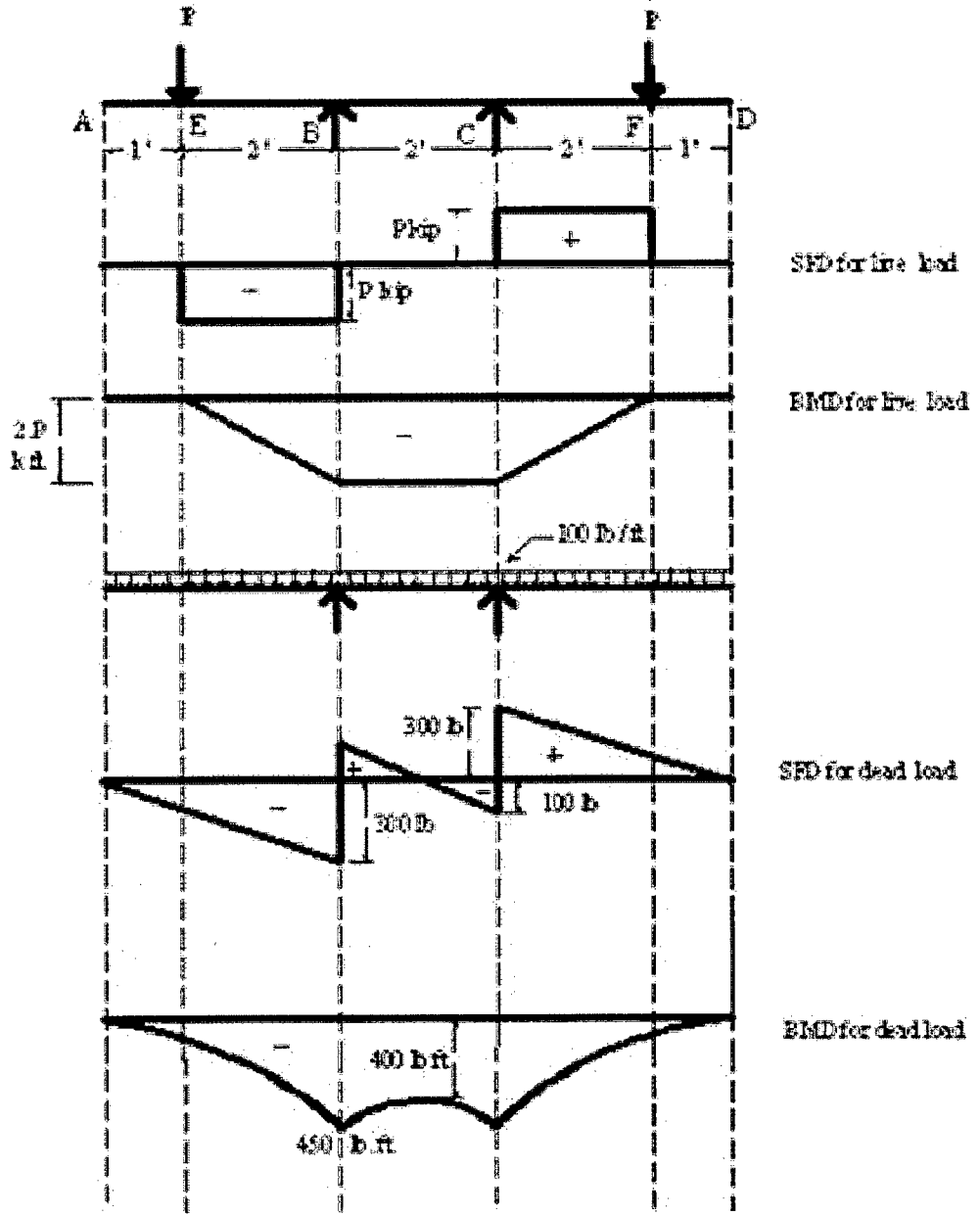
Figure 3.15 SFD and BMD for Three-Span Rectangular Beam.
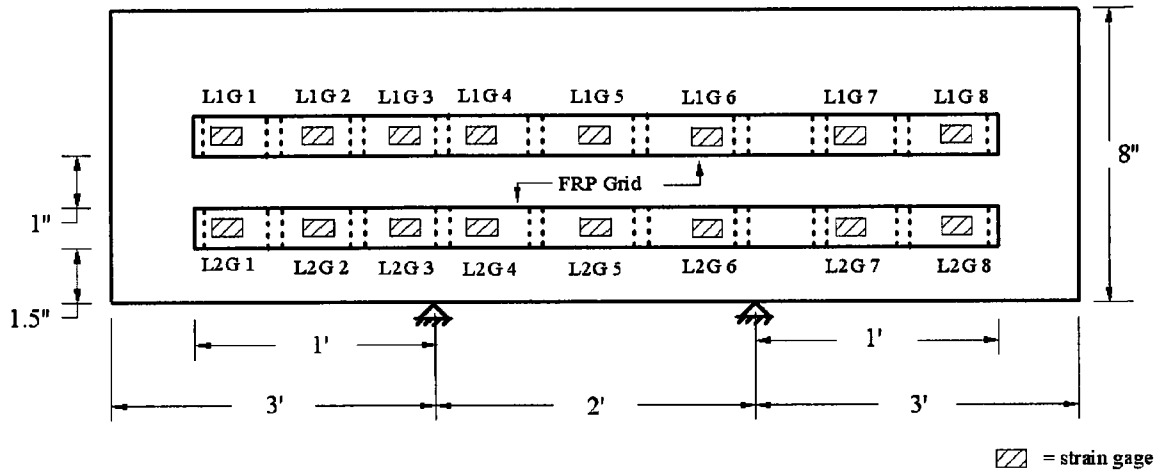
Strain Gage Designation:

Layer1 strain gages: L1G1 at 26", L1G2 at 30", L1G3 at 34", L1G4 at 39", L1G5 at 48", L1G6 at 57", L1G7 at 66" and L1G8 at 70" from left end of the beam.

Layer2 strain gages: L2G1 at 26", L2G2 at 30", L2G3 at 34", L2G4 at 39", L2G5 at 48", L2G6 at 57", L2G7 at 66" and L2G8 at 70" from left end of the beam.

Figure 3.16 Selected Strain Gage Locations for Beam 1 and Beam 2 (not to scale).

3.2.5 Test Procedure

A four-point bending test was conducted; the test load was applied in such a way that a negative bending moment was produced in the beam at the FRP grid's locations. The test set-up is similar to ASTM C 78.

The beams were loaded continuously at a constant rate of 2000 lbs/min until failure. The four-point bending tests were conducted using the MTS machine. The data collection system stored the strain and load data for every quarter second. For each load increment, data for the FRP strains and loads were collected. The applied loads and corresponding deflections at mid-span for each beam were measured during the tests.

3.2.6 <u>Material Characteristics</u>

3.2.6.1 <u>Concrete Compressive Strength</u>

The concrete cylinders were cast from the same batch delivered by a local ready mix truck to the Structural and Materials Laboratory at Louisiana Tech University. The concrete mix constituents are shown in Table 3.3.

Table 3.3 Concrete Mix Proportions.

Cement	489 - lb/yd^3
Fly Ash	122 - lb/yd^3
Coarse Aggregate Pea Gravel	1870 - lb/yd^3
Natural Sand	1325 - lb/yd^3
Admixture (900 P0Y-5)	18 - Oz/yd^3
Air Content	0.05
Slump	5 inch
Water	29.5 - gal/yd^3

The 4 x 8-inch concrete cylinders were cured in accordance with ASTM C511. The concrete compressive strength was determined in accordance with ASTM C39. The crushing load of each cylinder, average compressive strength of three cylinders and standard deviation for each testing are reported in Table 3.4. When the beam specimens were tested at 28 days, the compressive strength of the concrete was 5277 psi. The concrete strength development over time is shown in Figure 3.17.

Table 3.4 Average Concrete Compressive Strength.

Age	Crushing Load (lb)	Compressive Strength (psi)	Average Compressive Strength (psi)	Standard Deviation
1-day	19800	1575	1618	60
	21200	1687		
	20000	1591		
3-day	28200	2243	2381	153
	32000	2546		
	29600	2355		
7-day	56600	4503	4381	106
	54200	4312		
	54400	4328		
14-day	56800	4519	4567	126
	56200	4471		
	59200	4710		
28-day	69800	5553	5277	241
	65000	5171		
	64200	5107		
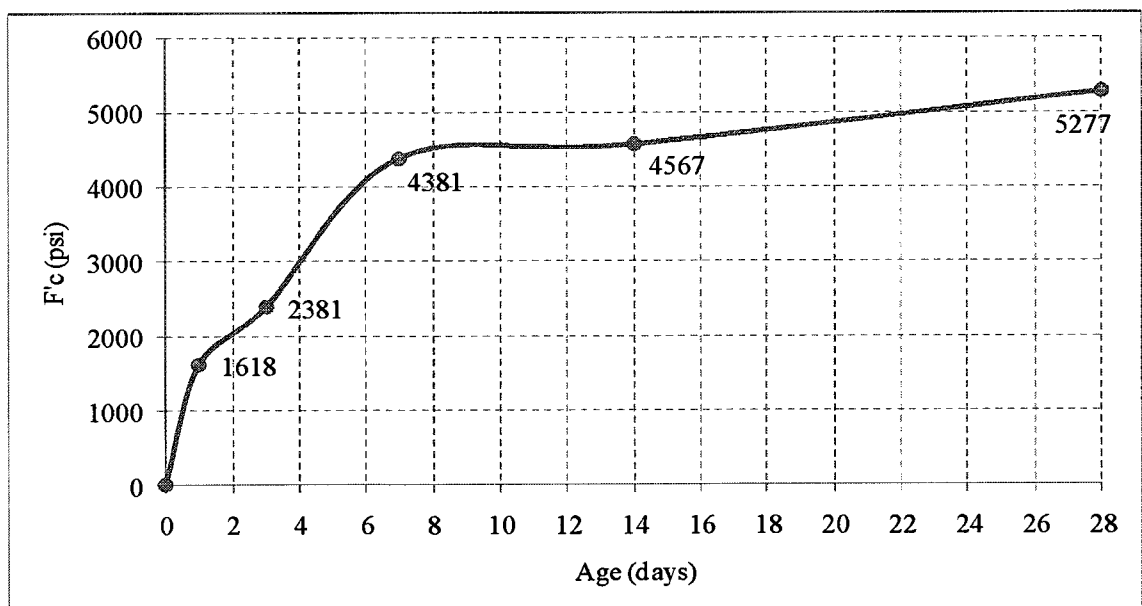
Figure 3.17 Concrete Average Compressive Strength.

3.2.6.2 FRP Material Properties

The material properties of FRP grid were obtained from the manufacturer (Fibergrate, Composite Structures), and are listed in Table 3.5.

Table 3.5 Material Properties Provided by Manufacturer.

MECHANICAL PROPERTIES	UNITS	VALUE
Tensile Stress, LW	psi	30,000
Tensile Modulus, LW	10^6 psi	2.5
Compressive Stress, LW	psi	30,000
Compressive Modulus, LW	10^6 psi	2.5
Flexural Stress, LW	psi	30,000
Flexural Modulus, LW	10^6 psi	1.8
Shear Modulus	10^6 psi	0.45
Short Beam Shear	psi	4,500
Punch Shear	psi	10,000
Bearing Stress, LW	psi	30,000
Area of 1 Inch Deep FRP per 9 inch width per Layer	in^2	1.43
Area of 1.25 Inch Deep FRP per 9 inch width per Layer	in^2	1.78

The pictures in APPENDIX B (Figure B.1 - B.6) shows the experimental work procedure (i.e., installing and fixing the strain gages to FRP grid, making the forms for beams, pouring concrete in beams, and testing of beams and cylinders) followed by structural testing of FRP grid reinforced decks.

3.3 <u>Experimental Work - Test for the Development Length</u>
<u>of FRP Grid</u>

3.3.1 <u>Purpose of the Test</u>

The test program presented here focused on the development length requirements for the FRP grids. ACI 440 guidelines provided equations for development length of the FRP bar. Till now, the ACI code has not discussed about the development requirements of the FRP grid and, also the code has not provided equations for the development length of the FRP grid. Here, the development lengths for two types of FRP grids of 1.00 deep and 1.25 inch deep was calculated using the available equations from the previous studies.

In the test program, one beam was reinforced with 1.00 inch deep FRP grid and another beam was reinforced with 1.25 inch deep FRP grid were designed and tested. The specimens were tested under the same support conditions. Loads, strains, deflections and ultimate load were measured for each test specimen and then experimentally obtained loads and strains were discussed.

3.3.2 <u>Development Length Equations</u>

The development length of the welded plain wire fabric or mesh is given by ACI 318-05, 12.8 as:

$$l_{db} \geq 0.27 \left(\frac{A_w}{S_w} \right) \cdot \left(\frac{f_y}{\sqrt{f'_c}} \right)$$

or, development length (l_{db}) should not be less than 6.0 inches.

Also, the development length of the welded deformed wire mesh or fabric is given by ACI 318-05, 12.7.2 as:

$$l_{db} \geq 0.20 \left(\frac{A_w}{S_w} \right) \cdot \left(\frac{f_y}{\sqrt{f_c'}} \right)$$

or, development length (l_{db}) should not be less than 8.0 inches,

where A_w = Area of an individual wire or longitudinal reinforcing bar to be developed

S_w = Spacing of the wire or longitudinal reinforcing bars

f_y = Yield strength of the non-prestressed reinforcement

f_c' = Compressive strength of the concrete.

The above two equations may be combined as:

$$l_{db} \geq \frac{A_{frp} \cdot f_{frp}}{\left(\frac{A_c / grid}{S_{trans}} \right) \cdot V_c},$$

where A_{frp} = Area of the longitudinal reinforcing bar

f_{frp} = Design strength of the FRP reinforcement

A_c /grid = Area of the concrete enclosed by one grid (one pair of longitudinal and

transverse bar)

V_c = Allowable shear strength of the concrete.

The proposed design equation for the development of the FRP grid

(Schmeckpeper, 1992) is:

$$l_{db} \geq 0.22 \frac{A_{frp} \cdot f_{frp}}{\left(\frac{A_c / grid}{S_{trans}} \right) \cdot \sqrt{f_c'}},$$

where $V_c = (4.6) \cdot \sqrt{f_c'}$.

The development length of two types of FIBERGATE FRP grids of 1.00 inch

deep and 1.25 inch deep can be calculated as:

1. The development length of the 1 inch deep FIBERGRATE CFRP grid:

    Average width of the grid $(W_{avg}) = 0.25$ inch

    Transverse or longitudinal spacing between the bars (S):

    $S_{trans} = S_{long} = 1.25$ inch

    $f'_c = 4000$ psi

    $f_{frp} = 30,000$ psi

    $A_{frp} = (1.0)\,(0.25) = 0.25$ in^2

    For in-line grid: $A_c/\text{grid} = (S - W_{avg})^2 = (1.25 - 0.25)^2 = 1.0$ in^2

    Assuming that FRP is stressed to 25 % of the ultimate:

    $$l_{db} \geq 0.22 \cdot \frac{(0.25) \cdot (0.25 \times 30,000)}{\left(\frac{1.0}{1.25}\right) \cdot \sqrt{4,000}}$$

    $l_{db} \geq 8.15\ inches$ \qquad (Say 9.0 inches).

    therefore, the development length of the 1.0 inch deep CFRP grid is 9.0 inches.

2. The development length of the 1.25 inch deep FIBERGRATE CFRP grid:

    Average width of the grid $(W_{avg}) = 0.25$ inch

    Transverse or longitudinal spacing between the bars (S):

    $S_{trans} = S_{long} = 1.25$ inch

    $f'_c = 4000$ psi

    $f_{frp} = 30,000$ psi

    $A_{frp} = (1.25)\,(0.25) = 0.3125$ in^2

    For in-line grid: $A_c/\text{grid} = (S - W_{avg})^2 = (1.25 - 0.25)^2 = 1.0$ in^2

    Assuming that FRP is stressed to 25 % of the ultimate:

$$l_{db} \geq 0.22 \cdot \frac{(0.3125) \cdot (0.25 \, X \, 30{,}000)}{\left(\frac{1.0}{1.25}\right) \cdot \sqrt{4{,}000}}$$

$$l_{db} \geq 10.19 \; inches \qquad \text{(Say 11.0 inches).}$$

therefore, the development length of the 1.25 inch deep CFRP grid is 11.0 inches.

3.3.3 Making of Test Specimens

The rectangular beam specimens were cast as per ACI 318-05 and ACI 440 guidelines. The first specimen had cross-sectional dimensions of 9 in. by 9 in. and a length of 24 in. The second specimen also had the same cross-sectional dimensions as the first one, with a length of 28 in. The two beams were reinforced with FRP grid.

The carbon fiber reinforced polymer (CFRP) used as the main reinforcement in the beams is shown in Figure 3.18. In the grid, the longitudinal or transverse bars are called ribs. The rib width was 0.25 in. and the height was 1.00 or 1.25 in. The open space between and among the ribs are called bays or cells. Each bay was 1.25 in. by 1.25 in. square.
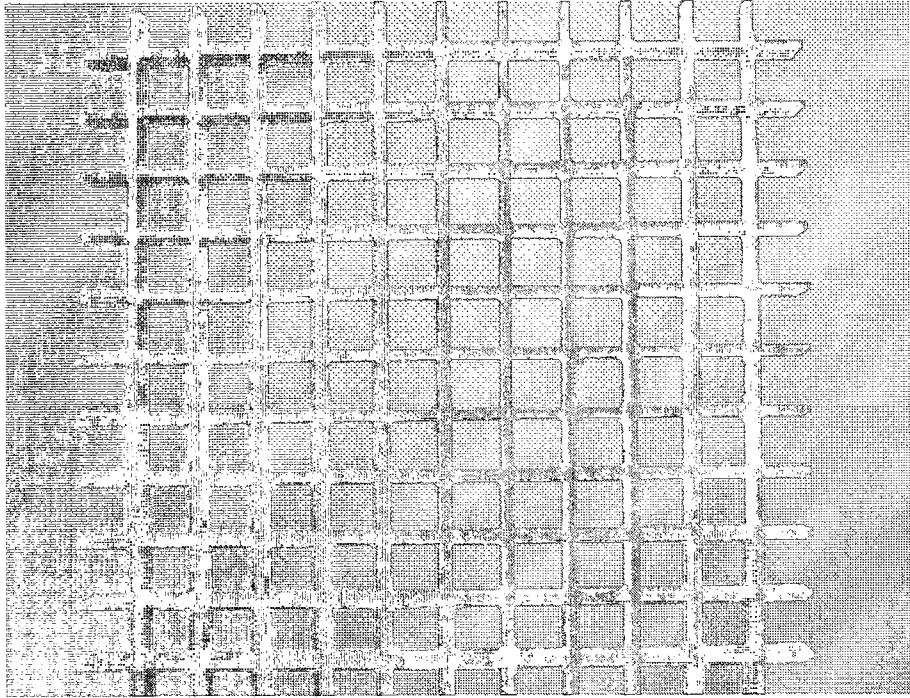
Figure 3.18 Commercially Available FIBERGATE CFRP Grid Used in Reinforcing Concrete Beams.

The first beam was reinforced with 1.00 in. deep FRP grid, and the beam was denoted as Beam 1. The grid was 18 in. long and 6 in. wide. The length of the grid was provided based on the development length requirements. Since, the development length of the 1.00 in. deep grid was 9 in. Hence, the 9 in. length was provided on either side of the point of application of the load or the critical section. Therefore, the total length of the grid provided was 18 in. The dimensions and cross-section details of Beam 1 are shown in Figures 3.19 and 3.20, respectively.
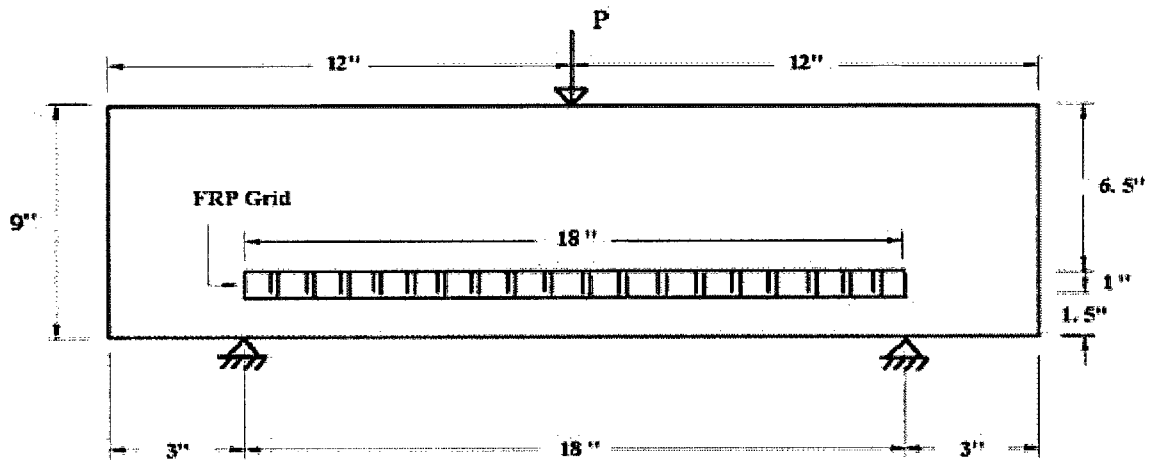
Figure 3.19 Beam 1 Dimensions (not to scale).
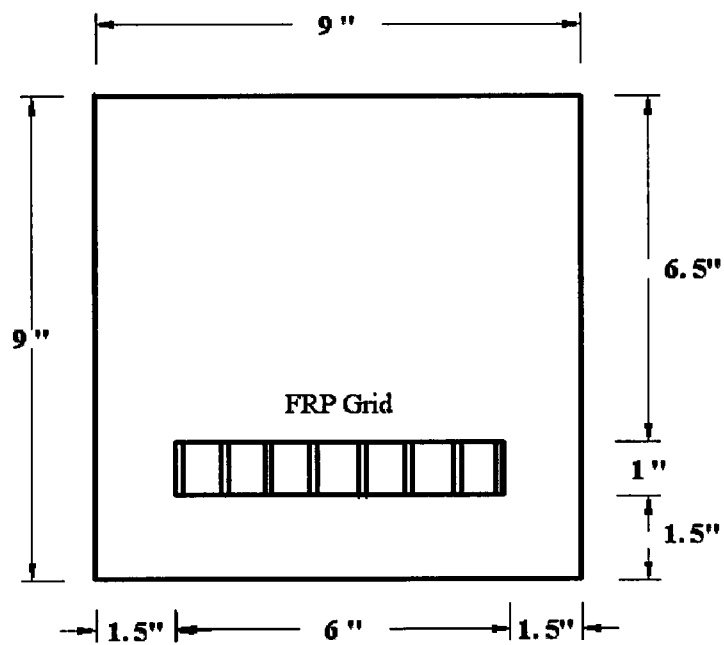
Figure 3.20 Beam 1 Cross-Section Details.

The second beam was reinforced with 1.25 in. deep FRP grid, and the beam was denoted as Beam2. The grid was 22 in. long and 6 in. wide. The length of the grid was provided based on the development length requirements. Since, the development length of the 1.25 in. deep grid was 11 in. Hence, the 11 in. length was provided on either side

of the point of application of the load or the critical section. Therefore, the total length of the grid provided was 22 in. The dimensions and cross-section details of Beam 2 are shown in Figures 3.21 and 3.22, respectively.
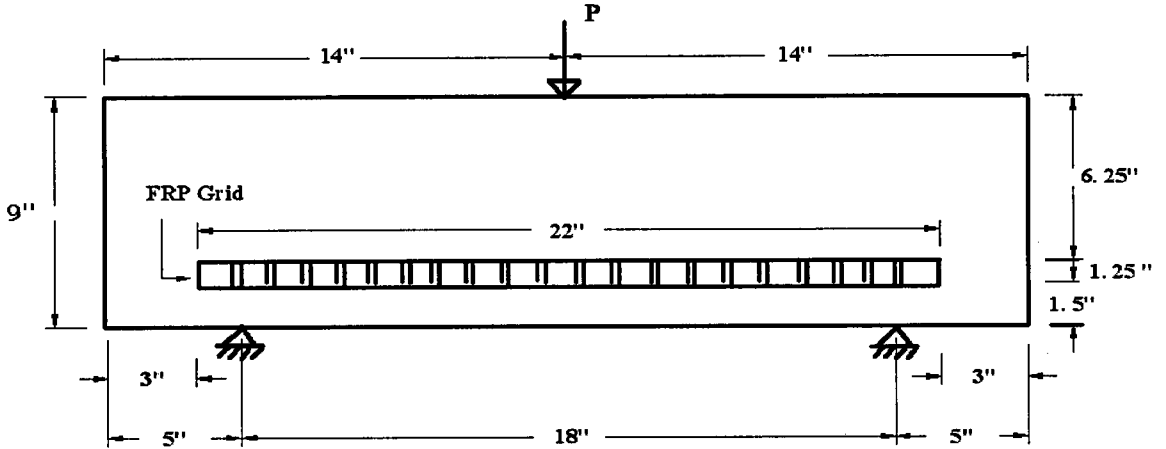
Figure 3.21 Beam 2 Dimensions (not to scale).
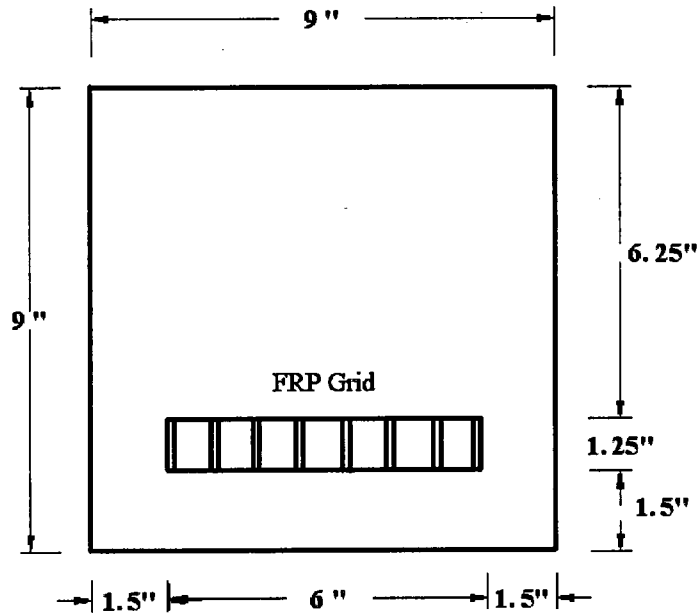
Figure 3.22 Beam 2 Cross-Section Details.

A minimum cover of 1.5 in. was provided to the grids as per the ACI code requirements. Shear reinforcement was not provided to the beams since the depth of the beam was not greater than 10 in. (ACI 318-05, 11.5.5.1). Both the rectangular beams were made from the concrete batch that was prepared in the Structural and Materials Laboratory at Louisiana Tech University.

3.3.4 Test Set-Up and Instrumentation

The two specimens were tested under a similar set-up. A concentrated load was applied at the mid-span of the beam. The applied load and the two supports are shown in Figures 3.19 and 3.21. The two supports were symmetric about the center of the beam. The specimen was kept on a high reaction stands of stiffened steel section. A roller was provided at each support and at the applied load. The purpose of the roller was to distribute the loads uniformly throughout the cross-section of the beam. The point load was applied on the beam by MTS hydraulic jack. The jack was started by a single automatic MTS electric pump.

Strain gages are fixed to the FRP grids to monitor the behavior of the beams and the reinforcement, and also to measure the strains and corresponding stresses in the FRP grids. The instrumentation used for the testing of each beam included Micro-Measurements N2A-06-10CBE-350 ohm strain gages with 1 in. gage length, a twenty-four channel data acquisition system and a deflectometer.

The shear force due to live load and the dead load was maximum at the supports. The bending moment due to live and dead load was maximum at the applied load. Hence, the strain gages were fixed at the locations on the grids where the bending moments and shear forces were high.

On each FRP grid, seven strain gages were fixed to measure the strains for the different applied loads. The strain gages were installed on the outer surface along the longitudinal direction. The locations of the seven strain gages in Beam 1 and Beam 2 are shown in Figures 3.23 and 3.24, respectively. A strain gage was installed at the mid-span and the other six gages were symmetric about the mid section. In both the beams, the strains gages were designated as Gage 1 through Gage 7 from the right end to the left end of the grid.
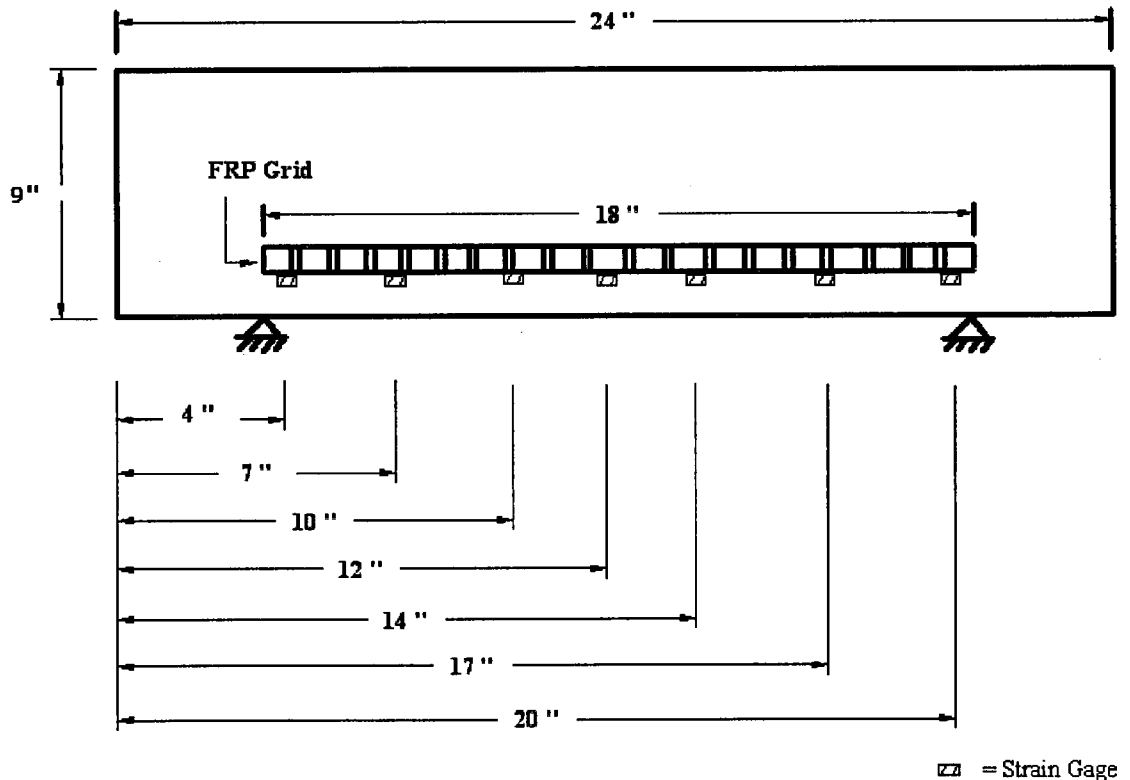
Figure 3.23 Selected Strain Gage Locations for Beam 1.
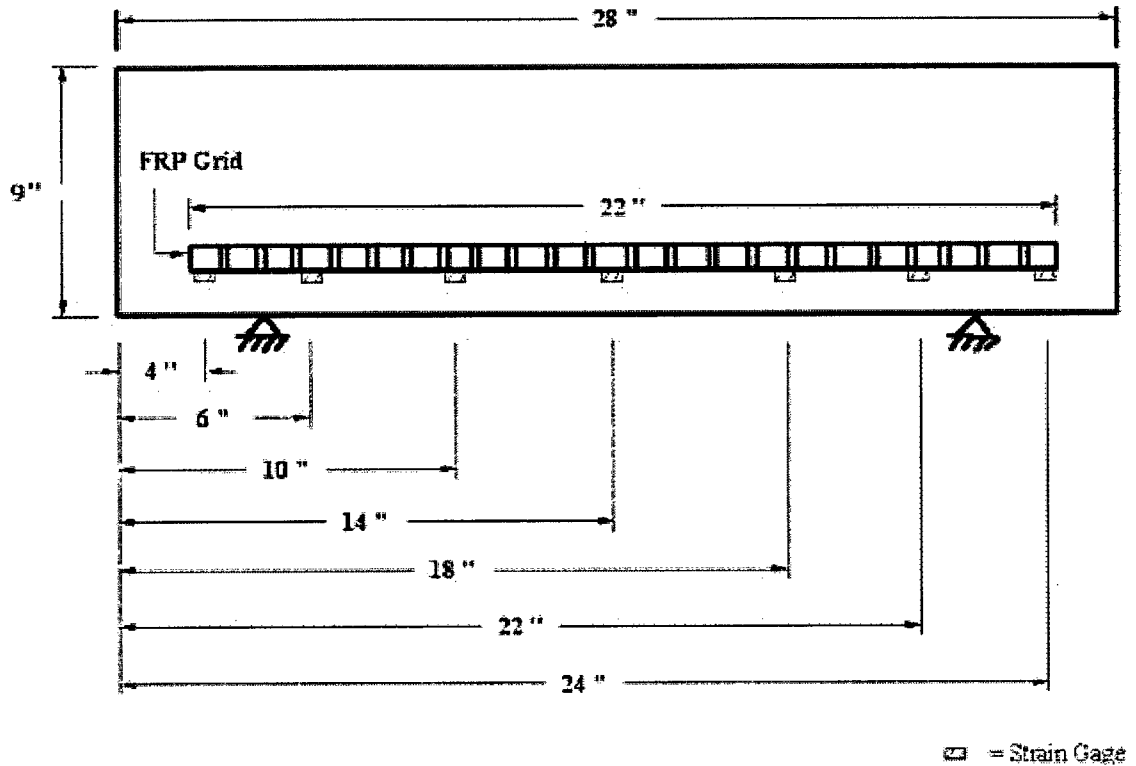
Figure 3.24 Selected Strain Gage Locations for Beam 2.

After fixing the strain gages to the grid, DSV cables were connected to the gages. Then, environmental protection coating was applied to the strain gages to keep them in good shape. Before testing the beams, the other end of the DSV cables were connected to the data acquisition system. The deflectometer was placed at the mid-span of the beam to measure the deflection during the test.

3.3.5 Test Procedure

The test was conducted to evaluate the development length requirements for the FRP grid. The test set-up and procedure is similar to ASTM C 78.

The three-point bending test was conducted using the MTS machine of capacity 55.0 kips. The beams were loaded continuously at a constant rate of 2000 lbs/min. until failure. The data collection system stored the resistance data for different time intervals.

The MTS machine also stored the load data for different time intervals. For each load increment, data for the resistances (FRP strains) and loads were obtained. During the test, the deflections were also measured at the mid-span of each beam at the applied load.

3.3.6 Material Characteristics

3.3.6.1 Concrete Compressive Strength

The concrete cylinders were cast from the same batch that was used for making the beams. The concrete mix was prepared in the Structural and Materials Laboratory at Louisiana Tech University. The concrete mix proportions are listed in Table 3.6.

Table 3.6 Concrete Mix Proportions.

Cement	$710 - lb/yd^3$
Coarse Aggregate	$1674 - lb/yd^3$
Natural Sand	$1334 - lb/yd^3$
Air Content (Mild Exposure)	0.035
Water	$270 - lb/yd^3$

The 4 x 8-inch concrete cylinders were cured in accordance with ASTM C511. The concrete compressive strength was determined in accordance with ASTM C39. The cylindrical specimens were tested for 1, 3, 7, 14, and 28 days. For each day of testing, three specimens were used. The crushing load of each cylinder, average compressive strength of three cylinders and standard deviation for each testing are reported in Table 3.7. When the beam specimens were tested at 28 days, the compressive strength of the concrete was 4743 psi. The concrete strength development over time is shown in Figure 3.25.

Table 3.7 Average Concrete Compressive Strength of the Cylinders.

Age	Crushing Load (lb)	Compressive Strength (psi)	Average Compressive Strength (psi)	Standard Deviation
1-day	17200	1369	1316	49
	16000	1273		
	16400	1305		
3-day	19600	1560	1602	148
	18600	1480		
	22200	1767		
7-day	37600	2992	3591	545
	51000	4058		
	46800	3724		
14-day	54600	4345	4122	199
	49800	3963		
	51000	4058		
28-day	56800	4520	4743	193
	61200	4870		
	60800	4838		
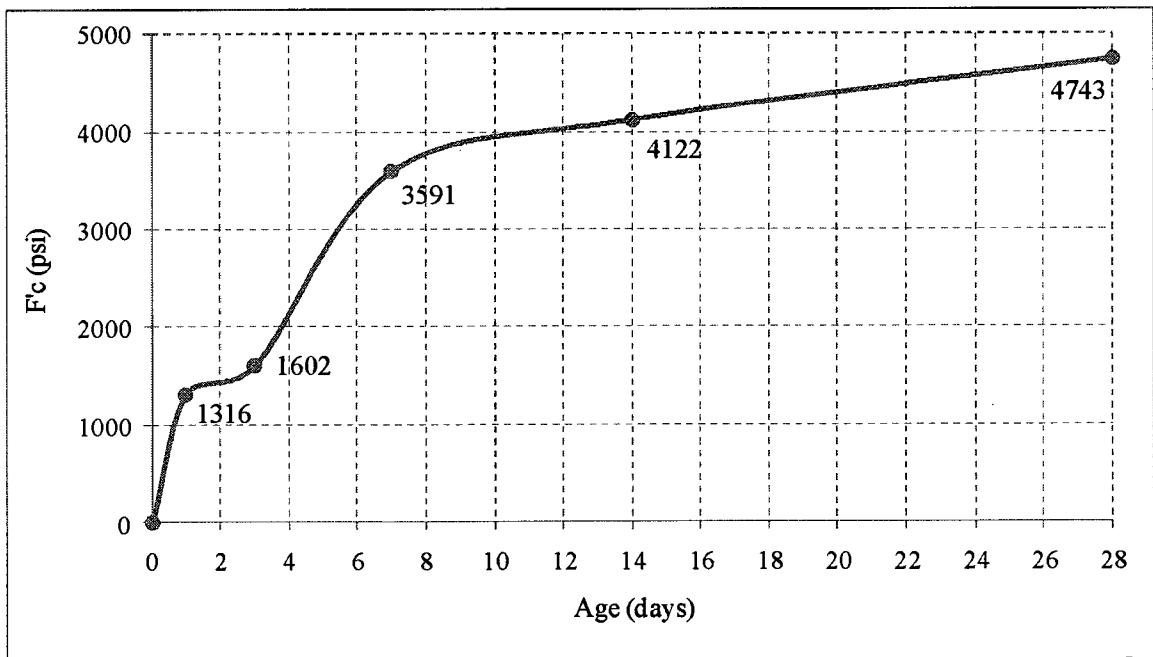
Figure 3.25 Concrete Average Compressive Strength.

3.3.6.2 FRP Material Properties

The material properties of FRP grid were obtained from the manufacturer (Fibergrate, Composite Structures). The properties were already listed in Table 3.5.

The pictures in APPENDIX B (Figure B.7 and B.8) show the experimental work procedure (i.e., pouring and testing of beams) followed by testing for the development length of FRP grid.

CHAPTER IV

DISCUSSION OF RESULTS

4.1 Theoretical Results - Structural Modeling of FRP Grid Reinforced Bridge Decks

4.1.1 Introduction

The results obtained from the finite element analyses described in the previous chapter were discussed in this section. The results from structural modeling and testing of FRP grid reinforced bridge decks were also presented in LTRC Report No. FHWA/LA.09/443 (Li and Saber 2009). The stresses in girders of open joint bridge and link slab bridge were obtained from the results and compared. A parametric study which was carried out to evaluate the effects of each design parameter such as grid geometry, grid mechanical properties, concrete strength and modulus, etc. on the structural behavior of the FRP grid reinforced link slab was presented in this chapter.

4.1.2 Analysis by Finite Element Method

The ANSYS software package was utilized to perform static analyses of the FE models described earlier. The results presented in this chapter were obtained for the case of applied vehicular load, dead loads and live load surcharge. The HS20-44 truck was placed on the first span deck to produce maximum continuity moment in the system and maximum tensile force in the link slab. This location was determined based on influence line analyses.

The four girders in the first span of the bridge were designated as S1G1, S1G2, S1G3, and S1G4. Similarly, girders in the second span of the bridge were designated as S2G1, S2G2, S2G3, S2G4, and girders in the third span of the bridge were designated as S3G1, S3G2, S3G3, and S3G4. The model with the girders is shown in Figure 4.1.
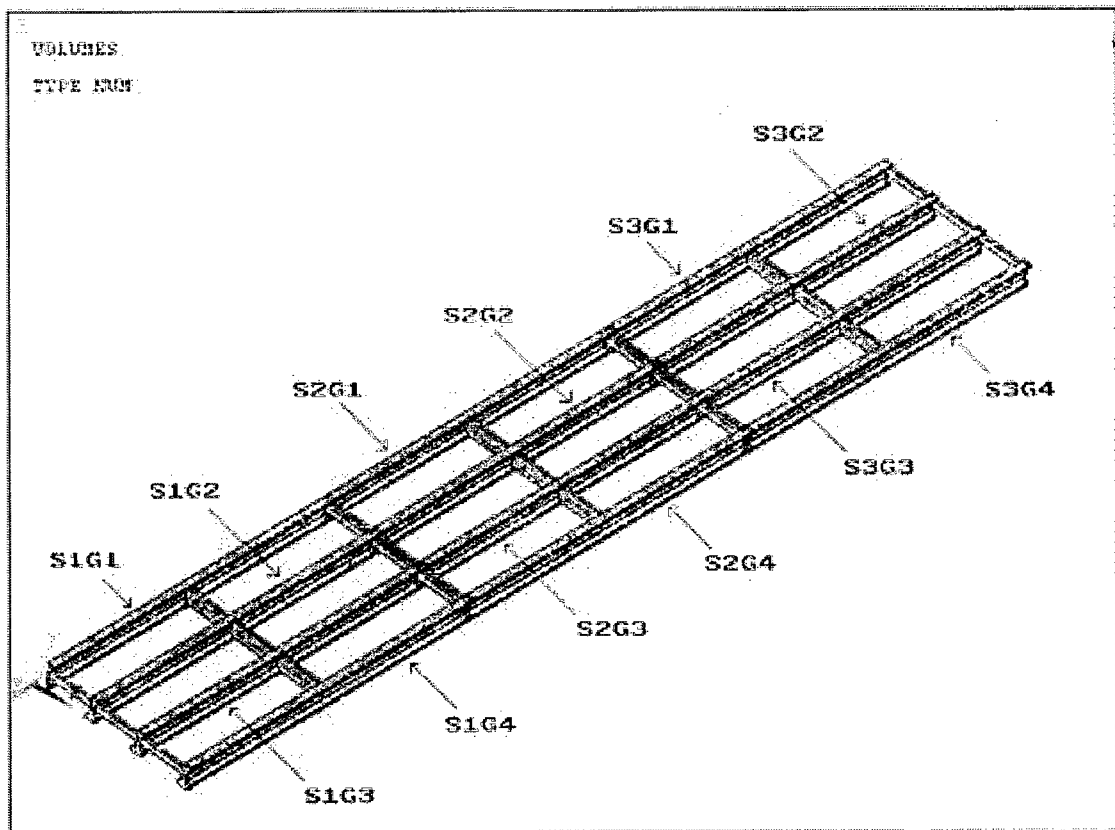
Figure 4.1 Model with the Girders.

4.1.3 Comparison between Open Joint Bridge and Link Slab Bridge

The two finite element models described earlier were compared. Comparison was done between the two models for the same bridge and loading configurations. This study was done for bridges with a 60 feet span length, 30 feet wide, 60 feet girder length and 8ft. 8 inch center-to-center spacing between two adjacent girders, with intermediate and

end diaphragms. The three span bridge model used in the analysis with one inch open joints is shown in Figure 4.2.
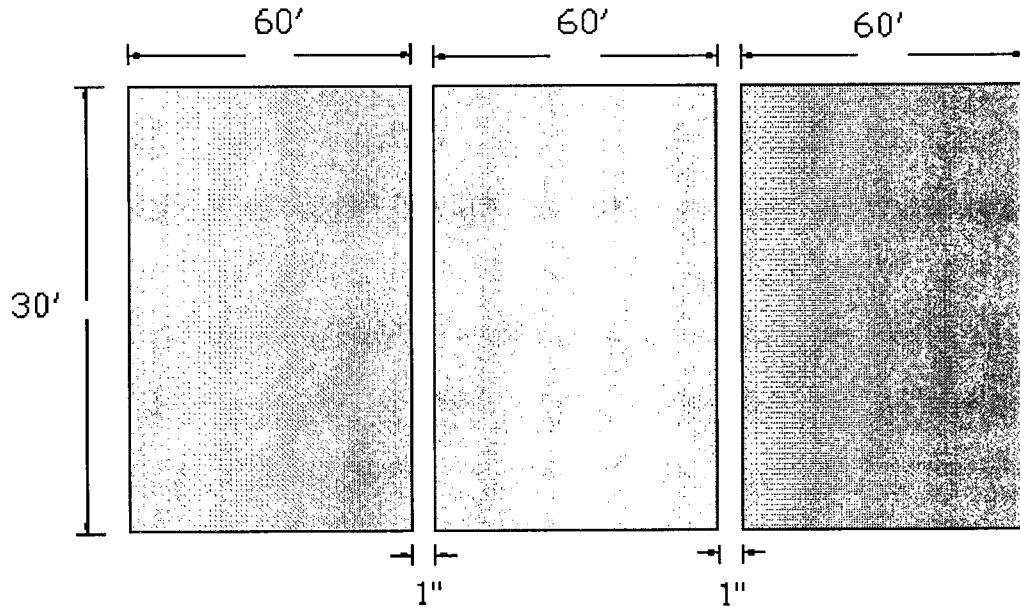
Figure 4.2 The Three-Span Bridge Model Used in the Analysis.

4.1.4 Girder Stresses

Span 1: The flexural/tensile stresses (Sz) for the bottom elements along the length of the first girder in the first span for the two bridge models are shown in Figure 4.3. The flexural stresses were higher in the open joint bridge than the link slab bridge at most of the locations. A maximum flexural stress difference of 124 psi was observed between two girders, at a distance of 596 inches (49 ft- 8 in.) from the left support. The flexural stresses were almost the same for a length of 192 inches (16 ft.) from the left support for both cases, but after that, stresses in the open joint bridge were much higher. It can be inferred from the figure that the continuity in decks reduce the flexural stresses in the girders.

Figure 4.3   Comparison between Flexural Stresses (Sz) for Bottom Elements of First Girder in First Span (S1G1).

The flexural stresses (tensile) for the bottom elements along the length of the second girder in the first span for the two bridge models are shown in Figure 4.4. The flexural stresses were higher in the open joint bridge than the link slab bridge at most of the locations. A maximum flexural stress difference of 150 psi was observed between two girders, at a distance of 596 inches (49 ft-8 in.) from the left support. The flexural stresses were almost the same for a length of 240 inches (20 ft.) from the left support for both cases, but after that, stresses in the open joint bridge were much higher.

57

Figure 4.4 Comparison between Flexural Stresses (Sz) for Bottom Elements of Second Girder in First Span (S1G2).

The flexural stresses (tensile) for the bottom elements along the length of the third girder in the first span for the two bridge models are shown in Figure 4.5. The flexural stresses were higher in the open joint bridge than the link slab bridge at most of the locations. A maximum flexural stress difference of 147 psi was observed between two girders, at a distance of 596 inches (49 ft-8 in.) from the left support. The flexural stresses were almost the same for a length of 216 inches (18 ft.) from the left support for both cases, but after that, stresses in the open joint bridge were much higher.

Figure 4.5 Comparison between Flexural Stresses (Sz) for Bottom Elements of Third Girder in First Span (S1G3).

The flexural stresses (tensile) for the bottom elements along the length of the fourth girder in the first span for the two bridge models are shown in Figure 4.6. The flexural stresses were higher in the open joint bridge than the link slab bridge at most of the locations. A maximum flexural stress difference of 105 psi was observed between two girders, at a distance of 572 inches (47 ft-8 in.) from the left support. The flexural stresses were almost the same for a length of 204 inches (17 ft.) from the left support for both cases, but after that, stresses in the open joint bridge were much higher.

Figure 4.6 Comparison between Flexural Stresses (Sz) for Bottom Elements of Fourth Girder in First Span (S1G4).

Span 2: The flexural stresses (tensile) for the bottom elements along the length of first girder in second span for two bridge models are shown in Figure 4.7. The flexural stresses were higher in the open joint bridge than the link slab bridge at all locations. A maximum flexural stress difference of 41 psi was observed between two girders, at a distance of 502 inches (41 ft-10 in.) from the left support.
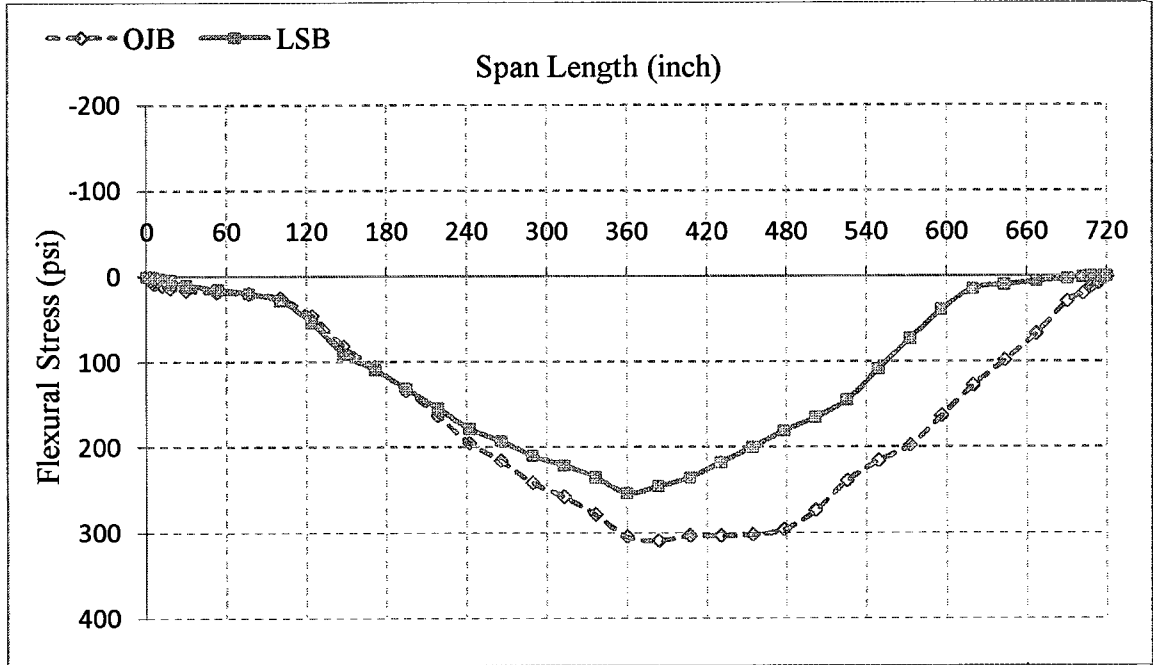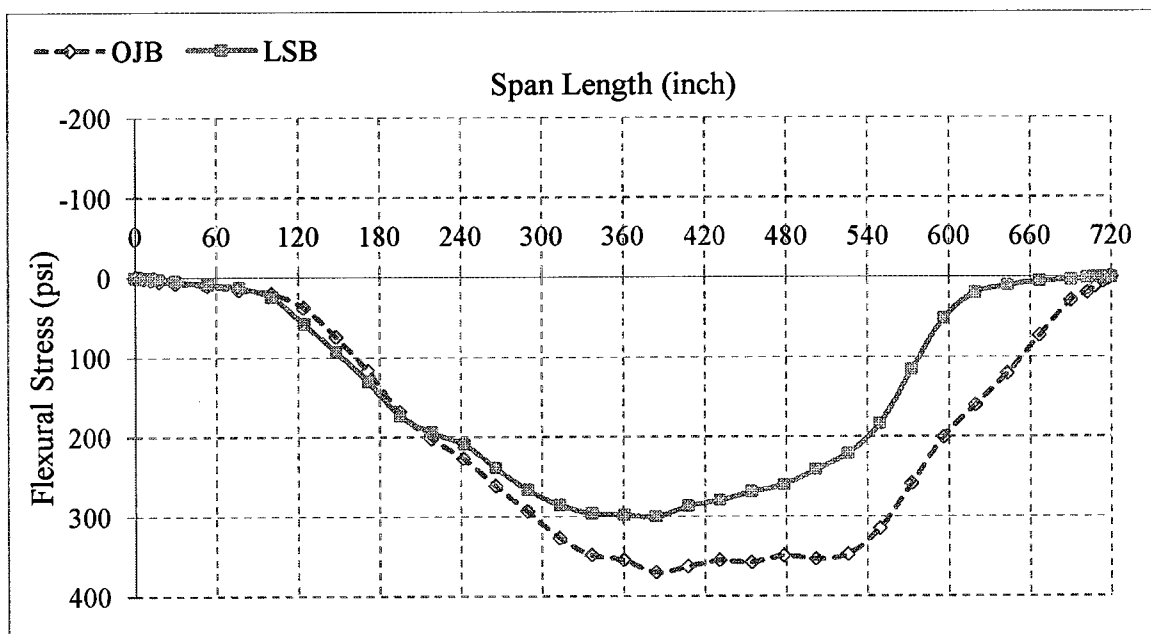
Figure 4.7 Comparison between Flexural Stresses (Sz) for Bottom Elements of First Girder in Second Span (S2G1).

The flexural stresses (tensile) for the bottom elements along the length of the second girder in the second span for the two bridge models are shown in Figure 4.8. The flexural stresses were higher in the open joint bridge than the link slab bridge at all locations. A maximum flexural stress difference of 40 psi was observed between two girders, at a distance of 525 inches (43ft-9 in.) from the left support.

The flexural stresses (tensile) for the bottom elements along the length of the third girder in the second span for the two bridge models are shown in Figure 4.9. The flexural stresses were higher in the open joint bridge than the link slab bridge at all locations. A maximum flexural stress difference of 40 psi was observed between two girders, at a distance of 478 inches (39 ft-10 in.) from the left support.

Figure 4.8 Comparison between Flexural Stresses (Sz) for Bottom Elements of Second Girder in Second Span (S2G2).
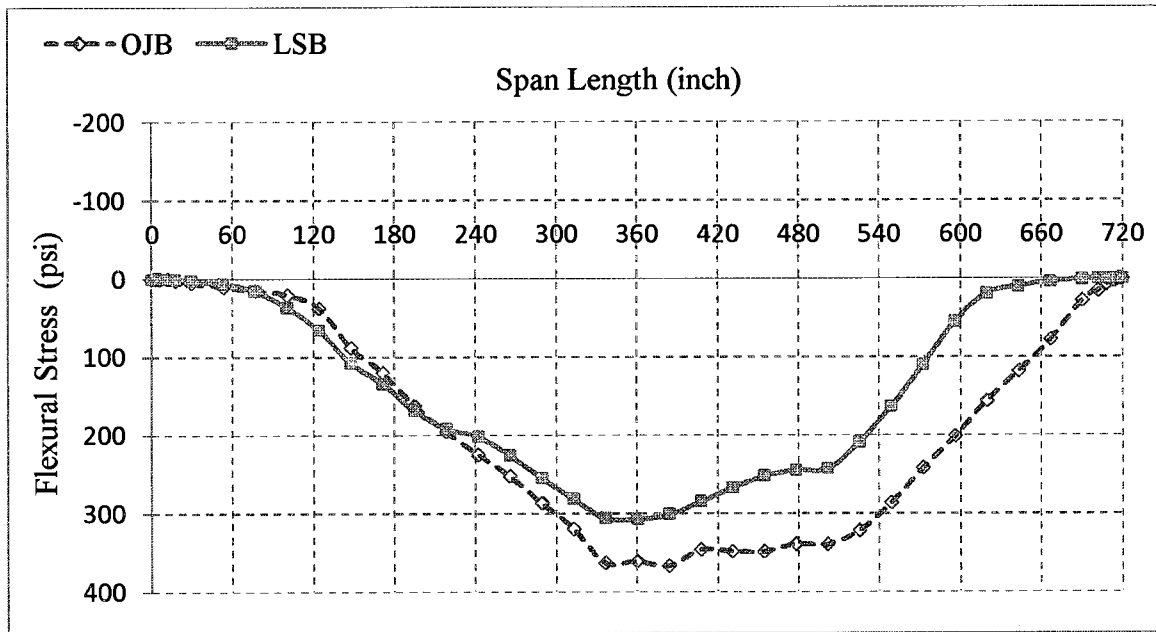

Figure 4.9 Comparison between Flexural Stresses (Sz) for Bottom Elements of Third Girder in Second Span (S2G3).

The flexural stresses (tensile) for the bottom elements along the length of the fourth girder in the second span for the two bridge models are shown in Figure 4.10. The

flexural stresses were higher in the open joint bridge than the link slab bridge at all locations. A maximum flexural stress difference of 38 psi was observed between two girders, at a distance of 336 inches (28 ft.) from the left support.
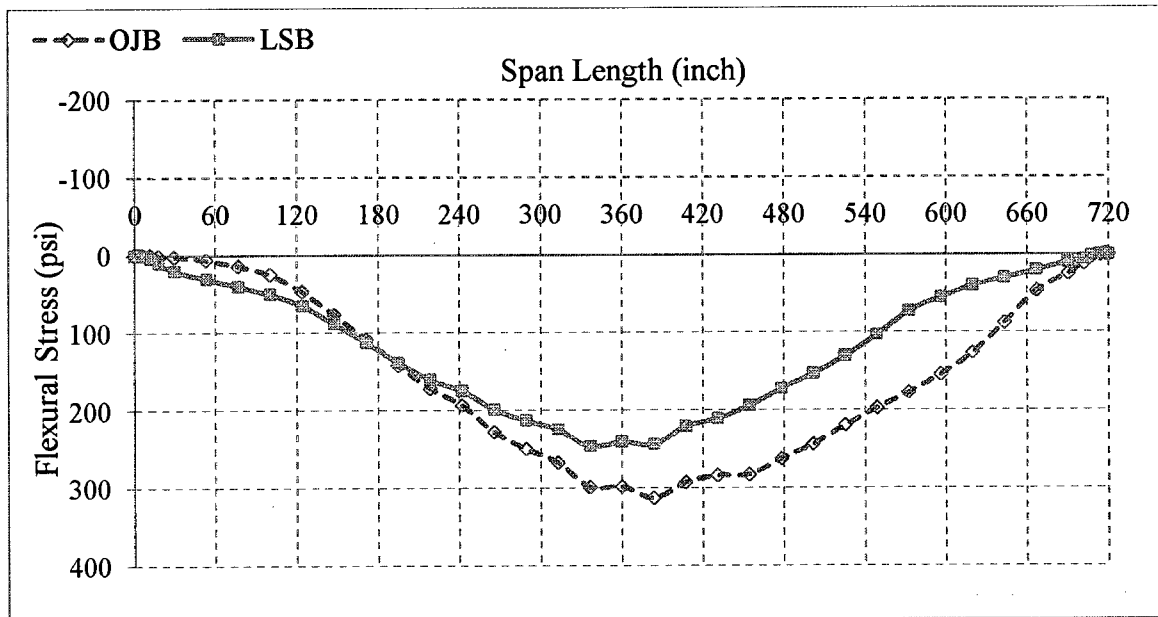

Figure 4.10 Comparison between Flexural Stresses (Sz) for Bottom Elements of Fourth Girder in Second Span (S2G4).

Span 3: The flexural stresses (tensile) for the bottom elements along the length of first girder in the third span for two bridge models are shown in Figure 4.11. A maximum flexural stress difference of 32 psi was observed between two girders, at a distance of 124 inches (10 ft- 4 in.) from the left support. The flexural stresses were higher in the open joint bridge up to 456 inches (38 ft.) from the left support and after that the flexural stresses were higher in the link slab bridge.
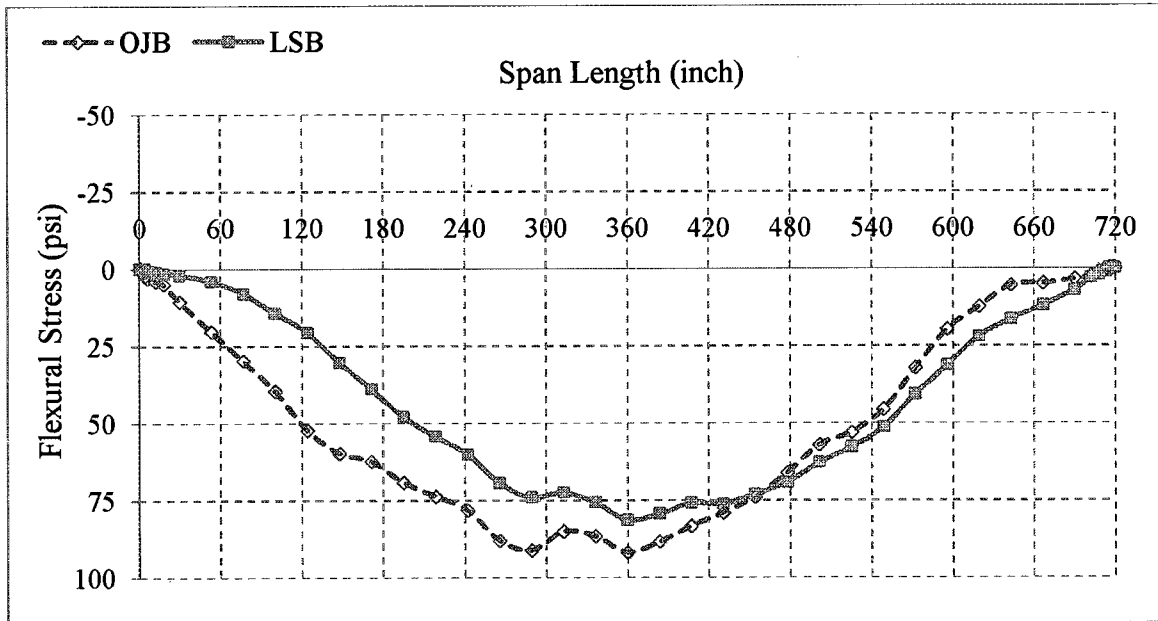
Figure 4.11 Comparison between Flexural Stresses (Sz) for Bottom Elements of First Girder in Third Span (S3G1).

The flexural stresses (tensile) for the bottom elements along the length of the second girder in the third span for two bridge models are shown in Figure 4.12. A maximum flexural stress difference of 31 psi was observed between two girders, at a 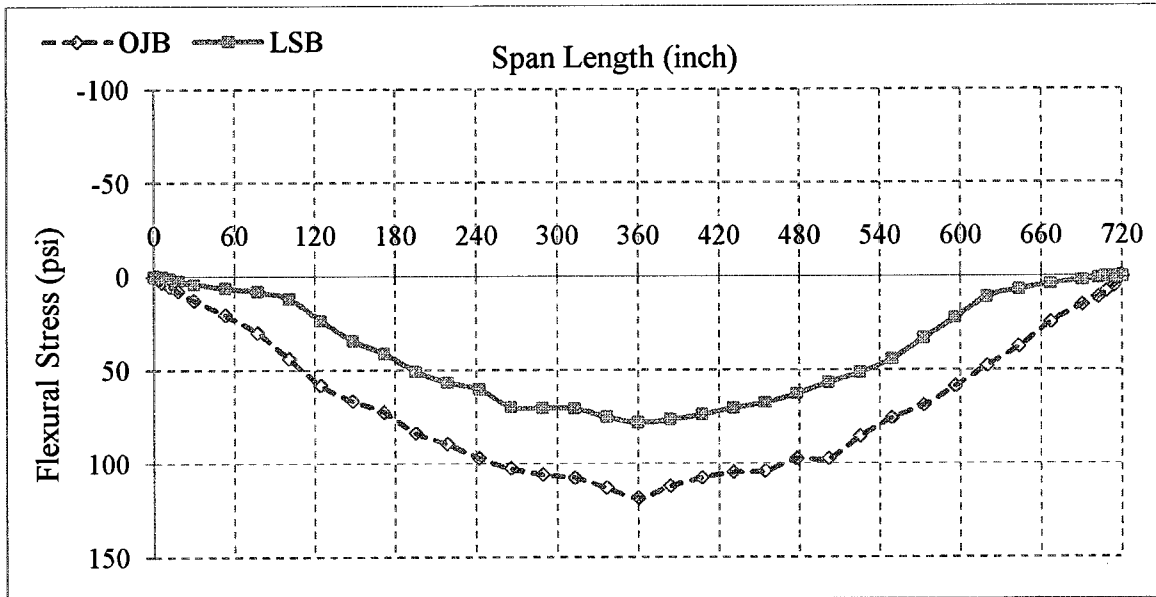distance of 148 inches (12 ft- 4 in.) from the left support. The flexural stresses were higher in the open joint bridge up to 480 inches (40 ft.) from the left support and after that the flexural stresses were high in the link slab bridge.

The flexural stresses (tensile) for the bottom elements along the length of the third girder in the third span for two bridge models are shown in Figure 4.13. A maximum flexural stress difference of 30 psi was observed between two girders, at a distance of 171 inches (14 ft- 3 in.) from the left support. The flexural stresses were higher in the open joint bridge up to 456 inches (38 ft.) from the left support and after that the flexural stresses were higher in the link slab bridge.
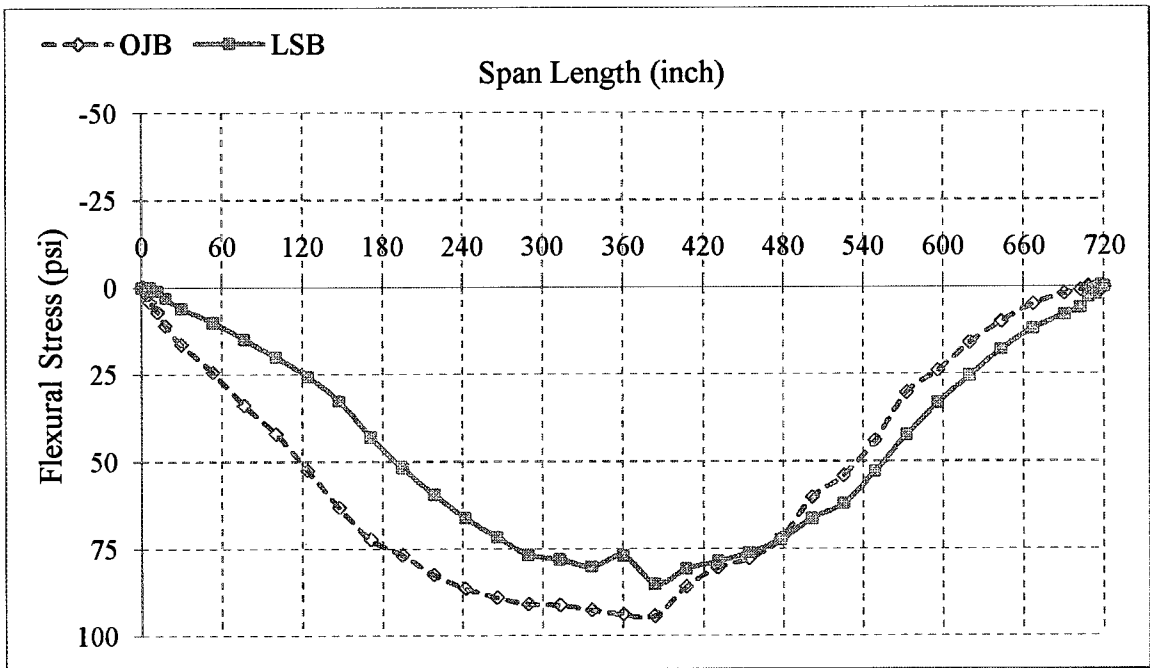
Figure 4.12 Comparison between Flexural Stresses (Sz) for Bottom Elements of Second Girder in Third Span (S3G2).
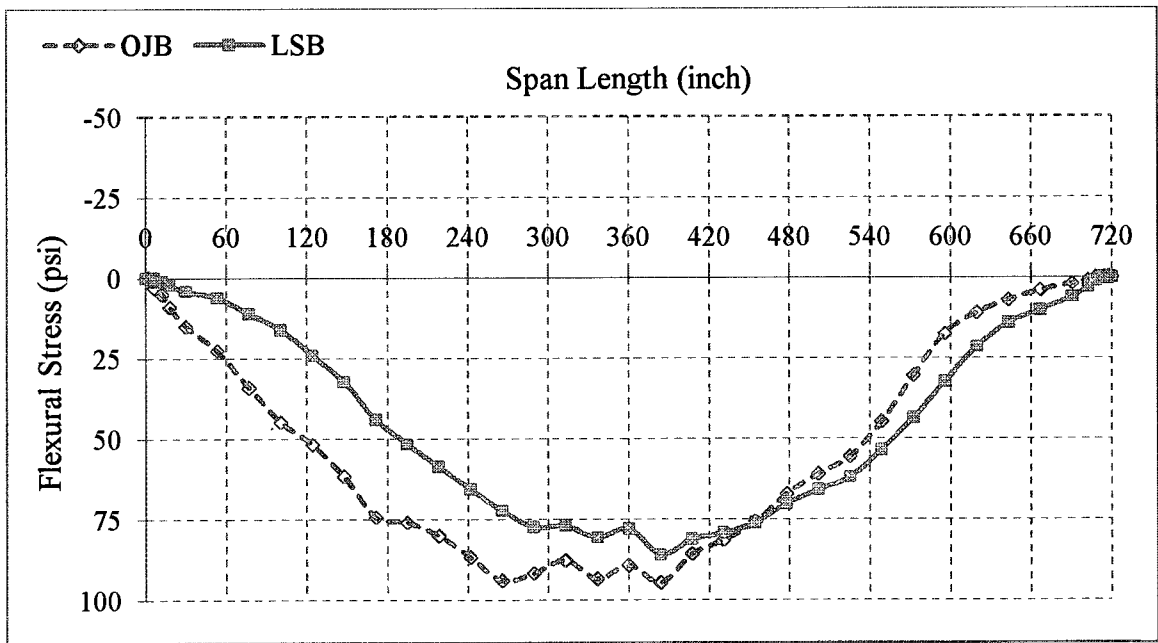
Figure 4.13 Comparison between Flexural Stresses (Sz) for Bottom Elements of Third Girder in Third Span (S3G3).

The flexural stresses (tensile) for the bottom elements along the length of the fourth girder in the third span for two bridge models are shown in Figure 4.14. A maximum flexural stress difference of 29 psi was observed between two girders, at a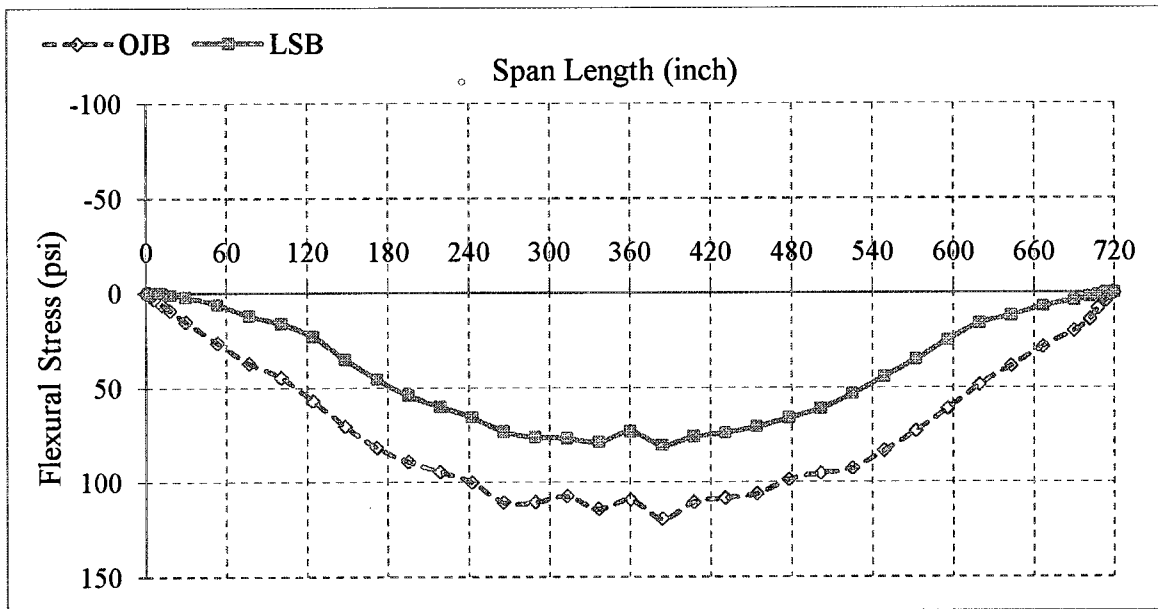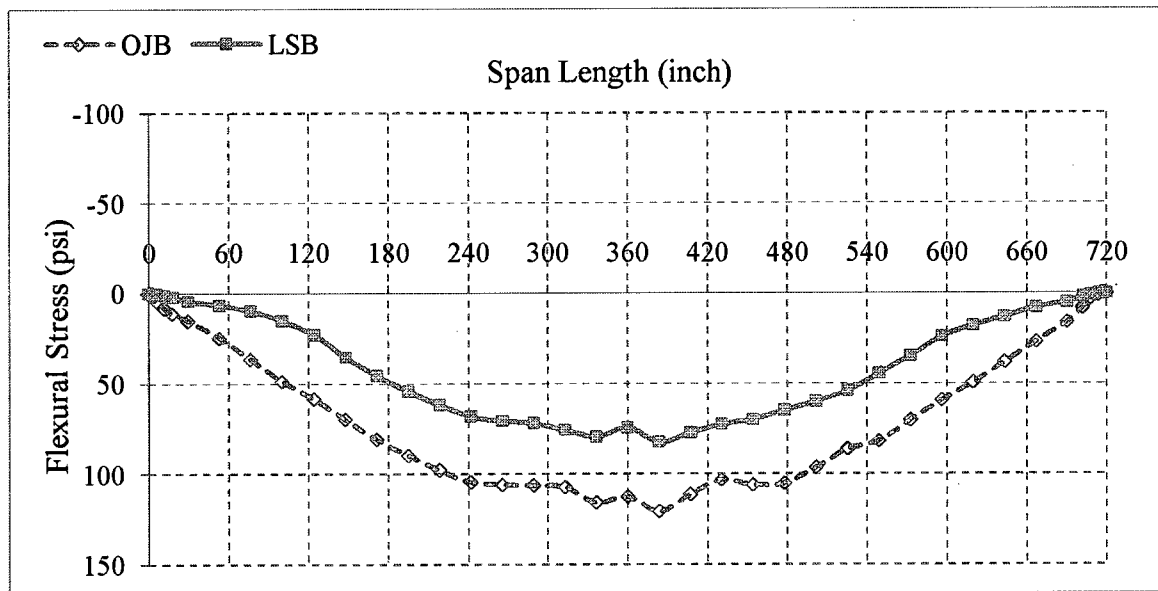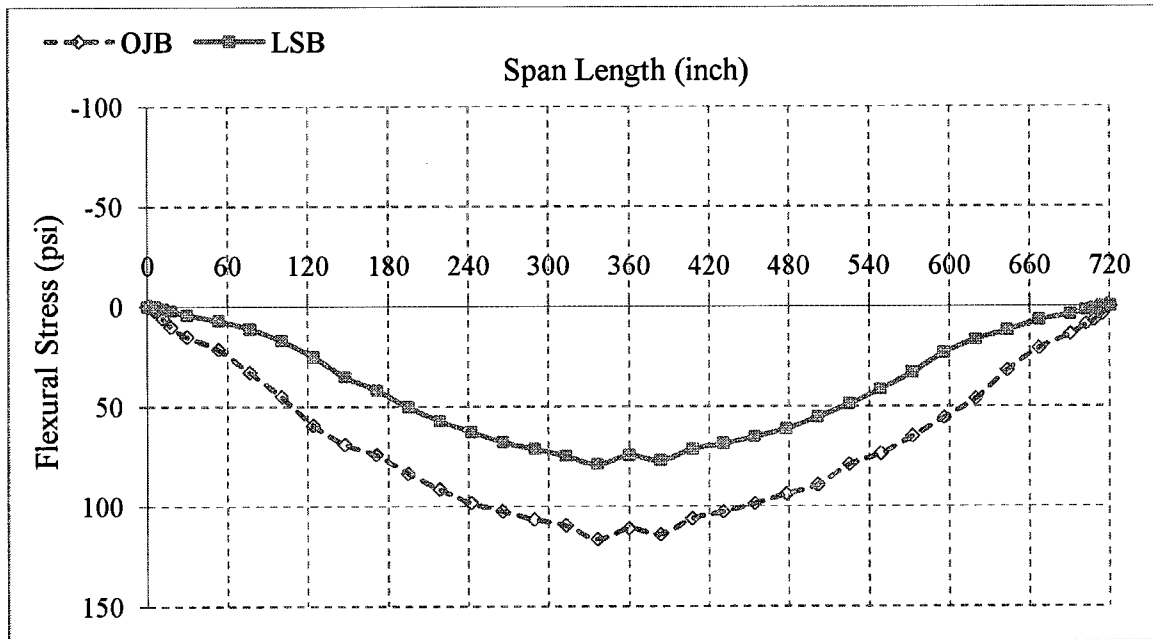 distance of 124 inches (10ft- 4 in.) from the left support. The flexural stresses were higher in the open joint bridge up to 456 inches (38 ft.) from the left support and after that the flexural stresses were higher in the link slab bridge.
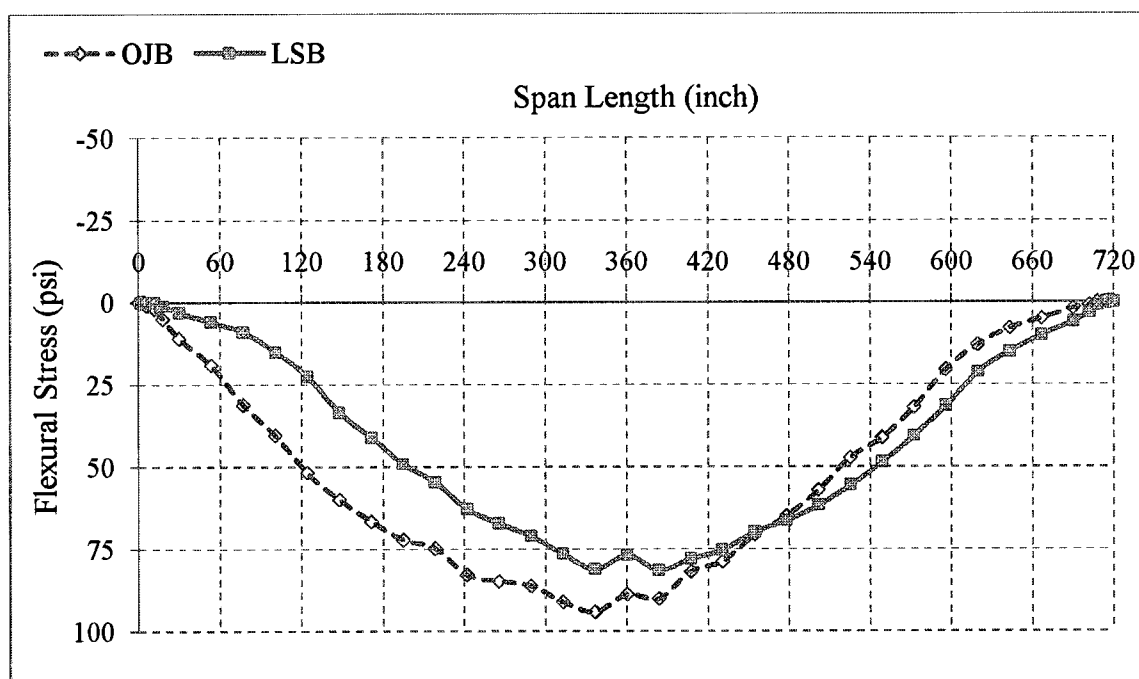
Figure 4.14 Comparison between Flexural Stresses (Sz) for Bottom Elements of Fourth Girder in Third Span (S3G4).

4.1.5 Maximum Flexural Stresses in Girders

The maximum flexural stresses in the twelve girders of the open joint bridge, the link slab bridge, and the percentage change in stresses of the open joint bridge compared with the link slab bridge are listed in Table 4.1. The stresses were higher in girders of the open joint bridge. The maximum decrease was 34% found in the girders of Span 2 of the

bridge, and the minimum decrease was 9% found in Span 3. The maximum effects in Span 1 where truck load was applied were min. 16% and max. 22%.

Table 4.1 Comparison between Maximum Flexural Stresses (Sz) for Bottom Elements for Bridge Girders.

Girder no.	Maximum Flexural Stress (psi)		% Decrease in Girder stresses due to Link Slab
	Open Joint Bridge (OJB)	Link Slab Bridge (LSB)	
S1G1	308.9	253.7	18 %
S1G2	370.5	300.6	19 %
S1G3	366.8	307.0	16 %
S1G4	312.8	245.6	22 %
S2G1	118.3	78.2	34 %
S2G2	119.3	80.4	33 %
S2G3	120.6	82.2	32 %
S2G4	116.5	78.7	32 %
S3G1	91.9	81.3	12 %
S3G2	94.3	85.2	10 %
S3G3	94.5	85.8	9 %
S3G4	94.0	81.2	14 %

4.1.6 Stresses in Bridge Decks

The maximum and minimum transverse, longitudinal and shear stresses in bridge decks of the open joint bridge and the link slab bridge are presented in Table 4.2. In bridge decks, the maximum and minimum transverse, longitudinal and shear stresses were found in the first deck of the open joint bridge or the link slab bridge, since the load was applied on the first span of the bridge. The maximum transverse stress was 48.7 psi

in the open joint bridge and the minimum transverse stress was -82.7 psi in the link slab bridge. The maximum longitudinal stress was 158.5 in the link slab bridge and the minimum longitudinal stress was -142.7 psi in the open joint bridge. The maximum shear was 224.7 psi in the open joint deck and the minimum shear stress was -15.9 psi in both the open joint bridge and the link slab bridge.

Table 4.2 Maximum and Minimum Transverse, Longitudinal and Shear Stresses in Deck Slabs of Open Joint Bridge and Link Slab Bridge.

Span 1:

Result	Open Joint Deck		Link Slab Deck		% Decrease in Deck Stresses due to Link Slab
Transverse Stress (Sx)	Max.	48.7	Max.	42.4	13%
Longitudinal Stress (Sz)	Min.	-142.7	Min.	-91.1	36%
Shear Stress (Syz)	Max.	224.7	Max.	127.2	43%
	Min.	-15.9	Min.	-15.9	0%

Span 2:

Result	Open Joint Deck		Link Slab Deck		% Decrease in Deck Stresses due to Link Slab
Transverse Stress (Sx)	Max.	-1.8	Max.	-0.6	67%
Longitudinal Stress (Sz)	Min.	-49.8	Min.	-9.5	81%
Shear Stress (Syz)	Max.	3.7	Max.	3.5	5%

Span 3:

Result	Open Joint Deck		Link Slab Deck		% Decrease in Deck Stresses due to Link Slab
Transverse Stress (Sx)	Min.	-4.9	Min.	-4.2	14%
Longitudinal Stress (Sz)	Min.	-39.1	Min.	-10.0	74%
Shear Stress (Syz)	Max.	3.7	Max.	3.1	16%
	Min.	-14.5	Min.	-0.8	94%

4.1.7 Stresses in Link Slabs

The maximum and minimum transverse, longitudinal and shear stresses in two link slabs are sreported in Table 4.3. Slabs 1 and 2 were joined by link Slab 1, and Slabs 2 and 3 were joined by link Slab 2. The stresses were higher in link slab 1 than the link slab 2 because the truck was placed on Span 1 of the bridge. Maximum and minimum stresses were either at the top surface or the bottom surface of the link slab.

Table 4.3 Maximum and Minimum Stresses in Link Slabs at the Top and the Bottom of Bridge Deck.

Result	Link Slab 1		Link Slab 2	
	Stress (psi)		Stress (psi)	
Transverse stress (Sx)	Max.	76.5	Max.	33.4
	Min.	-12.6	Min.	-5.4
Longitudinal stress (Sz)	Max.	332.8	Max.	151.9
	Min.	-146.7	Min.	-28.4
Shear Stress(Syz)	Max.	7.8	Max.	10.6
	Min.	-4.0	Min.	-1.5

**4.1.7.1 Longitudinal Stresses along the
Depth of the Link Slabs**

The longitudinal stresses along the depth or thickness of the link slabs are shown

in Figure 4.15. The stresses at the bottom element and at the top element of the link Slab1

were -146.7 psi and 332.8 psi respectively. The stresses at the bottom element and at the

top element of the s link slab2 were -28.4 psi and 151.9 psi respectively. The longitudinal

stresses varied from compression to tension from the bottom to the top elements of both

link slabs.
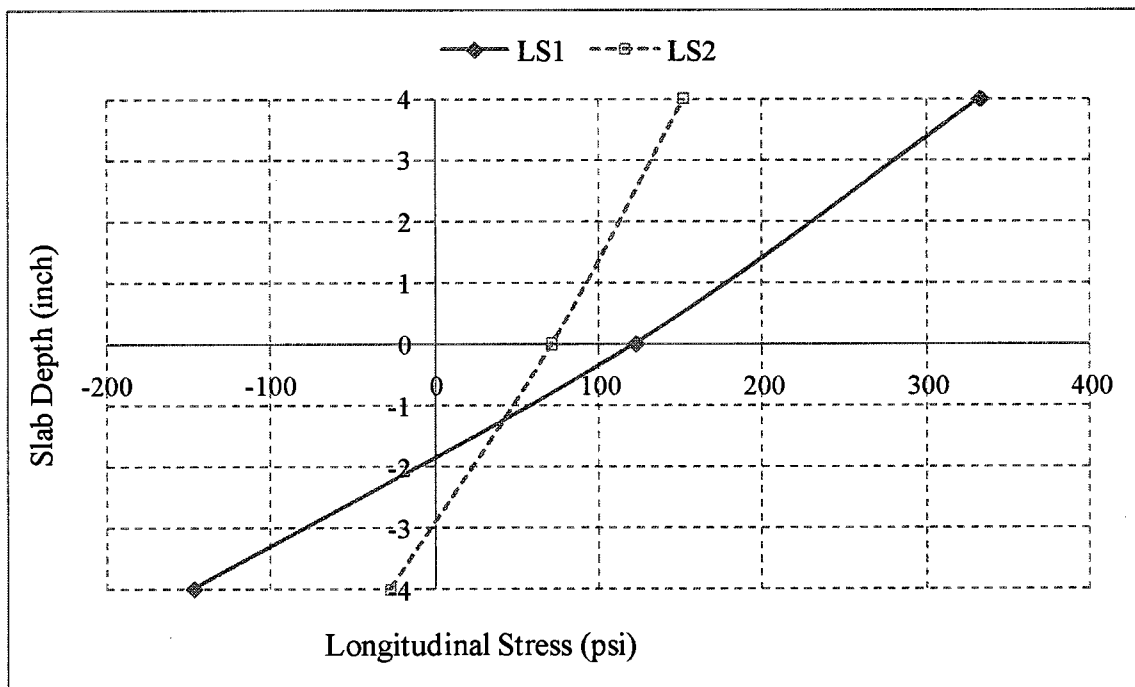
Figure 4.15 Variation of Longitudinal Stress along the Depth of the Link Slabs.

**4.1.7.2 Longitudinal Stress along the Length
of the Link Slabs for Top Elements**

The longitudinal stresses along the length of the link slabs are shown in Figure

4.16. The maximum longitudinal stresses were 176.1 psi and 89.6 psi for link Slab1 and

2, respectively. The X and Y co-ordinates for these top elements were 347 inches and 53 inches (at one end of the link slab), respectively. Along the length of the link slab, all top elements for both link slabs were in tension. The maximum and minimum longitudinal stresses were higher in the link Slab 1 than in the link Slab 2 because the truck load was placed in the first span of the bridge and the link slab 1 was connecting Span 1 and Span 2 decks of the bridge.

4.1.7.3 Longitudinal Stress along the Length of the Link Slabs for Bottom Elements

The longitudinal stresses along the length of the link slabs are shown in Figure 4.17. The minimum longitudinal stresses were -42.1 psi and 2.6 psi for link slab 1 and 2, respectively. The X and Y co-ordinates for these bottom elements were 347 inches and 45 inches (at one end of the link slab), respectively. Along the length of the link slab, the bottom elements of link slab 2 were in tension.
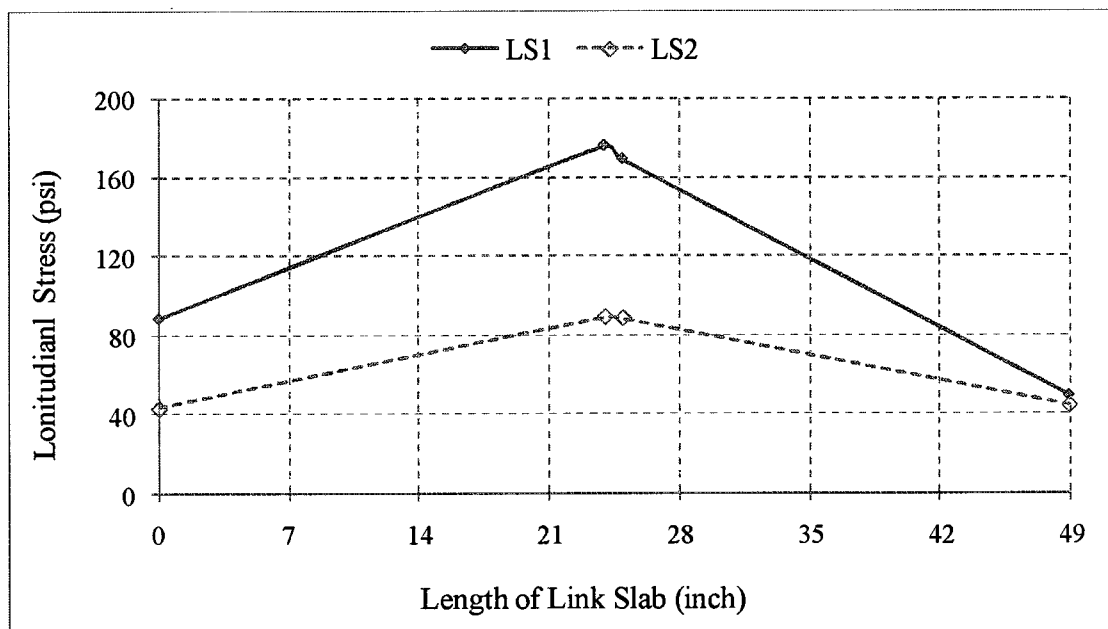
Figure 4.16 Variation of Longitudinal Stress along the Length of the Link Slabs for Top Elements.
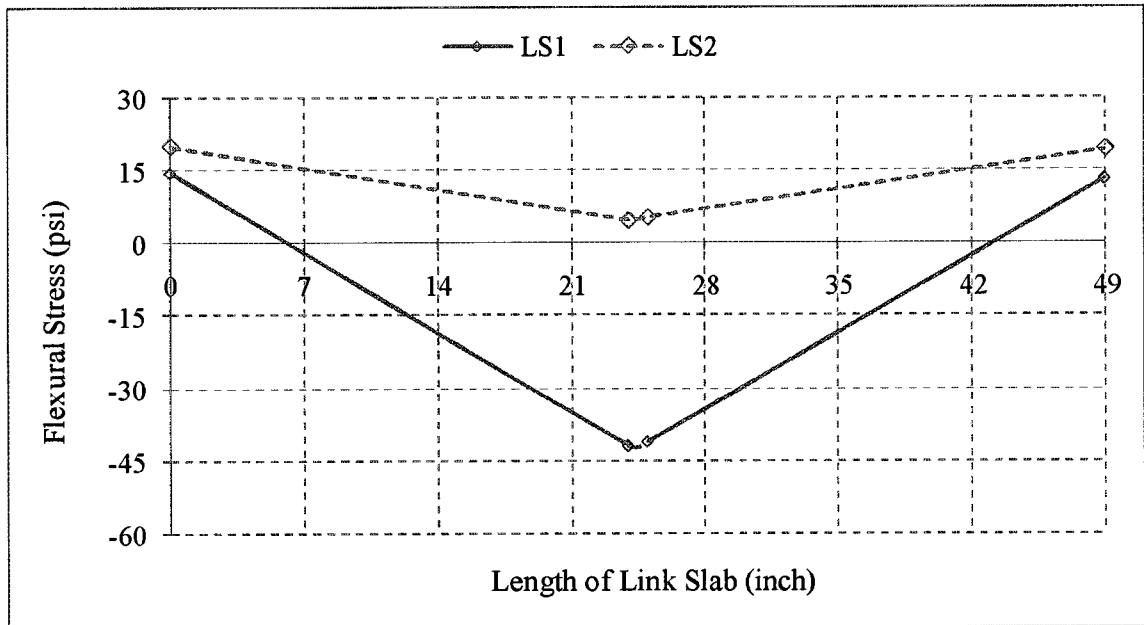
Figure 4.17 Variation of Longitudinal Stress along the Length of the Link Slabs for Bottom Elements.

4.1.7.4 Longitudinal Stresses in FRP Layers of the Link Slabs

The longitudinal stresses in FRP layers of link Slab 1 and link Slab 2 are shown in Figures 4.18 and 4.19, respectively. The top, middle and bottom FRP layers in both link slabs were designated as Layer 1, Layer 2 and Layer 3, respectively. The maximum stresses in all the layers (except Layer 2 in link Slab 1) of both link slabs were found at the locations where a 1-inch open joint was closed. The maximum stresses in Layer 1, Layer 2, Layer 3 of link Slab 1 were 118.1 psi, 57.3 psi, and 38.3 psi, respectively. Also, the maximum stresses in Layer 1, Layer 2, Layer 3 of link Slab 2 were 83.6 psi, 52.9 psi, and 45.8 psi, respectively.
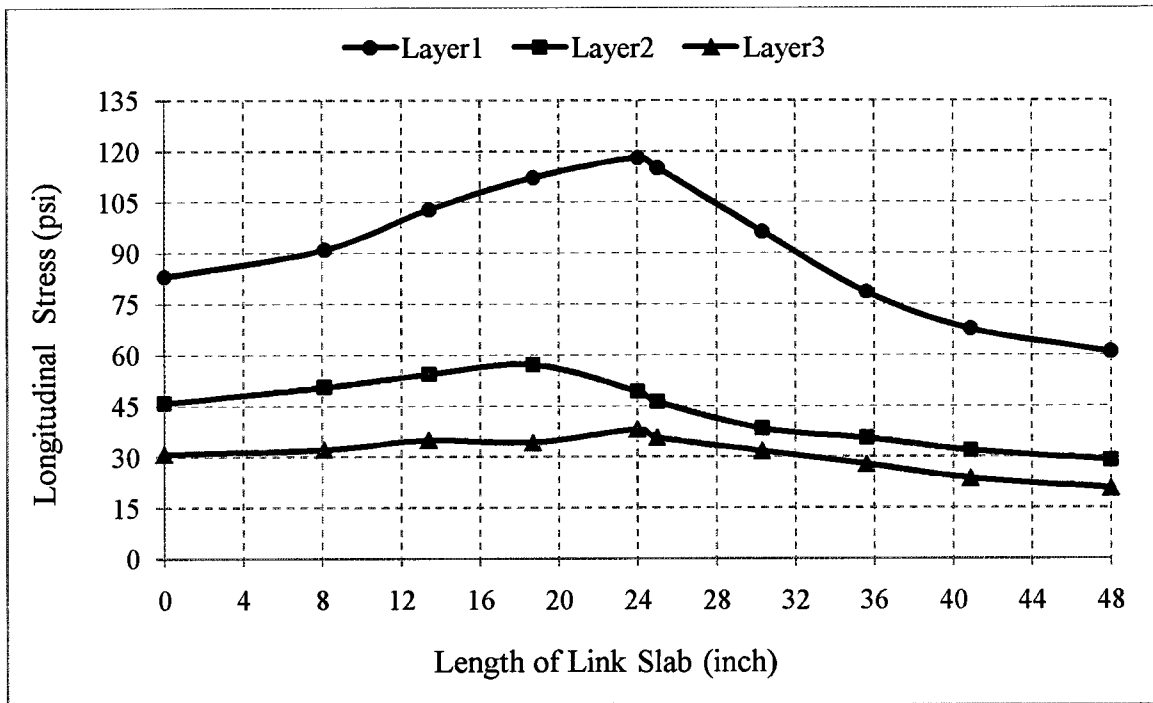
Figure 4.18 Longitudinal Stress (Sz) in FRP Layers for Link Slab 1.
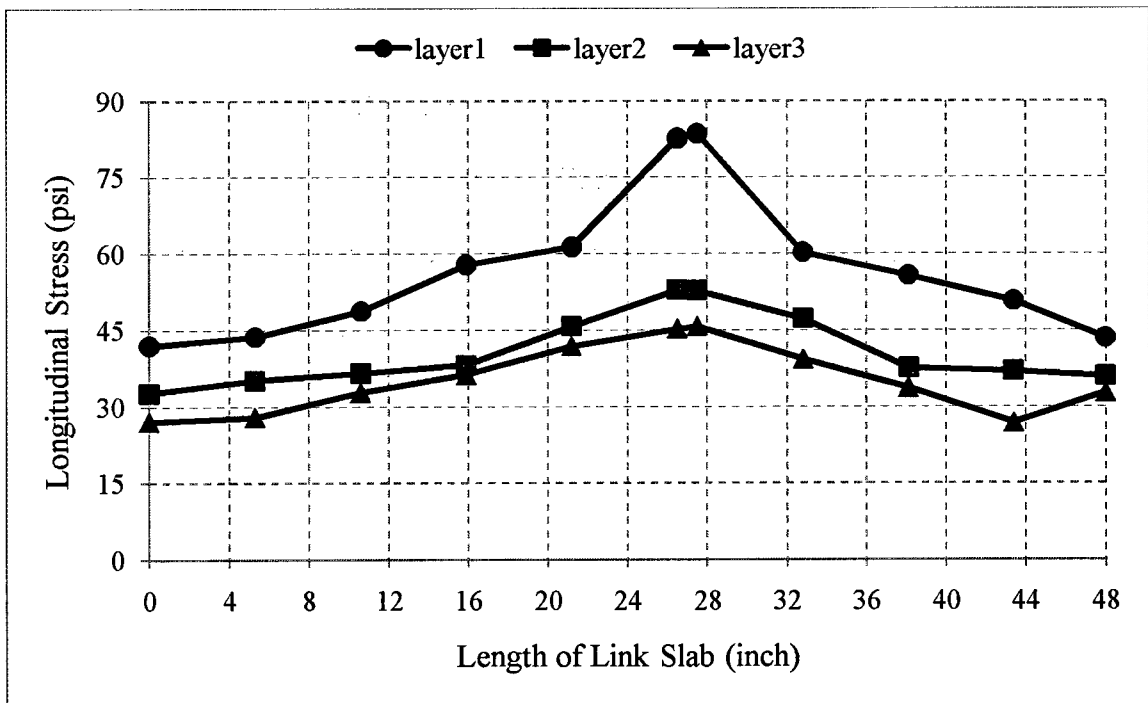
Figure 4.19 Longitudinal Stress (Sz) in FRP Layers for Link Slab 2.

4.2 Experimental Results - Structural Testing of FRP Grid Reinforced Decks

4.2.1 General Form and Behavior of Specimen

The specimens were designed to be under reinforced so that yielding of the steel precedes the crushing of the concrete in compression. Large strains in the reinforcing steel and FRP grids were expected at failure, and deflection of the beam at the collapse point was substantial (L/240) accompanied by excessive cracking, as shown in Figures 4.20 and 4.21 for Beam 1 and Beam 2, respectively.

Figure 4.20 Beam 1 at Collapse.
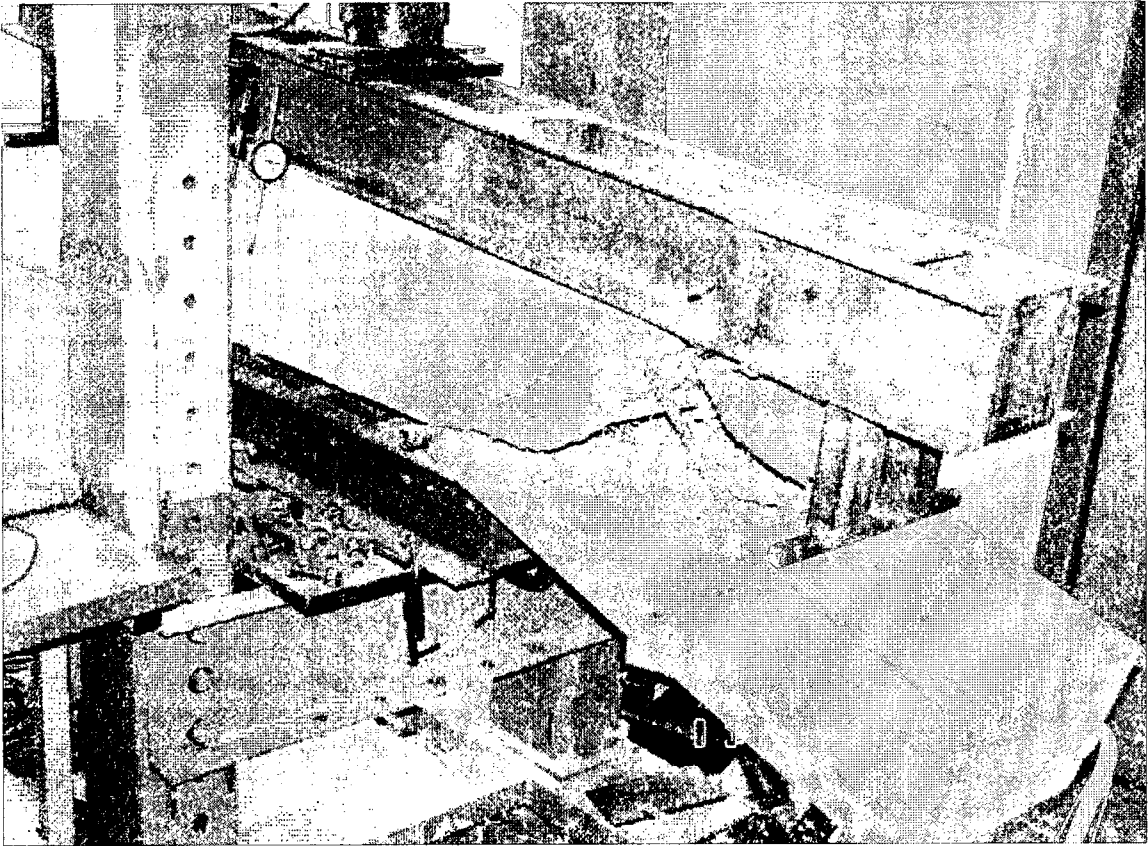
Figure 4.21 Beam 2 at Collapse.

The load deflection response of the specimens exhibited three regions of behavior, as shown in Figures 4.22 and 4.23. At low applied loads, the stiffness of the reinforced concrete beam was relatively high, indicating that the concrete behaved in a linear elastic manner. As the load increased, the bending stress in the extreme fibers increased until the tensile strength at the top of the section of the concrete was reached. This caused flexural cracks to form, first in the constant moment region, then through the beam cantilever section. As the flexural cracks developed in the span, the member stiffness was reduced and thus sudden change in the slope of the curve is shown in Figures 4.22 and 4.23. The response after the cracking load was approximately linear due to the post cracking stiffness. The maximum deflection for each beam was about L/240.

After the concrete in the tension zone cracked, the reinforcing steel and FRP grid carried the tensile forces due to applied loads. As the applied load increased, the tensile stress in the steel increased and reached its yield magnitude. At this point the beam's stiffness decreased due to the loss of material stiffness and the ability of the section to support the tensile stress was reduced. This was shown by the second change in the slope of the load-deflection response at the yield load. The yield plateau in the slope-deflection curve for Beam 2 was longer than that of Beam 1, which indicated that Beam 2 was more ductile than Beam 1, although the area of the FRP grids in Beam 2 were greater than Beam 1.
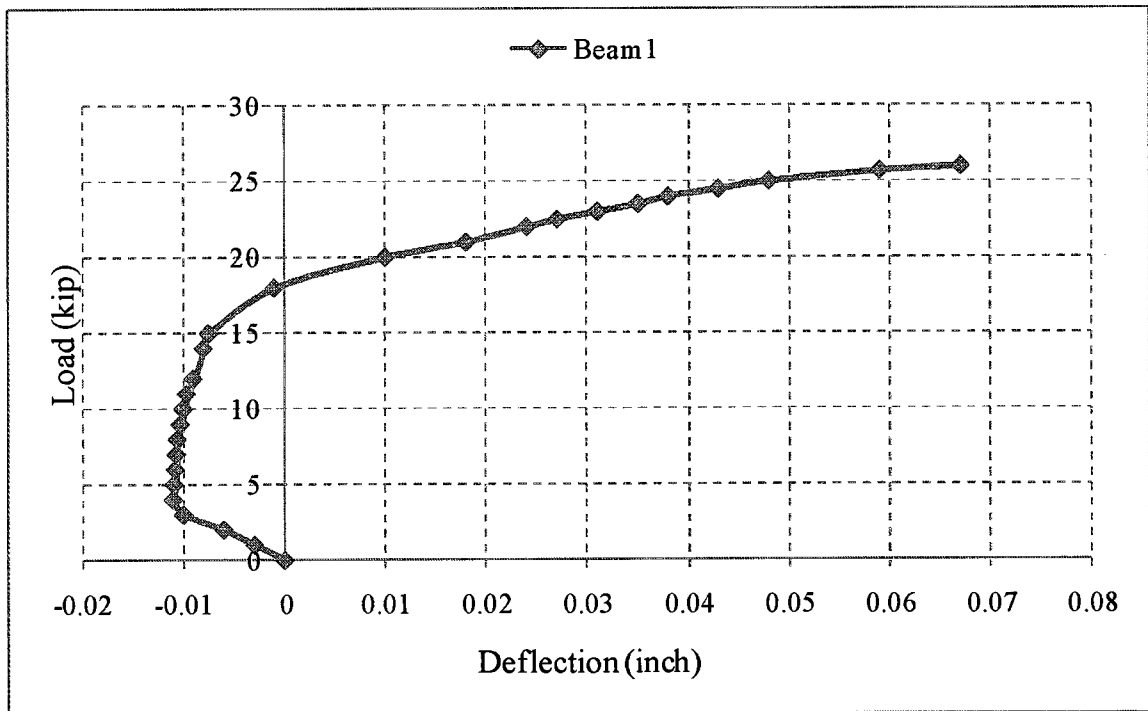
Figure 4.22 Experimental Load Deflection Response for Beam 1.
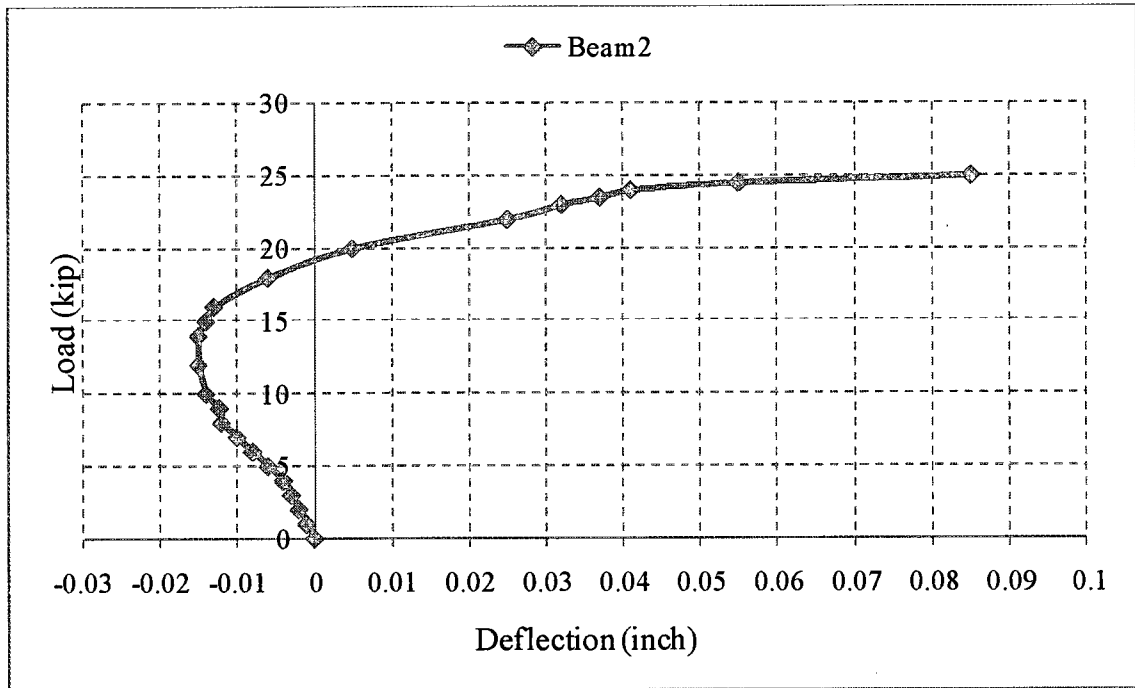
Figure 4.23 Experimental Load Deflection Response for Beam 2.

The flexural cracks formed in the constant moment region (i.e., between the supports) extended vertically and then became wider. These cracks initiated in the shear span at collapse. The cracks initially extended vertically, and then continued towards the load points in a diagonal fashion. Then the beams collapsed as shown in Figures 4.20 and 4.21.

4.2.2 Beam1 Failure

The longitudinal strains in the FRP Grids due to the applied loads were recorded. The locations of the 2-inch strain gages along the FRP Grids were shown in Figure 3.16. The strain data for Beam1, with 1" FRP Grid, are presented in Figures 4.24 through 4.28. Some of the strain gages that were installed on the FRP Grid failed during the tests, so no data was available at their locations.

In Figures 4.24 and 4.25, the strain data in the cantilever section indicated that the longitudinal strain distribution followed the bending moment diagram. In Figures 4.26 and 4.27, the data obtained from the strain gages indicated that at higher loads the longitudinal strains in the shear spans increased above those of a linear variation. This showed that strains were not proportional to the applied moment at these locations. At ultimate conditions, the axial strain in the FRP Grid varied linearly along the end of the FRP Gird and the point of load. Based on the previous discussion, it was concluded that the bond between the FRP Grid and concrete is uniform. Moreover, the data in Figures 4.26 and 4.27 indicated that the variations in the strain with the load at the beam center were slightly higher than those close to the load point, but the two curves were of similar form. As the applied load increased, the rate of change in the strains in the shear span was higher than that in the constant moment region. The higher rates demonstrated the initiation and progress of cracking in the region close to the support. The high level of strains in the shear span explained the flexure-shear cracking in the collapse mechanism for the beam.

The strain data from Layer 1 and 2 in Beam 1 at loads close to failure is shown in Figure 4.28. The strain distribution in these FRP grids followed the moment diagram.

Figure 4.24 Distribution of Longitudinal Strain along FRP Grid for Layer 1 in Beam 1.
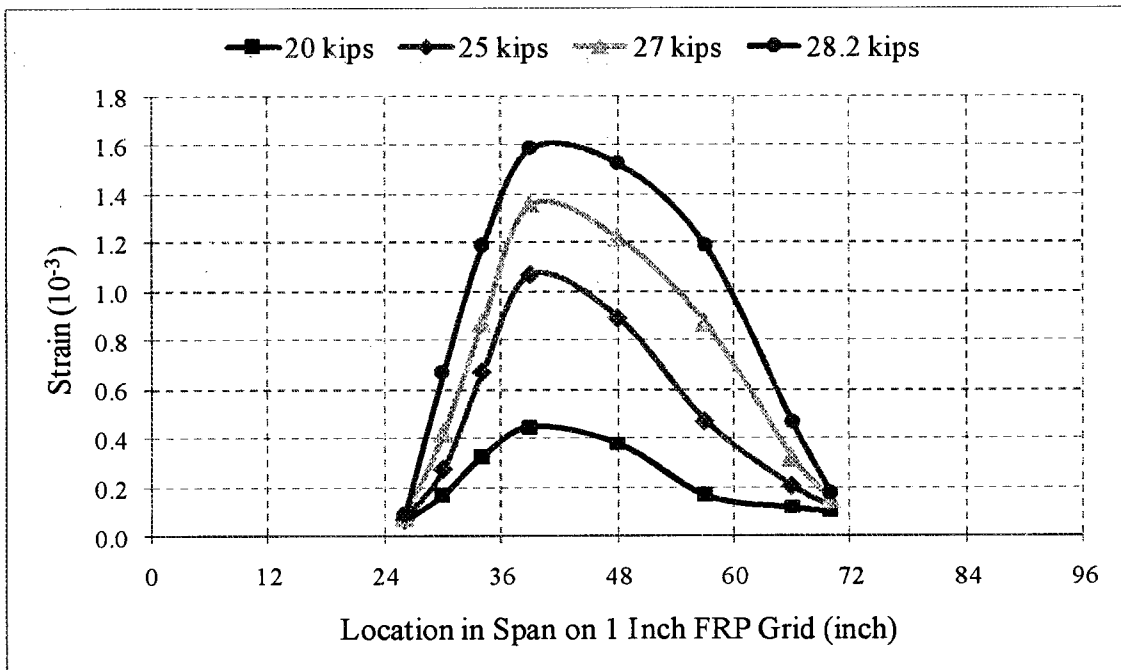
Figure 4.25 Distribution of Longitudinal Strain along FRP Grid for Layer 2 in Beam 1.
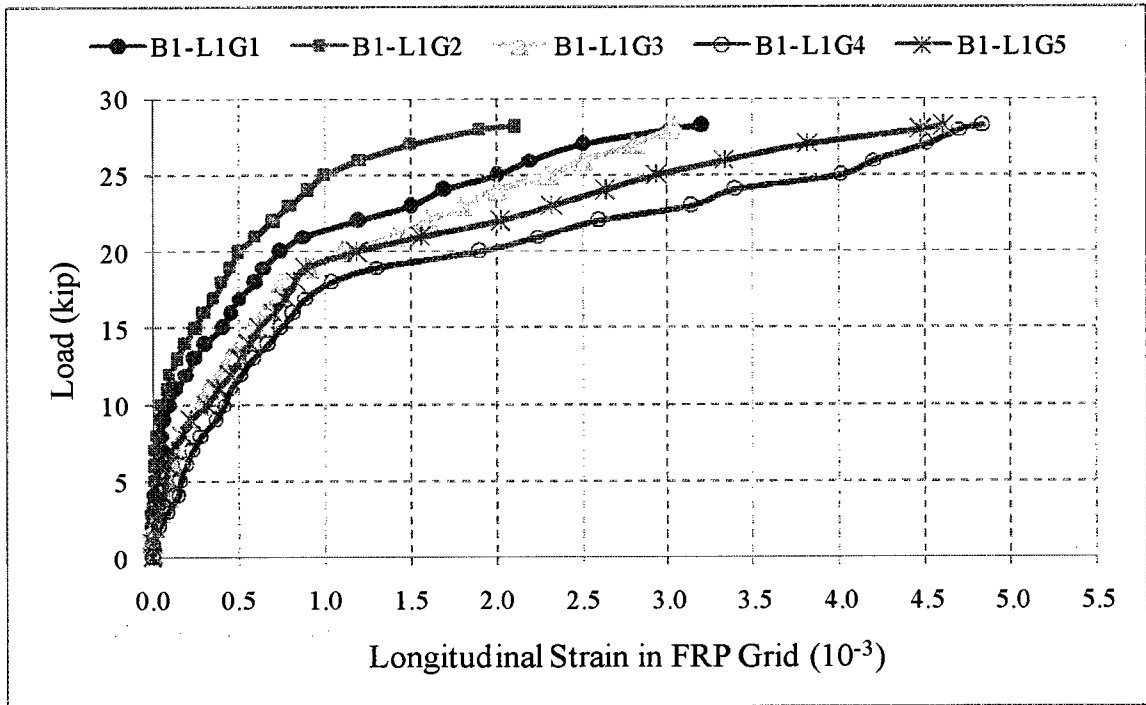
Figure 4.26 Typical Load/Strain along FRP Grid for Layer 1 in Beam 1.
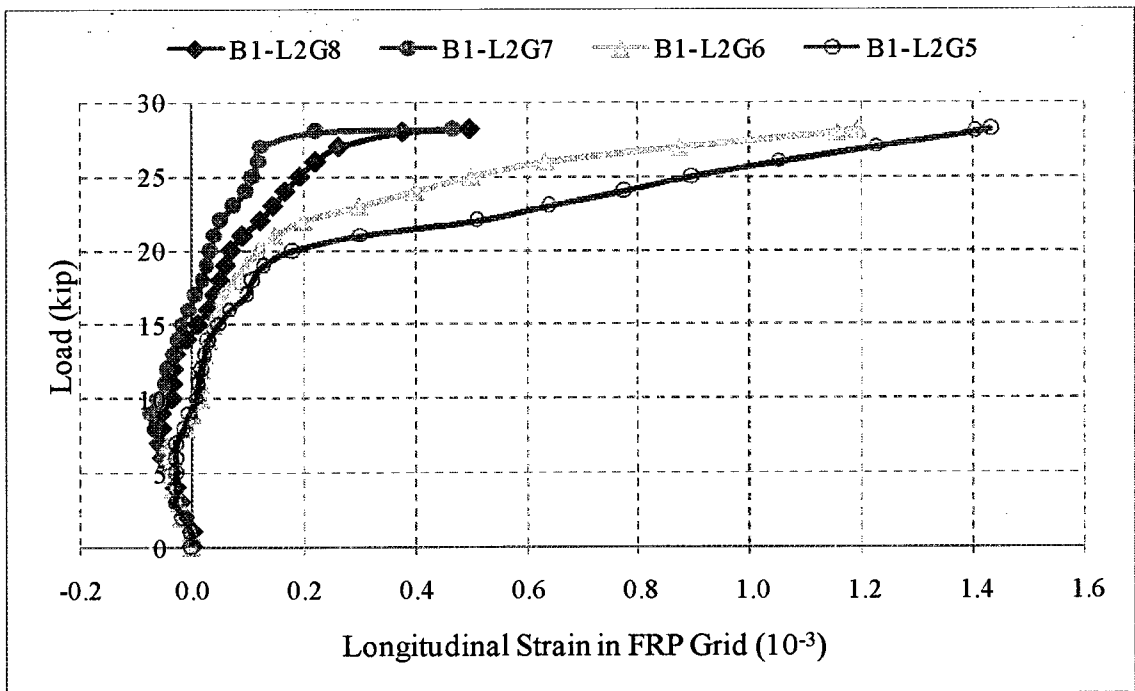
Figure 4.27 Typical Load/Strain along FRP Grid for Layer 2 in Beam 1.
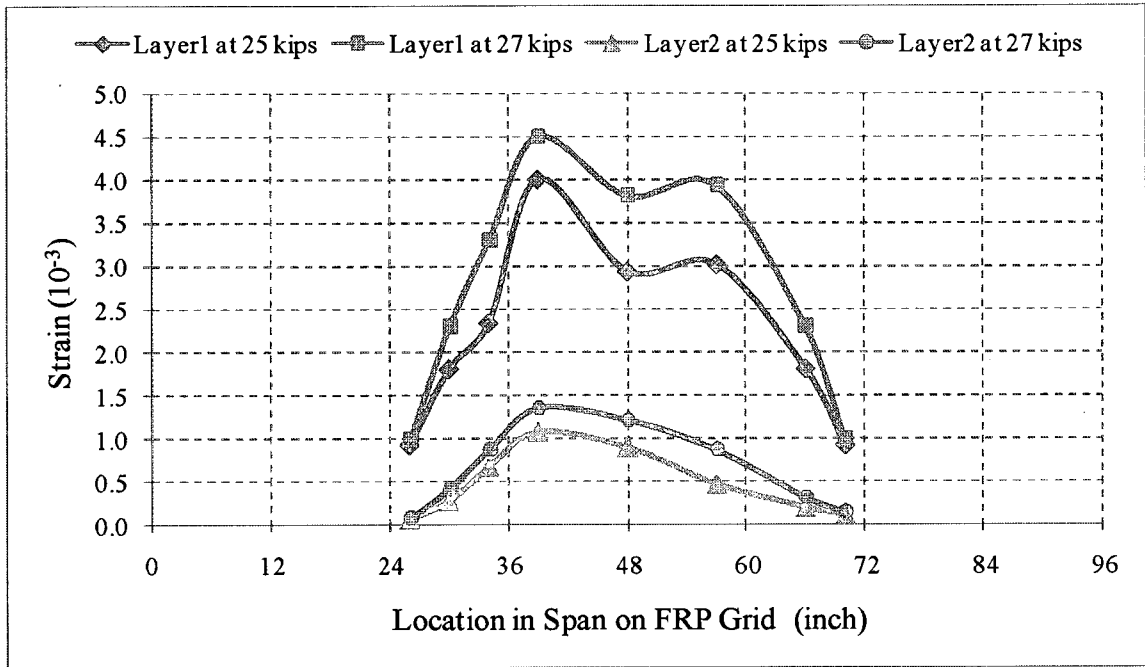
Figure 4.28 Longitudinal Strain along FRP Grids for Beam 1.

4.2.3 Beam 2 Failure

The same discussion presented above applies to the behavior for Beam 2 with two 1.25" FRP Grid which are shown in Figures 4.29 through 4.32.
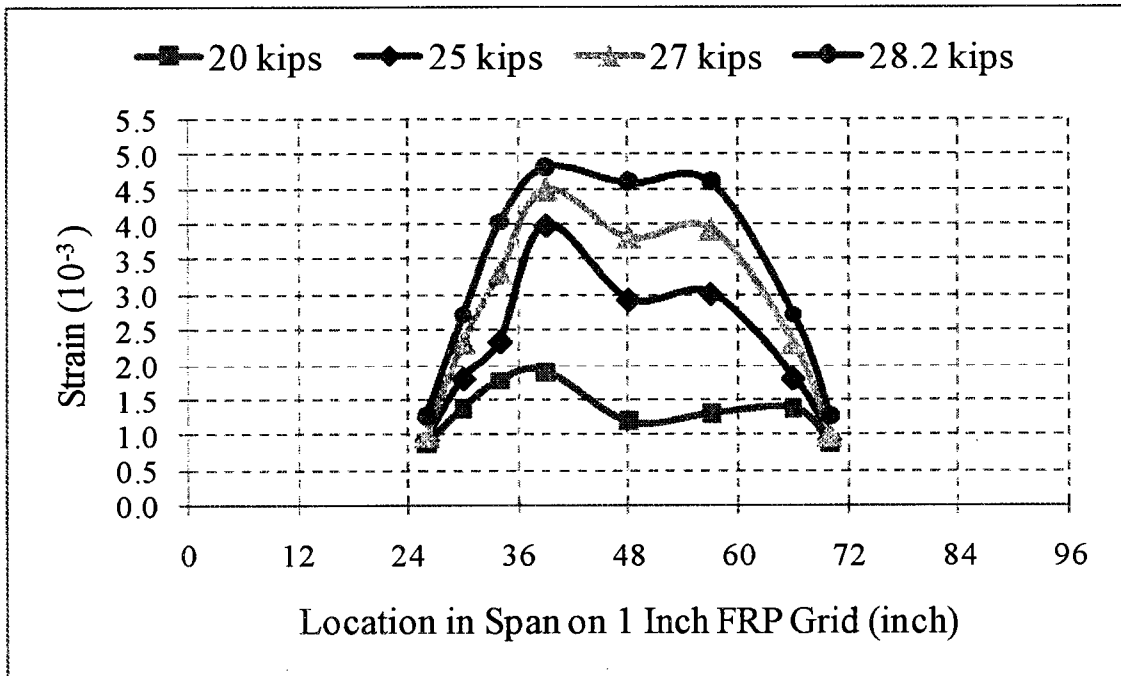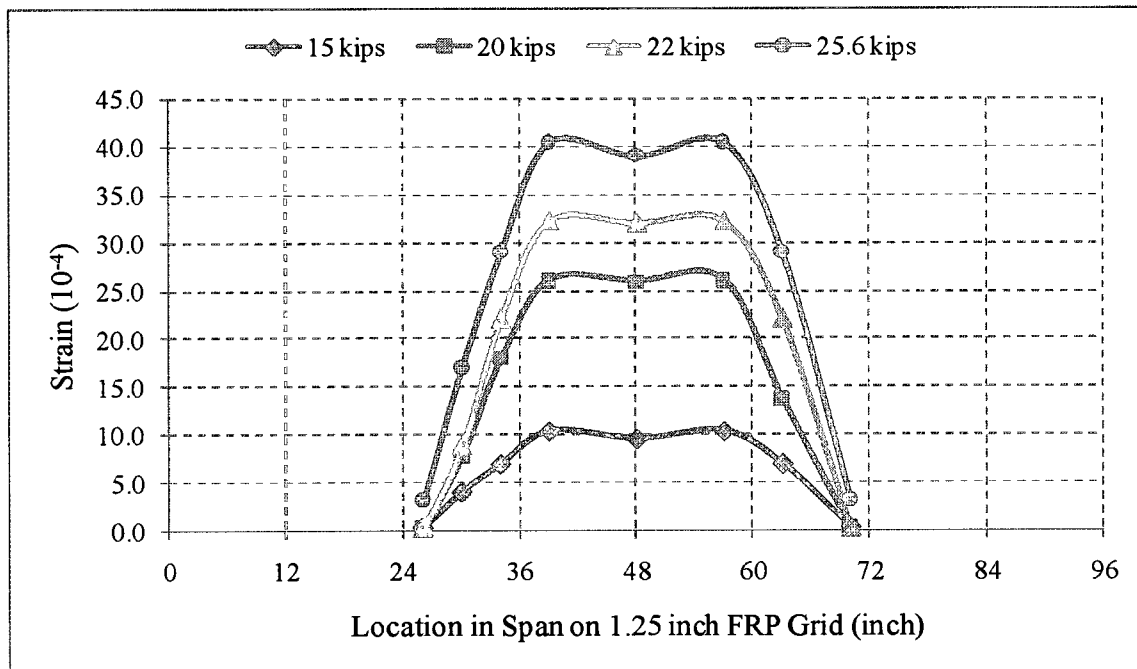
Figure 4.29 Distribution of Longitudinal Strain along FRP Grid for Layer 1 in Beam 2.
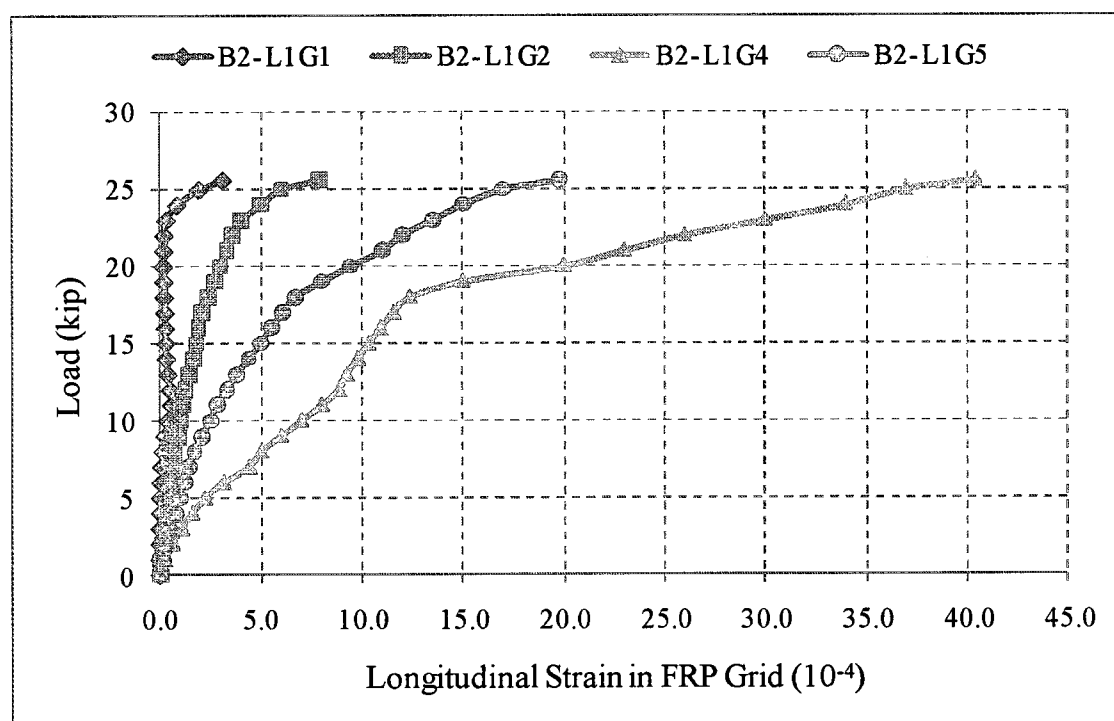
Figure 4.30 Typical Load/Strain along FRP Grid for Layer 1 in Beam 2.
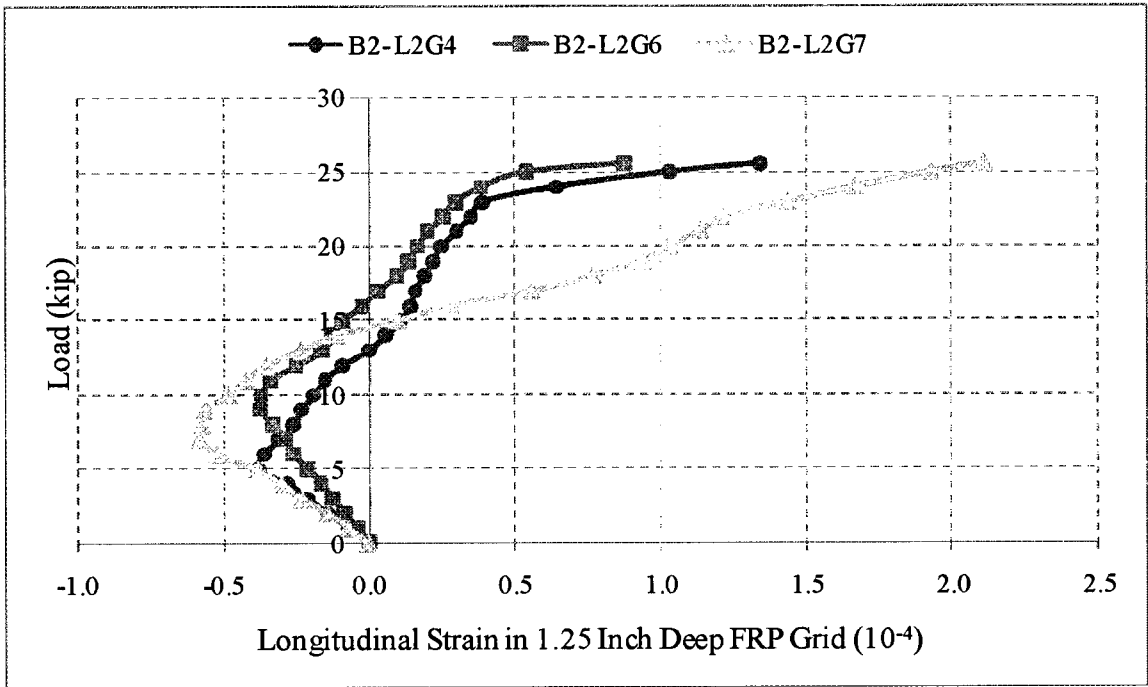
Figure 4.31 Typical Load/Strain along FRP Grid for Layer 2 in Beam 2.
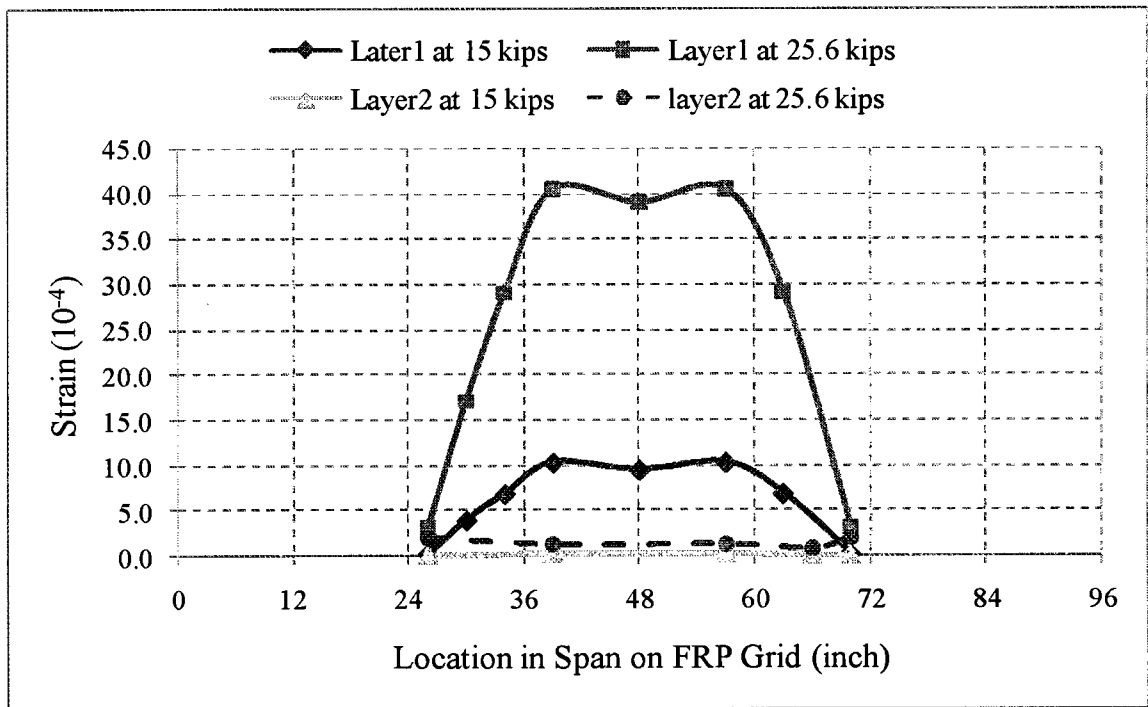
Figure 4.32 Longitudinal Strain along FRP Grids for Beam 2.

The test results for the two beam specimens were presented in Sections 4.2.4 and 4.2.5. The discussion will be given on the overall load/deflection and strain responses up to failure and the mode of failure of the specimens. The beams were designed to have ductile failure at the ultimate load, as would be the case for existing bridge decks in service.

4.2.4 Load-Deflection Behavior

All specimens were tested in a four-point bending configuration. The ultimate loads and corresponding deflections for both beams were measured during the tests.

The load carrying capacity of Beam 1 was more than that of Beam 2. The load deflection behavior of Beam 1 is shown in Figure 4.33. The stiffness of the beam was relatively high until the applied load reached 18.0 kips because the measured deflections were low. When the applied load reached 26.0 kips, the deflectometers were removed to avoid damaging them during the test. The beam collapsed at an applied load of 28.2 kips.
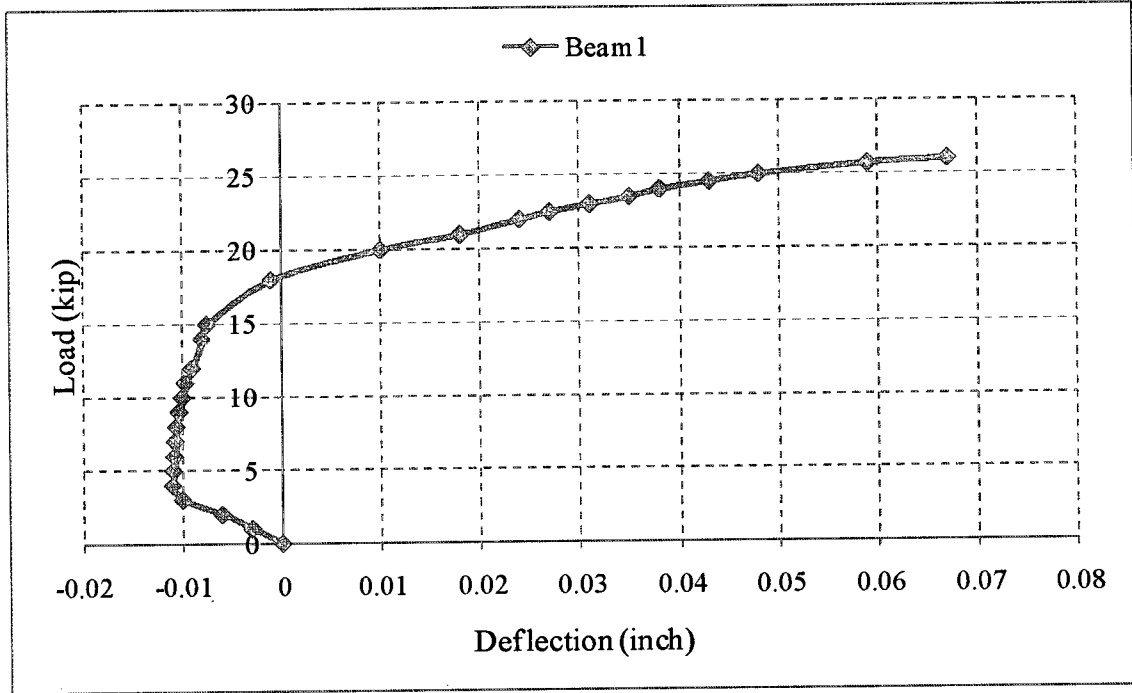
Figure 4.33 Experimental Load Deflection Behavior of Beam 1.

The load deflection behavior of Beam 2 is shown in Figure 4.34. The stiffness of the beam was relatively high until the applied load reached 19.0 kips because the measured deflections were low. When the applied load reached 25.0 kips, the deflectometer were removed to avoid damaging them during the test. The beam collapsed at an applied load of 25.6 kips.
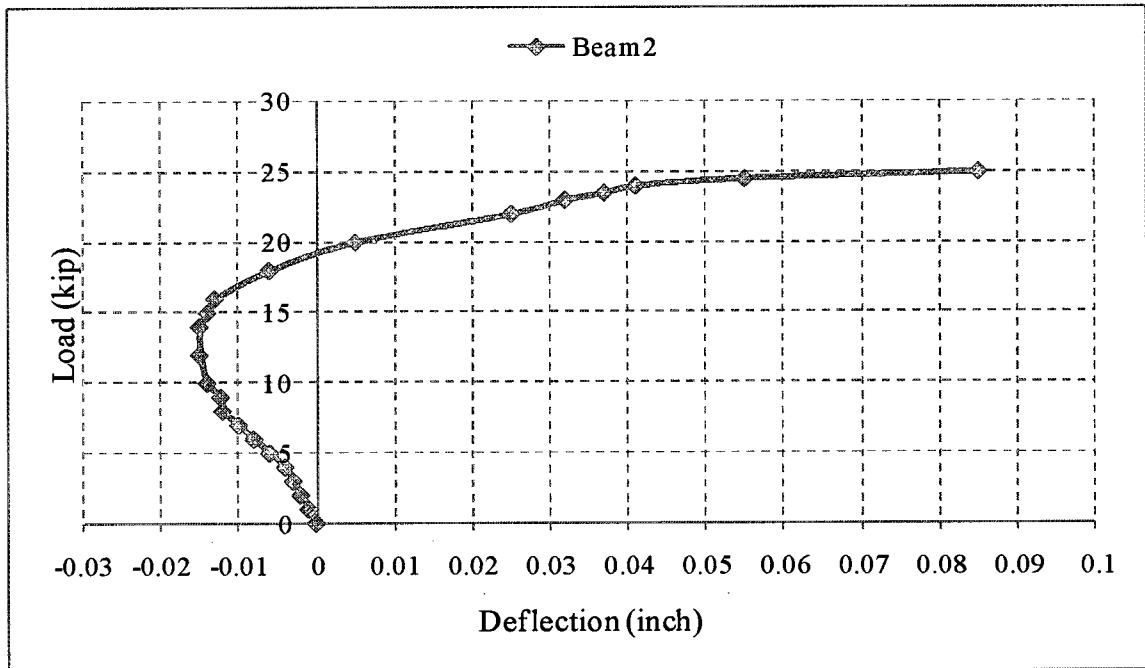
Figure 4.34 Experimental Load Deflection Behavior of Beam 2.

4.2.5 Strains in the Beams

4.2.5.1 Beam 1 Layer 1

For Layer 1 in Beam 1, eight strain gages were installed to monitor the strain distribution. The strains measured were tensile strains in all the gages at different applied loads for the ultimate load test. These measurements indicated that the grid was in tension. Among all the gages, maximum tensile strain was found in Gage 4 (B1-L1G4), which was located just to the right of the left support. The maximum strain was 4.8 milli strains at the ultimate load of 28.2 kips. The tensile modulus of the grid was 2.5×10^3 ksi. Therefore, the tensile stress corresponding to maximum tensile strain was 12.0 ksi which is 40% of the maximum tensile stress recommended by the manufacturer, as shown in Table 3.5. The load-strain relationship was linear up to the load level of 17 kips when the

beam began to yield. The load-strain distribution of Gage 4 in Layer 1 (B1-L1G4) is shown in Figure 4.35.
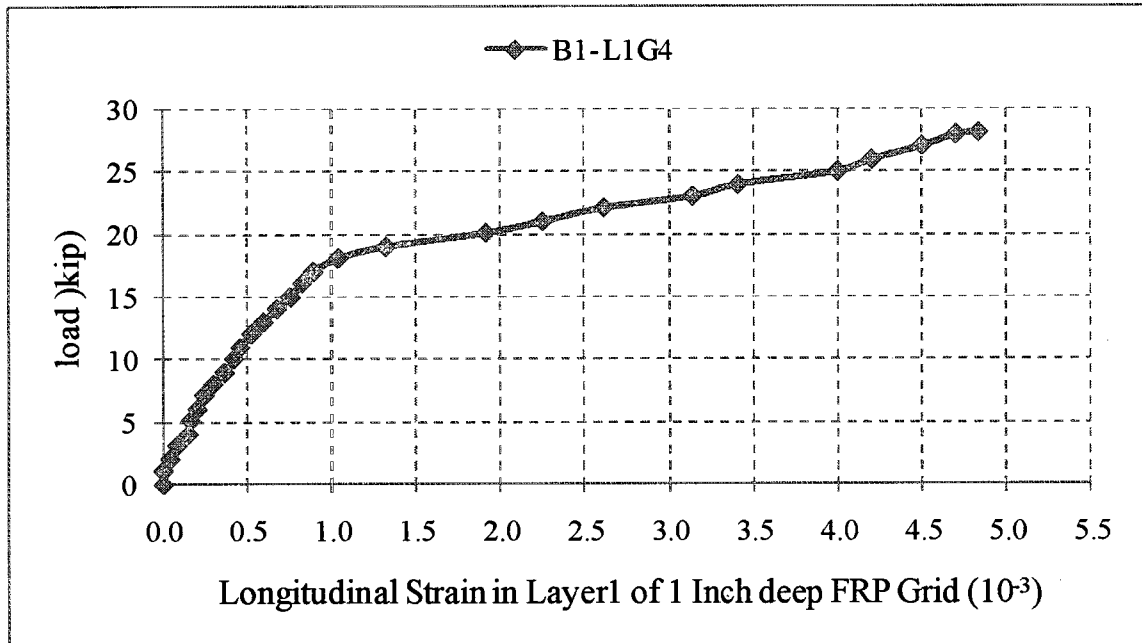
Figure 4.35 The Load-Strain Distribution in Gage 4 in Layer 1 (L1G4) for Beam 1.

Figure 4.36 shows the load-strain distribution of Gage 5 in Layer 1 (B1-L1G5) located at the center of the grid and the beam. The change in the strains were low up to the load level of 19 kips, and after that, change in strains were higher until the ultimate load was reached.

Figure 4.37 shows the load-strain distribution of Gage 6 in Layer 1 (B1-L1G6) located just to the left of the right support. The load-strain relationship was almost linear up to the load level of 21 kips when the beam began to yield.

Figure 4.36 The Load-Strain Distribution in Gage 5 in Layer 1 (L1G5) for Beam 1.
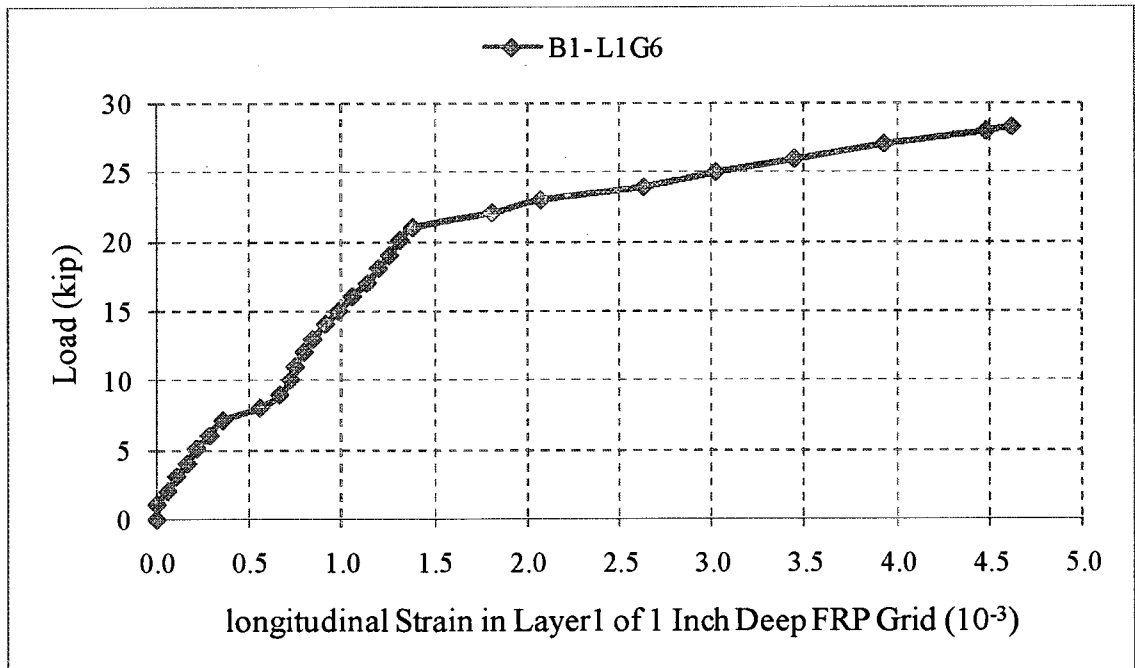
Figure 4.37 The Load-Strain Distribution in Gage 6 in Layer 1 (L1G6) for Beam 1.

The strain distribution for Layer 1 of Beam 1 (B1-L1) is presented in Figure 4.38.

The figure indicated that as the applied load increases towards its maximum value, the

distribution of strain in the FRP grid became unsymmetrical.
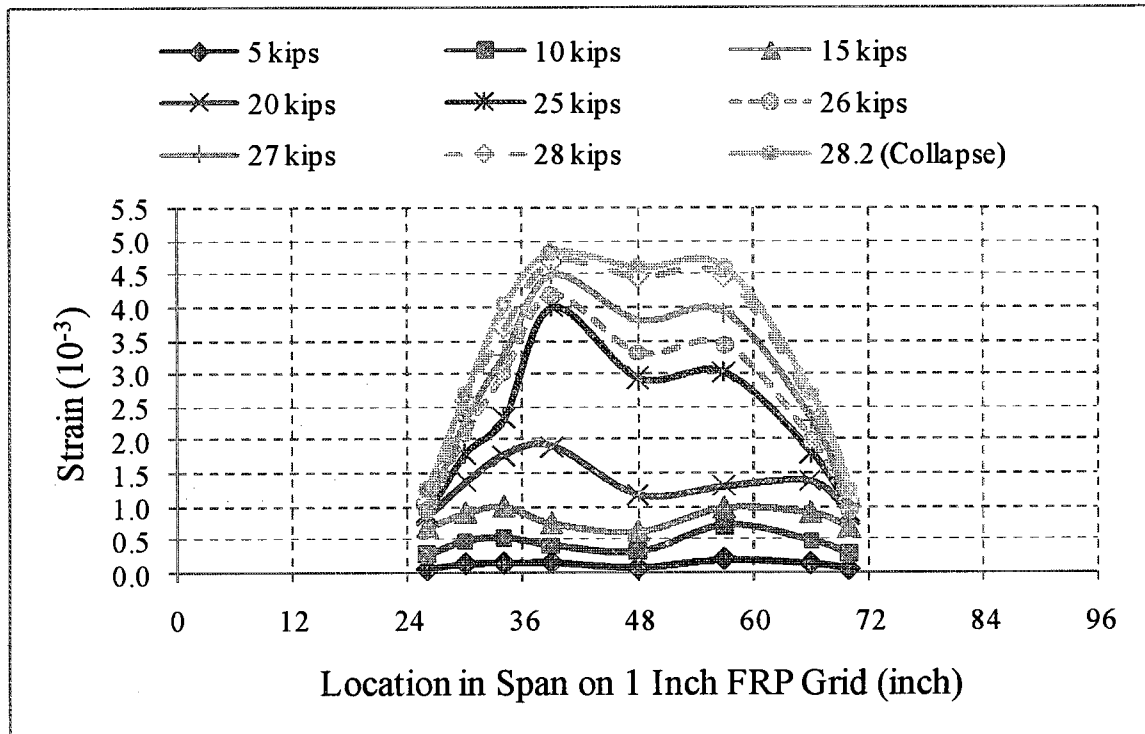
Figure 4.38 Distribution of Longitudinal Strain along FRP Grid in Layer1 for Beam1
(B1-L1).

The strain Gages 4 and 6 in Layer 1 of Beam 1 (B1-L1) were symmetric about the

center-line. The strain distribution for these gages indicated that the strains were similar

at different applied loads as shown in Figure 4.39.
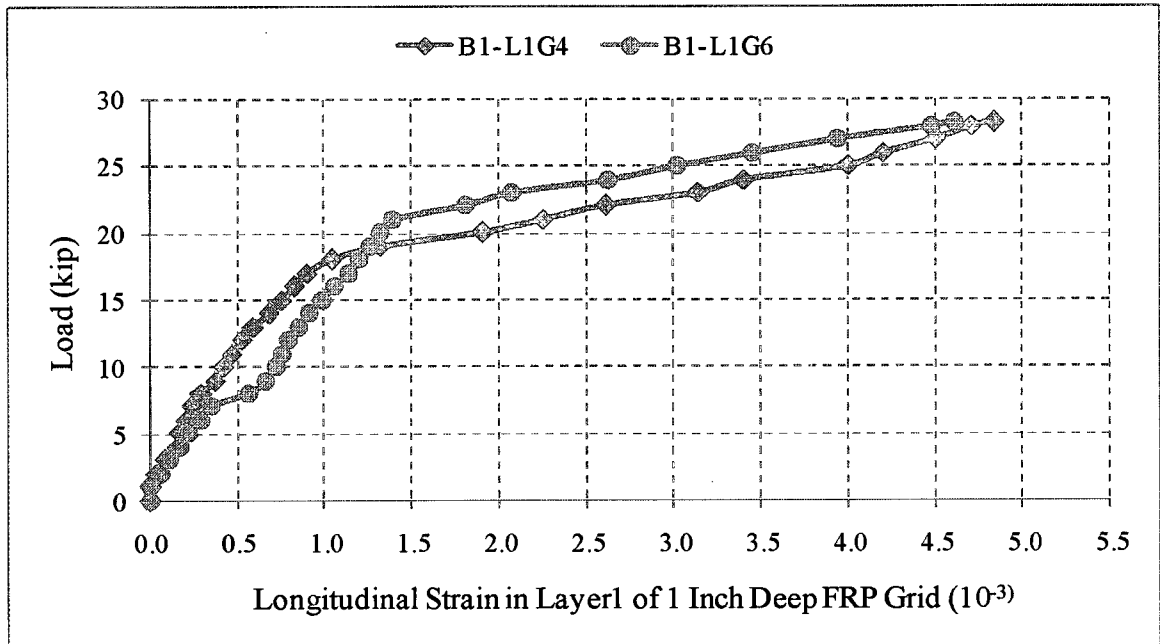
Figure 4.39   The Load-Strain Distribution in Two Symmetric Gages in Layer 1 for Beam1.

4.2.5.2 Beam 1 Layer 2

For Layer 2 in Beam 1, eight strain gages were installed to monitor the strain distribution. The locations of the 2-inch strain gages along the FRP grid in Layer 2 of Beam1 were shown in Figure 3.16. The strains measured were compressive strains in all the gages up to an applied load of 9 kips. Then the measured strains were changed to tensile strains for the ultimate load test. These measurements indicated that the grid was in compression till the applied load reached a value of 9 kips, then the grid was in tension. Among all the gages, the maximum compressive strain was found in Gage 7 (B1-L2G7) located at 66 inches from the left end of the beam as shown in Figure 3.16, at an applied load of 9 kips. The load-strain distribution of Gage 7 in Layer 2 (B1-L2G7) is shown in Figure 4.40. The maximum compressive strain was (-0.074) milli strains. The compressive modulus of the grid was 2.5x 10^3 ksi. Therefore, the compressive stress

corresponding to the maximum compressive strain was 0.18 ksi, which is 0.6% of the

maximum compressive stress recommended by the manufacturer.

Figure 4.40 The Load-Strain Distribution in Gage 7 in Layer 2 (B1-L2G7) for Beam 1.

The maximum tensile strain was found in Gage 4 (B1- L2G4) which was located

just right of the left support. The maximum strain was 1.6 milli strains at the ultimate

load 28.2 kips. The tensile modulus of the grid was 2.5 x 10^3 ksi. Therefore, the tensile

stress corresponding to the maximum tensile strain was 3.98 ksi, which is 13.3% of the

maximum tensile stress. The load-strain distribution of Gage 4 in Layer 2 (B1- L2G4) is

shown in Figure 4.41.
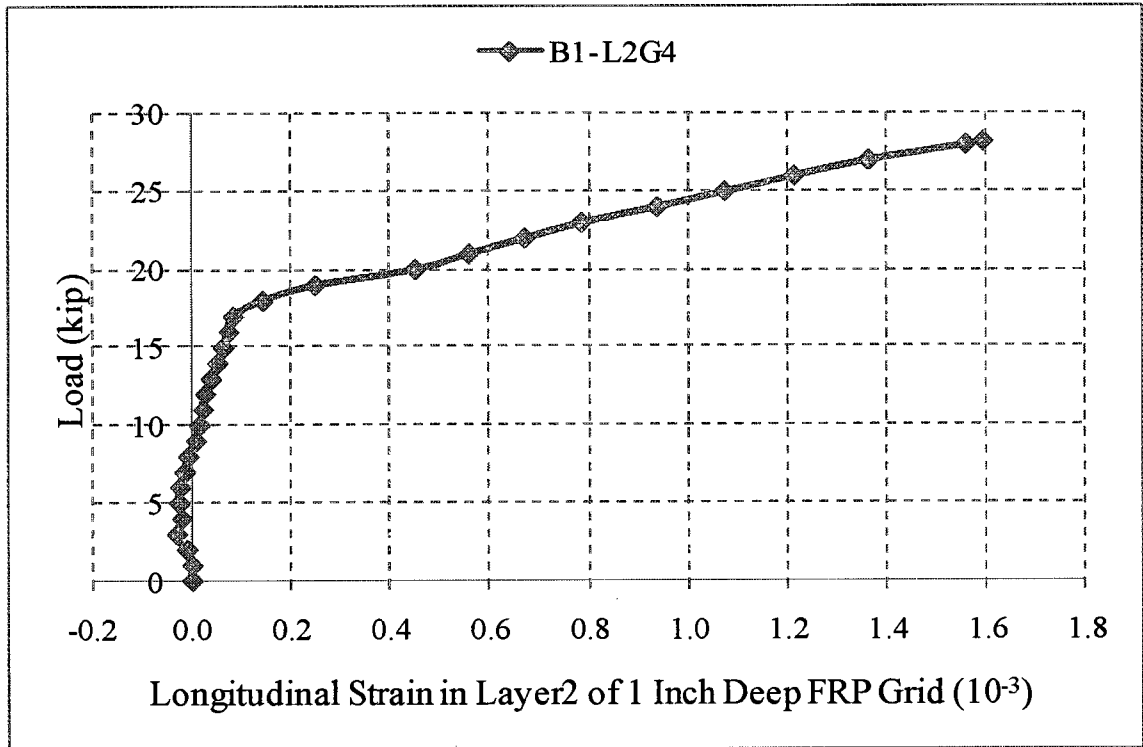
Figure 4.41 The Load-Strain Distribution in Gage 4 in Layer 2 (L2G4) for Beam 1.

The strain Gages 4 and 6 in Layer 2 of Beam 1 were symmetric about the center-line. Figure 4.42 shows the strain distribution for these gages which indicated that the strains were similar up to an applied load of 17 kips.
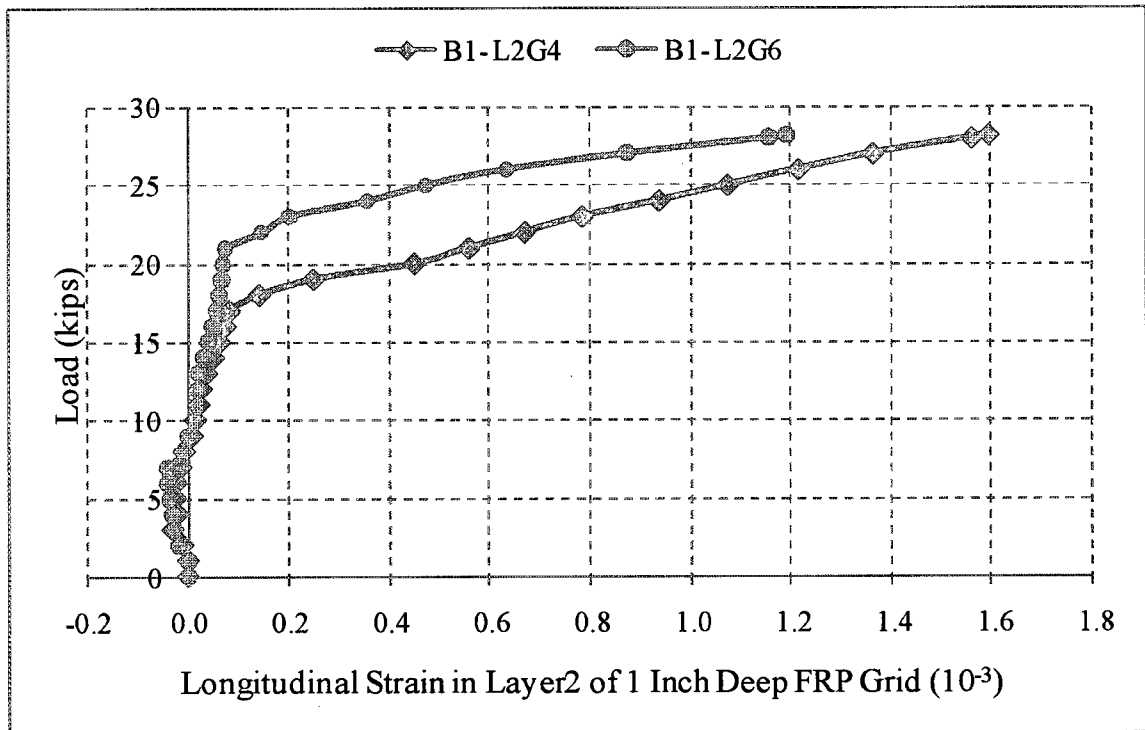
Figure 4.42 The Load-Strain Distribution in Two Symmetric Gages in Layer 2 for Beam1 (B1-L2).

4.2.5.3 Beam 2 Layer 1

For Layer 1 in Beam 2, eight strain gages were installed to monitor the strain distribution. The strains measured were tensile strains in all the gages at different applied loads for the ultimate load test. These measurements indicated that the grid was in tension. Among all the gages, maximum tensile strain was found in Gage 4 (B2-L1G4), which was located just right of the left support. The maximum strain was 4.0 milli strains at the ultimate load of 25.6 kips. The tensile modulus of the grid was 2.5×10^3 ksi. Therefore, the tensile stress corresponding to the maximum tensile strain was 10.1 ksi, which is 34% of the maximum tensile stress recommended by the manufacturer, as shown in Table 3.5. The load-strain distribution of Gage 4 in Layer 1 (B2- L1G4) is shown in Figure 4.43.
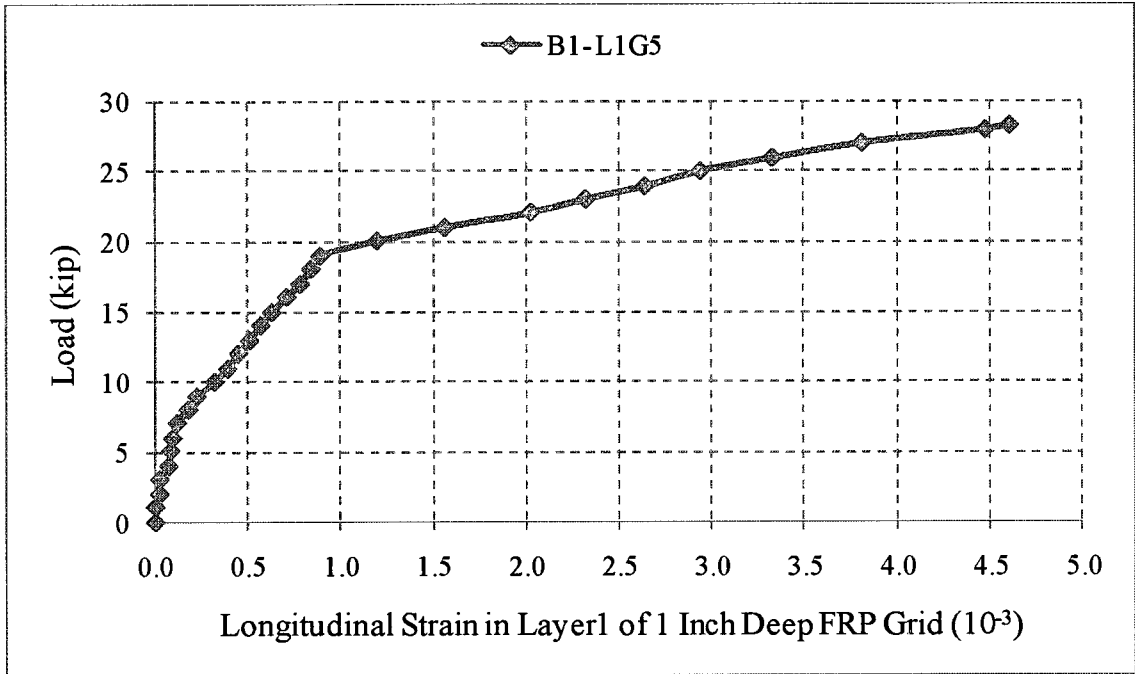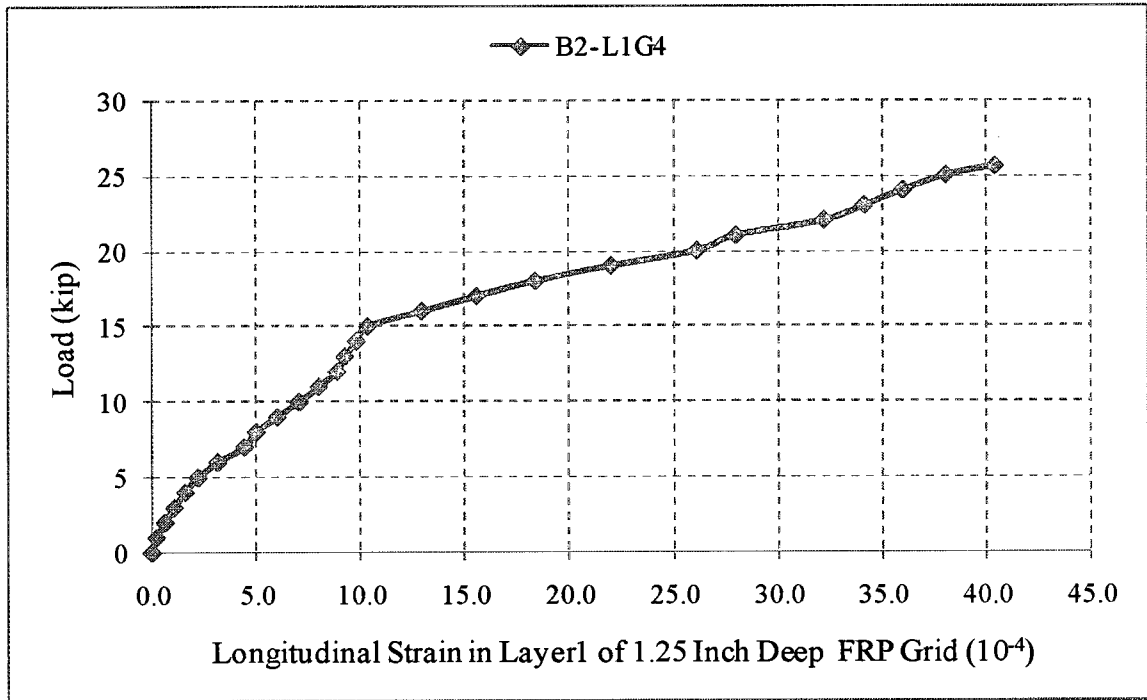
Figure 4.43 The Load-Strain Distribution in Gage 4 in Layer 1 (B2-L1G4) for Beam 2.

Figure 4.44 shows the load-strain distribution of Gage 5 in Layer 1 (B2-L1G5) located at the center of the grid and the beam. At higher loads, strain varied linearly with the applied loads.

For Layer 1 in Beam 2, the strain distribution in all gages at different applied loads is presented in Figure 4.45.
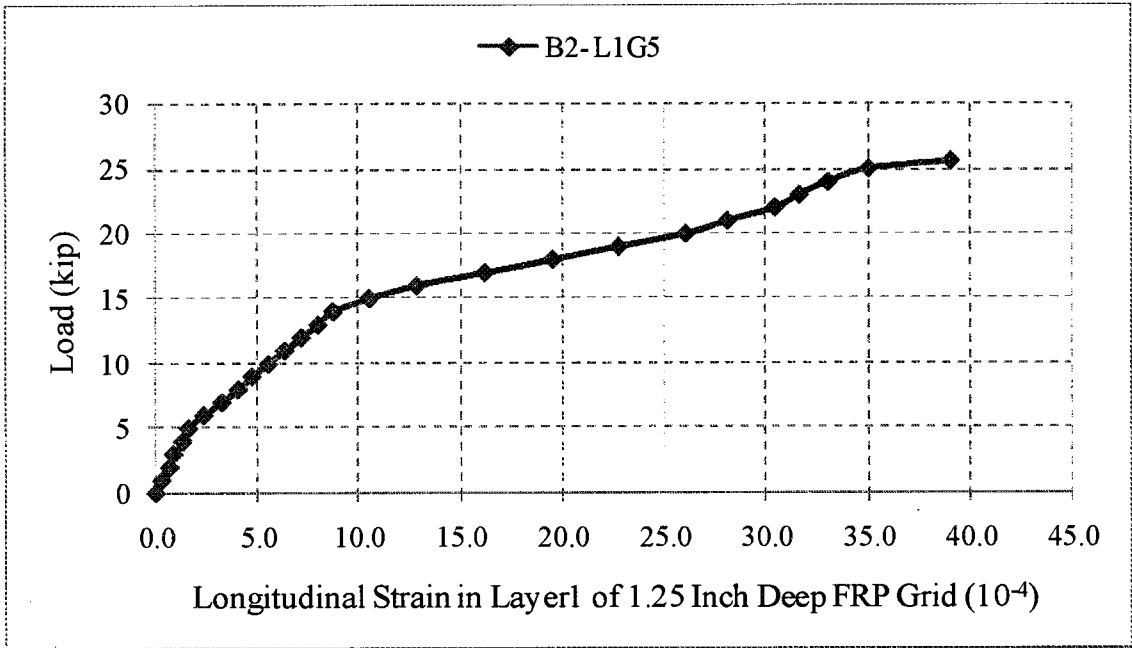
Figure 4.44 The Load-Strain Distribution in Gage 5 in Layer 1 (B2- L1G5) for Beam 2.
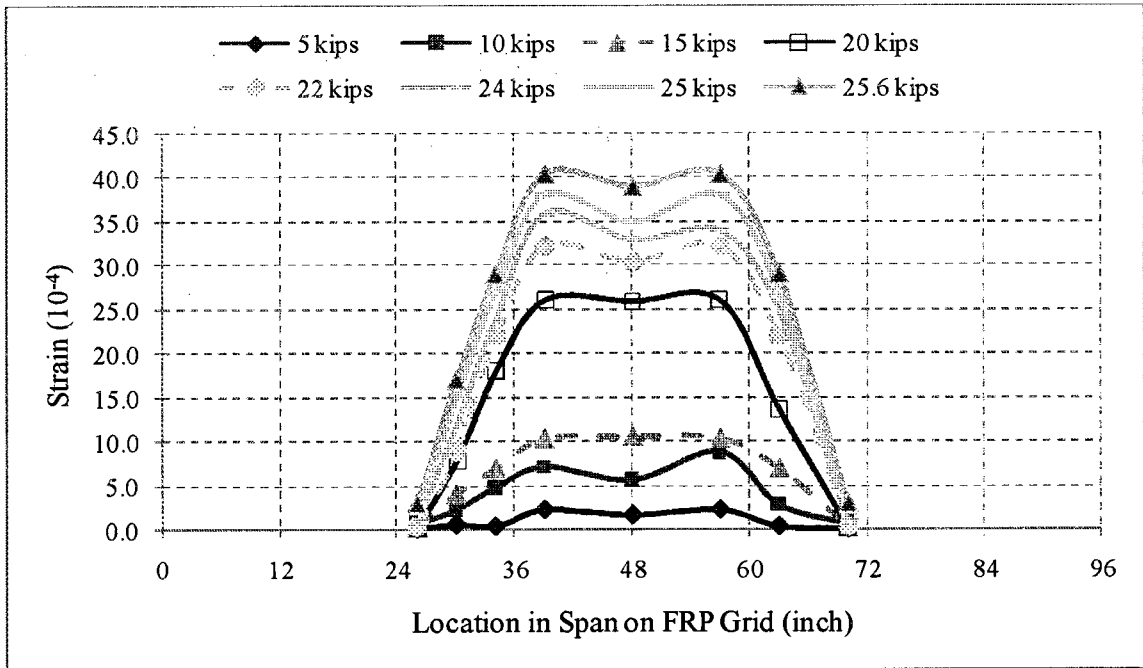
Figure 4.45 Distribution of Longitudinal Strain along FRP Grid in Layer 1 for Beam 2 (B2-L1).

4.2.5.4 Beam 2 Layer 2

For Layer 2 in Beam 2, strain gages were installed to monitor the strain distribution. The locations of the 2-inch strain gages along the FRP grid in Layer 2 of Beam 2 were shown in Figure 3.16. The strains measured were compressive strains in all the gages up to an applied load of 14 kips. After that, the measured strains were changed to tensile strains for the ultimate load test. These measurements indicated that the grid was in compression till the applied load reached a value of 14 kips, then the grid was in tension. Among all the gages, the maximum compressive strain was found in Gage 7 (B2-L2G7) located at the right end of the grid, as shown in Figure 3.16, at an applied load of 7 kips. The load-strain distribution of Gage 7 in Layer 2 (B2-L2G7) is shown in Figure 4.46. The maximum compressive strain was (-0.058) milli strains. The compressive modulus of the grid was 2.5×10^3 ksi. Therefore, the compressive stress corresponding to the maximum compressive strain was 0.15 ksi, which is 0.5% of the maximum compressive stress recommended by the manufacturer.
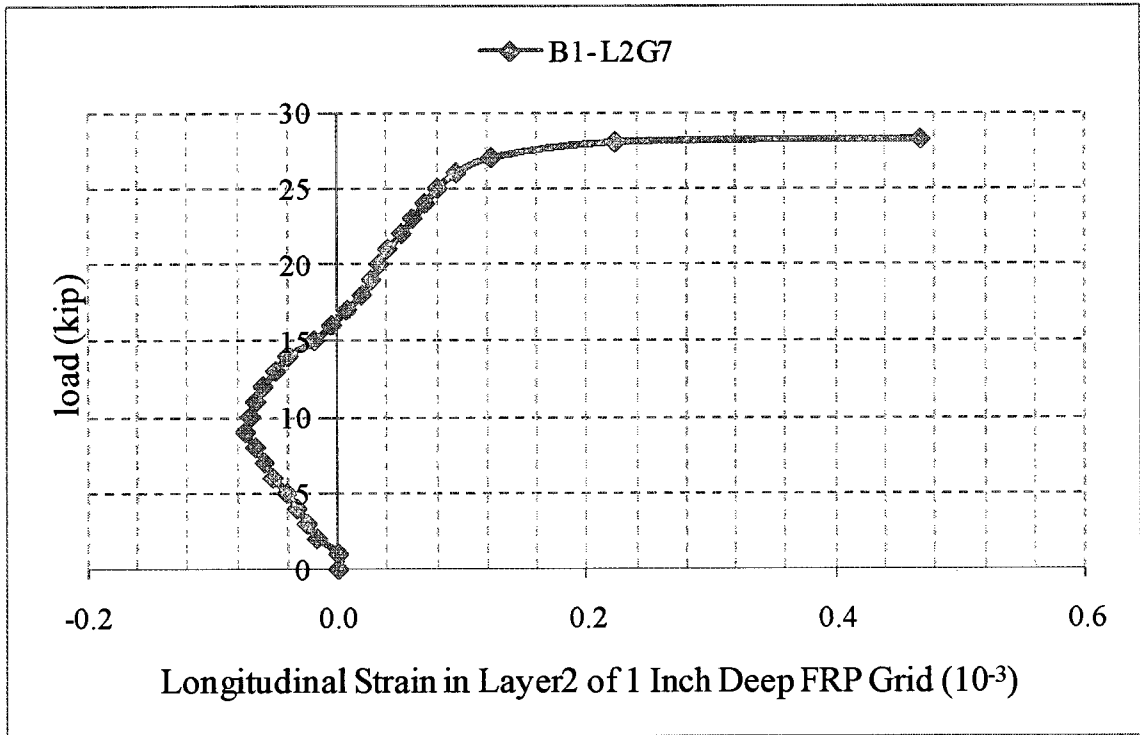
The maximum tensile strain was also found in Gage 7 (B2-L2G7). The maximum strain was 0.21 milli strains at the ultimate load of 25.6 kips. The tensile modulus of the grid was 2.5×10^3 ksi. Therefore, the tensile stress corresponding to maximum tensile strain was 0.53 ksi, which is 1.8% of the maximum tensile stress.
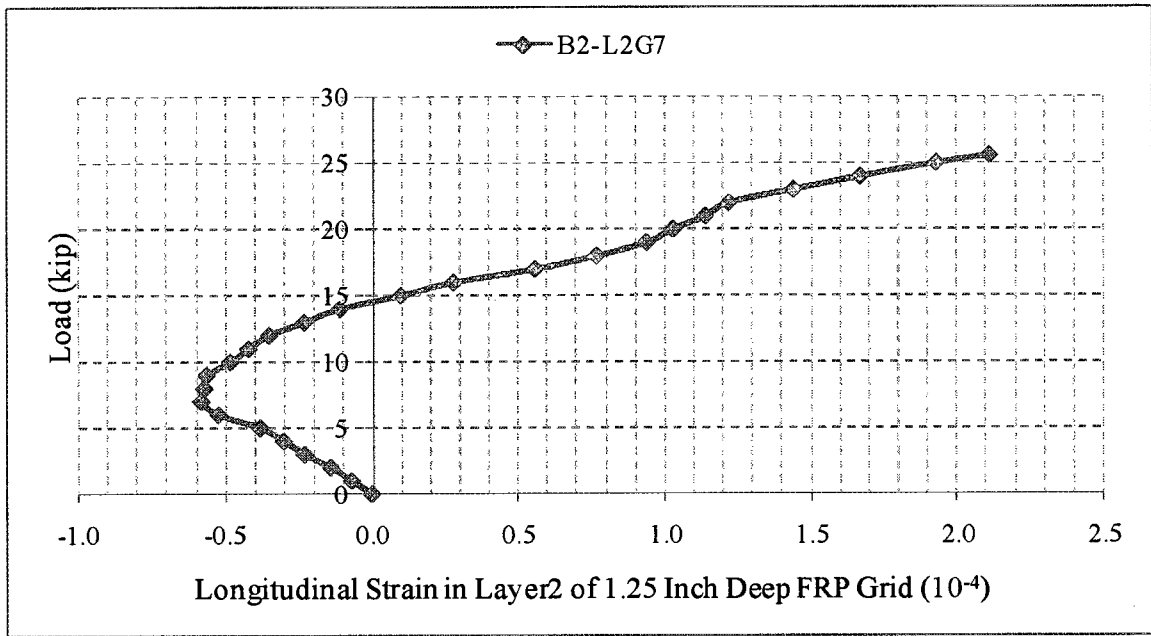
Figure 4.46 The Load-Strain Distribution in Gage 7 in Layer 2 (B2-L2G7) for Beam 2.

The load-strain distribution of Gage 2 in Layer 2 (B2-L2G2) is shown in Figure 4.47. The strains measured were compressive strains in the gage up to an applied load of 11 kips. After that, the measured strains were changed to tensile strains for the ultimate load test.
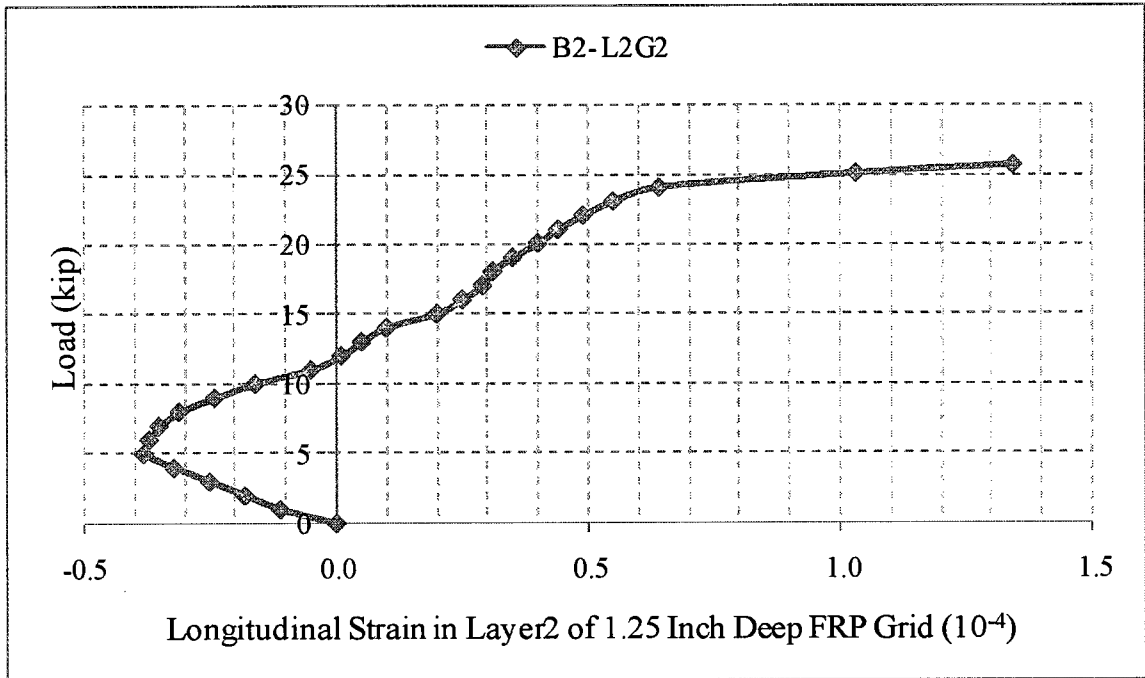
Figure 4.47 The Load-Strain Distribution in Gage 2 in Layer 2 (B2-L2G2) for Beam 2.

4.3 Experimental Results - Test for the Development Length of FRP Grid

The results obtained from beams that were tested for the development length requirements of the FRP grid were discussed in this section. The load deflection behavior, crack pattern and crack progression and failure mechanism of the beams were discussed. Also, the applied loads and corresponding strains in the beams were discussed. The maximum stresses in the FRP grids were calculated from the strains at the ultimate loads.

4.3.1 Results of Three-Point Bending Test

The load deflection behavior of Beam 1 and Beam 2 are shown in Figures 4.48 and 4.49, respectively. The stiffness of the FRP grid reinforced beam was relatively high at low applied loads (until 11 to 12 kips), which implies that the concrete beam behaved in a linear elastic manner. Increasing the load further, flexural crack initiated at the point of application of the load on the bottom surface, where bending moment due to live load and dead load was maximum. Due to the flexural crack, there was a slight change in the slope of the deflection curve as the member stiffness was reduced.
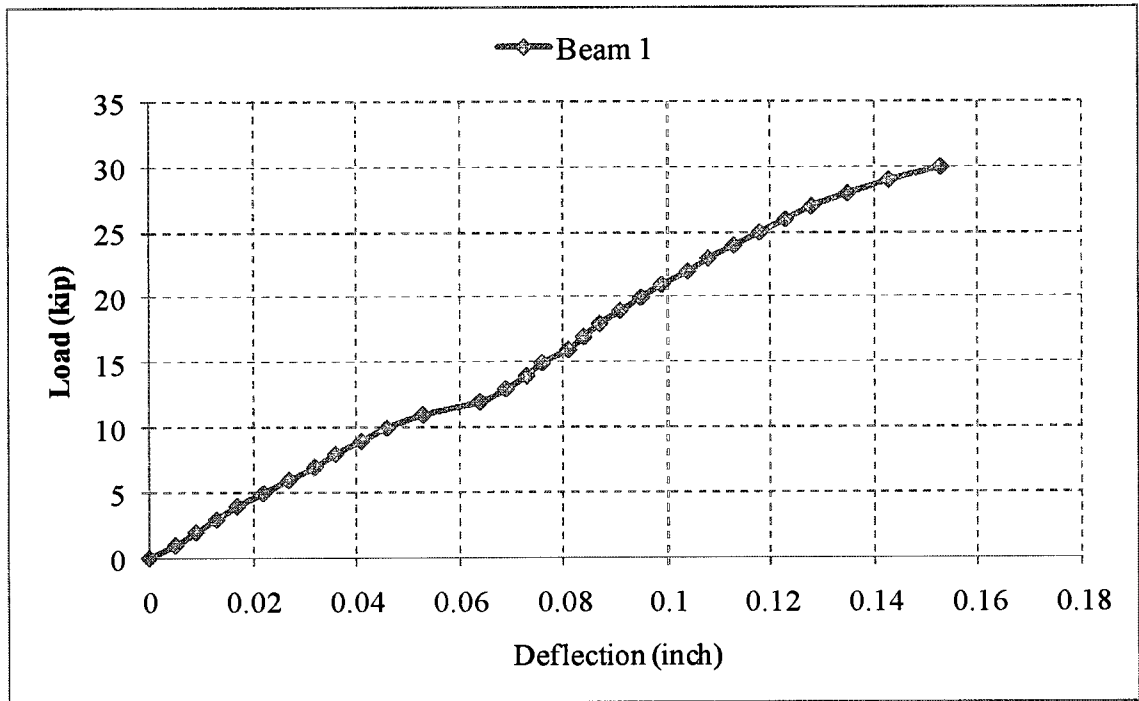
Figure 4.48 Experimental Load-Deflection Behavior of Beam 1.

The observed maximum deflection in Beam 1 was 0.153 inch at an applied load of 30 kips, and in Beam 2, the deflection was 0.173 inch at an applied load of 37 kips. The load-deflection curve also indicated that both beams showed less ductility as compared with the typical steel reinforced beams. It confirms that FRP reinforcement is a brittle material. The modulus of elasticity of the FRP grid reinforcement (1.8×10^6 psi) is much less than the steel reinforcement (29×10^6 psi). Hence, the deflection was significantly high in a beam reinforced with FRP grids.
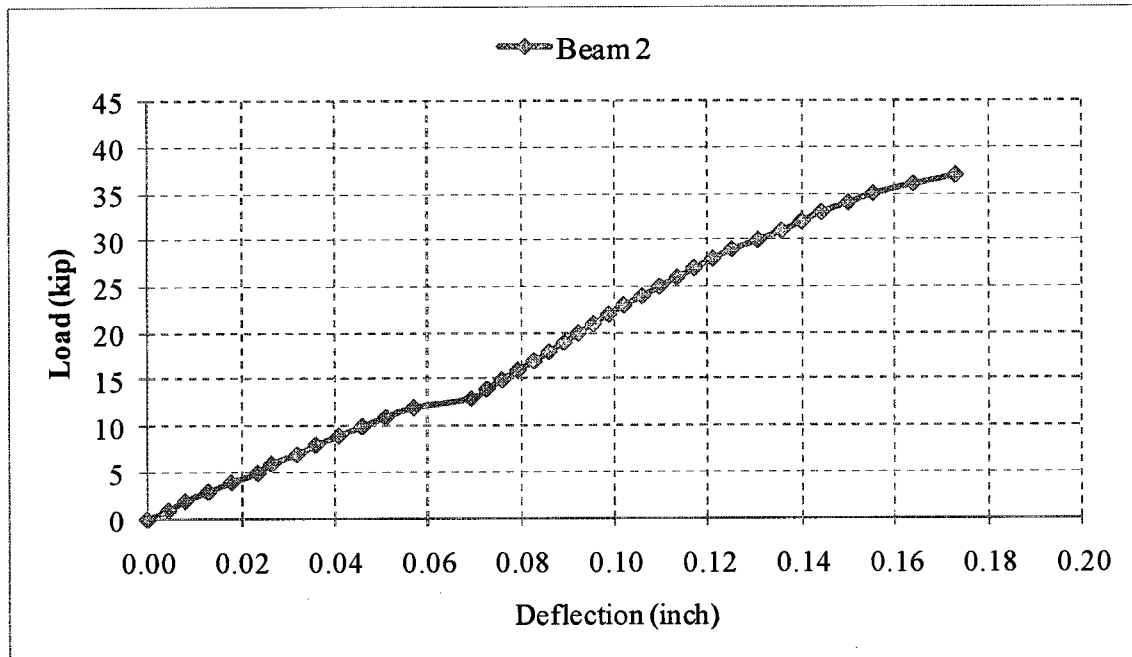
Figure 4.49 Experimental Load-Deflection Behavior of Beam 2.

The crack propagation and failure mechanism of Beam 1 and Beam 2 are shown in Figures 4.50 and 4.51. The beams were collapsed due to the shear tension failure. The yielding of the FRP reinforcement preceded the crushing of the concrete in compression as expected. Since, the beams were designed as under-reinforced. The large strains in the FRP reinforcement were expected at failure.

The beams were failed in shear as expected, since the flexural capacity of the beam was higher than shear capacity. The shear reinforcement was not provided since the depth of the beam was not greater than 10 inches.
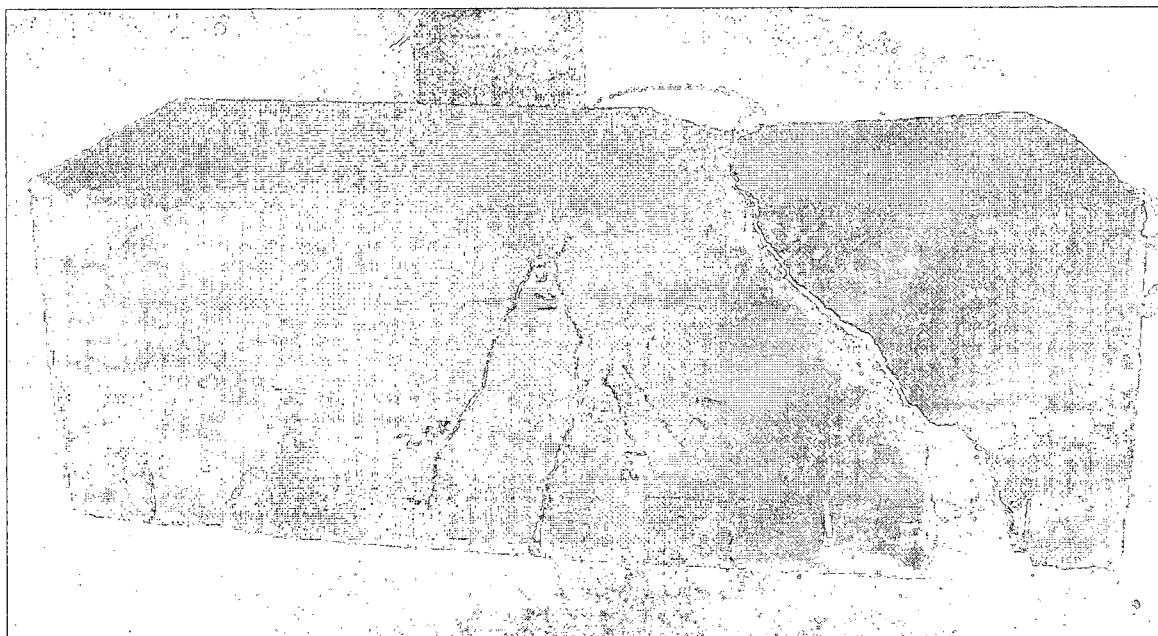
Figure 4.50 Shear Tension Failure of Beam 1.

Figure 4.51 Shear Tension Failure of Beam 2.

From the failure mechanism of the two beams, the beams failed in shear tension and FRP grids cracked, but there was no relative slip between the FRP grid and the concrete. This was due to the mechanical anchorage or interlocking between the concrete and the FRP grid. It confirms that the bond between the FRP grid and the concrete was highly improved.

4.3.2 Strains in Beams

The strain gages were installed in the beams to monitor the behavior of the FRP grid reinforcement. The applied loads and the corresponding resistances in FRP grid were collected for each load increment. Then, the strains in FRP were calculated from the resistances. In each beam, seven strain gages were installed.

Large strains were observed in FRP grid of each beam as expected. Among all the gages in Beam 1, the maximum tensile strain was obtained in Gage 4, which was located at the mid-span of the beam shown in Figure 3.23. Load-strain distribution of Gage 4 in Beam 1 is shown in Figure 4.52. The maximum strain was 12.6 milli strains at an applied load of 25.0 kips, even though the ultimate load carried by the beam was 32.3 kips. The gage failed when the applied load reached 25 kips. The tensile modulus of the grid was 2.5×10^3 ksi. Therefore, the tensile stress corresponding to the maximum tensile strain was 31.5 ksi, which was equal to the maximum tensile stress of the FRP grid. Even though the FRP grid reinforcement reached the maximum tensile capacity at 25.0 kips, after that, the beam had resisted till 32.3 kips and then collapsed.
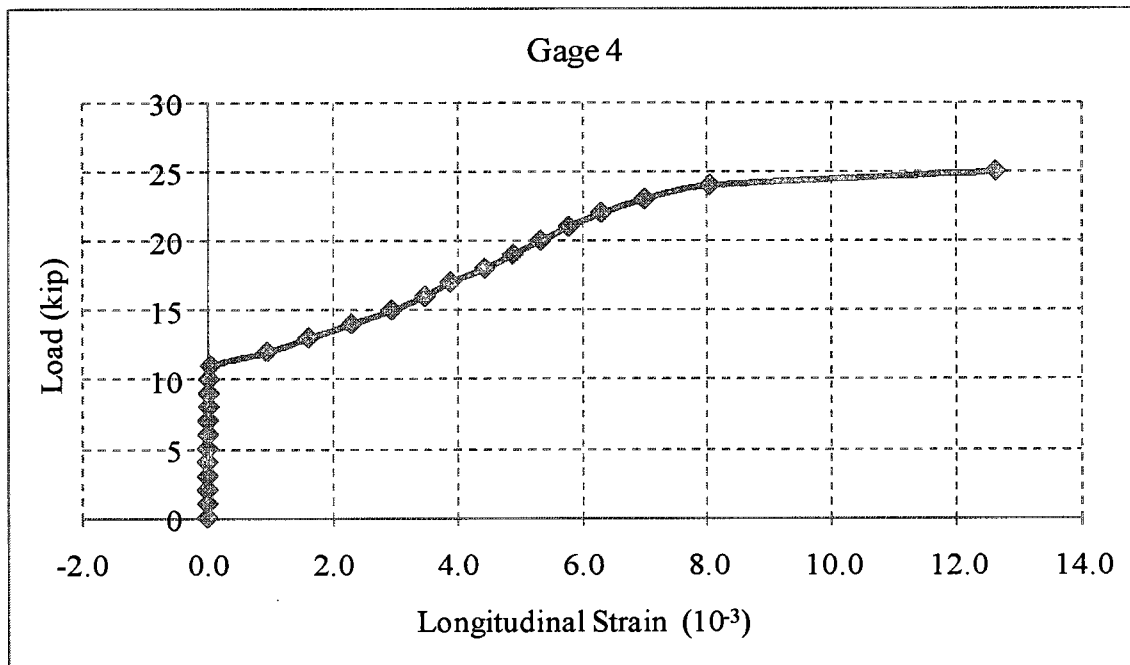
Figure 4.52 The Load-Strain Distribution in Gage 4 for Beam 1.

Among all the gages in Beam 2, the maximum tensile strain was obtained in gage4, which was located at the mid-span of the beam shown in Figure 3.24. Load-strain distribution of Gage 4 in Beam 2 is shown in Figure 4.53. The maximum strain was 12.3 milli strains at an applied load of 33.0 kips, even though the ultimate load carried by the beam was 39.4 kips. The gage failed when the applied load reached 33 kips. The tensile modulus of the grid was 2.5×10^3 ksi. Therefore, the tensile stress corresponding to the maximum tensile strain was 30.7 ksi, which was about the maximum tensile stress of the FRP grid (30 ksi). Even though the FRP grid reinforcement reached the maximum tensile capacity at 33.0 kips, after that, the beam had resisted till 39.4 kips and then collapsed.

Beam 1 had taken an extra load of 7.3 kips and Beam 2 had also taken an extra load of 6.4 kips after the longitudinal reinforcement of FRP grid reached its ultimate capacity. The reason could be the two or three dimensional load-transfer mechanism of

the FRP grid for carrying extra loads; whereas conventional steel reinforcement provides only a one-dimensional load transfer, and failure occurs in steel reinforced beams when reinforcement reaches its ultimate capacity. The longitudinal and transverse sections in the grid provided more efficient load-transfer between the FRP grid reinforcement and the concrete due to the mechanical interlocking.
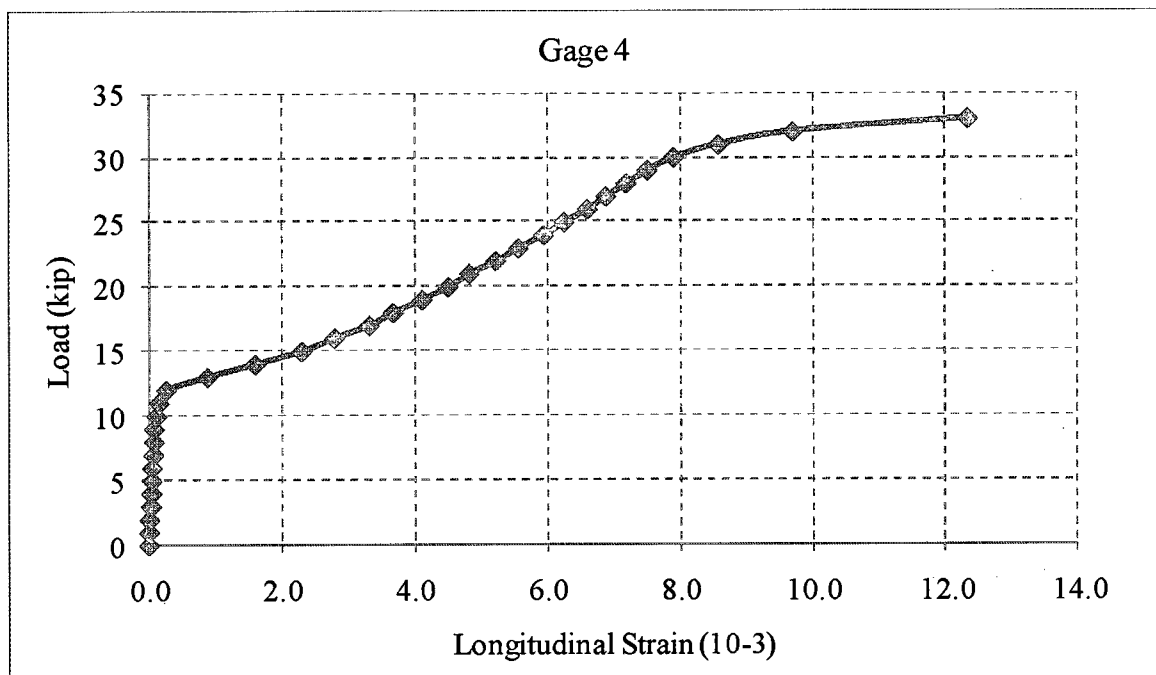
Figure 4.53 The Load-Strain Distribution in Gage 4 for Beam 2.

CHAPTER V

CONCLUSIONS AND RECOMMENDATIONS

5.1 General Summary and Conclusions

The research presented herein describes the development of durable link slabs for jointless bridge decks based on using FRP Grid for reinforcement. Specifically, the ductility of the FRP material was utilized to accommodate bridge deck deformations imposed by girder deflection, temperature variations, and concrete shrinkage. It would also provide a solution to a number of deterioration problems associated with bridge deck joints.

In this study, finite element models were used to investigate the behavior of a bridge with link slabs. The models were one with the open joints and another with the joints closed over the supports. The length of the link slab was determined theoretically to be equal to 5% of the span of the girders. The maximum flexural stresses in the link slab bridge were lower than those in the bridge with the open joint. Due to the link slab,

- The flexural stresses in the girders in span 1 were reduced by a range of 16 and 22%; in span 2 it was between 32 and 34%; and in span 3 it was between 9 and 14%.

In the bridge decks, the maximum and minimum transverse, longitudinal and shear stresses were found in the first deck of the open joint bridge or the link slab bridge, where the load was applied. All the stresses in the bridge deck were reduced due to thelink slab. The reduction of these stresses in span 1 of the three-span model considered were as follows:

- The transverse stresses were reduced by 13%, the longitudinal stresses were reduced by 36%, and the shear stresses were reduced by 43%.

The experimental work was conducted to determine the behavior and strength of the jointless bridge decks under static loading. The jointless decks could be achieved by replacing expansion joints by a link slab that could join the bridge decks of the adjacent spans without imposing any continuity in the bridge girders. The link slab would be subjected to tensile forces due to negative moment that developed at the location of the joint. The link slab panel was cut into beam specimens to determine the strength of the link slab against tensile forces. The test program included two test specimens: (1) a reinforced concrete beam with two layers of 1.00 inch deep FRP grids; and (2) a similar concrete beam with two layers of 1.25 deep FRP grids. A four-point bending test was conducted; the load was applied so that a negative bending moment was produced in the beam at the FRP grid's locations.

The specimens were designed to be under reinforced so that yielding of the steel precedes the crushing of the concrete in compression. Large strains in the reinforcing steel and FRP grids were expected at failure, and deflection of the beam at collapse was substantial (L/240) accompanied by excessive cracking. At low applied loads the stiffness of the reinforced concrete beam was relatively high, indicating that the concrete

behaved in a linear elastic manner. As the load increased, the bending stress in the extreme fibers increased until the tensile strength at the top of the section of the concrete was reached. This caused flexural cracks to form, first in the constant moment region, then through the beam cantilever section. As the flexural cracks developed in the span, the member stiffness was reduced, and thus the sudden change in the slope of the curve. The response after the cracking load was approximately linear due to the post cracking stiffness. The maximum deflection for each beam was about L/240.

After the concrete in the tension zone cracked, the reinforcing steel and FRP grid carried the tensile forces due to applied loads. As the applied load increased, the tensile stress in the steel increased and reached its yield magnitude. At this point the beam stiffness decreased due to the loss of material stiffness and the ability of the section to support the tensile stress was reduced. This was shown by the second change in the slope of the load-deflection response at the yield load. The yield plateau in the slope-deflection curve for Beam 2 was longer than that of Beam 1, which indicated that Beam 2 was more ductile than Beam 1, although the area of the FRP grids in Beam 2 were greater than Beam 1.

The flexural cracks formed in the constant moment region (i.e., between the supports) extended vertically and became wider. These cracks initiated in the shear span at collapse. The cracks initially extended vertically, and then progressed towards the load points in a diagonal fashion.

Another set of experimental work was conducted to verify the development length requirements for the FRP grid using the available equations from previous studies. The

load-deflection curve indicated that both beams showed less ductility as compared with typical steel reinforced beams. It confirms that FRP reinforcement is a brittle material.

The beams failed in shear as expected, since the flexural capacity of the beam was higher than shear capacity. From the failure mechanism of the two beams, the beams failed in shear tension and FRP grids cracked, but there was no relative slip between the FRP grid and the concrete. This was due to the mechanical anchorage or interlocking between the concrete and the FRP grid. It confirms that the bond between the FRP grid and the concrete was highly improved.

Large strains were observed in FRP grid of each beam as expected. The strains in both beams are as follows:

- Among all the gages in Beam 1, the maximum strain was 12.6 milli strains at an applied load of 25.0 kips, even though the ultimate load carried by the beam was 32.3 kips. Therefore, the tensile stress corresponding to the maximum tensile strain was 31.5 ksi, which was equal to the maximum tensile stress of the FRP grid.

- Among all the gages in Beam 2, the maximum strain was 12.3 milli strains at an applied load of 33.0 kips, even though the ultimate load carried by the beam was 39.4 kips. Therefore, the tensile stress corresponding to the maximum tensile strain was 30.7 ksi, which was about the maximum tensile stress of the FRP grid (30 ksi).

Since the two beams had taken an extra load of 6-8 kips after the reinforcement (FRP grid) reached its ultimate capacity. The reason could be the two or three dimensional load-transfer mechanism of the FRP grid, where as conventional steel

reinforcement provides only a one-dimensional load transfer. The longitudinal and transverse sections in the grid provided more efficient load-transfer between the FRP grid reinforcement and the concrete due to the mechanical interlocking. Therefore, the FRP grid reinforcements enhanced the load transfer mechanism, leading to a higher load carrying capacity and higher stiffness. Hence, it can be concluded that the provided development length for the FRP grid was good enough to maintain a bond between concrete and FRP reinforcement.

5.2 Recommendations

The results of the theoretical and experimental work presented in this report confirmed the advantages of FRP grids used to eliminate expansion joints in the bridge decks. The link slab technique will improve the behavior of the bridge and reduce the maintenance cost of the bridge decks. Based on the results of this study:

- It is recommended that the FRP grid link slab technique be considered in repair and retrofit of bridge decks after extensive field work to test the required mechanical properties at the bridge deck joints.

- It is recommended that the link slab technique can be used during new construction of the bridge decks.

- It is recommended that future research focus on cyclic tests of full-scale bridge link slab to be compared with those of conventional concrete bridge slabs.

- It is recommended that the analytical and experimental results be compared with data collected from field-level testing of the link slab. If the analytical and experimental results are supported by these data, then serious

consideration should be given to implementing an installation program using FRP grid link slab.

ACRONYMS, ABBREVIATIONS & SYMBOLS

AASHTO = American Association of State Highway and Transportation Officials

ACI = American Concrete Institute

AGS = Advanced Grid-Stiffened

ASTM = American Society for Testing and Materials

CFRP = Carbon Fiber Reinforced Polymer

FRP = Fiber Reinforced Polymer

GFRP = Glass Fiber Reinforced Polymer

ft = Foot

ksi = 1,000 Pounds per Square Inch

kip = 1,000 lb

LA-DOTD = Louisiana Department of Transportation and Development

lb = Pound

LRFD = Load Resistance Factor Design

LSB = Link Slab Bridge

LTRC = Louisiana Transportation Research Center

NEFMAC = New Fiber Composite Material for Reinforced Concrete

OJB = Open Joint Bridge

psi = Pounds per Square Inch

APPENDIX A

A.1 ANSYS INPUT DATA FOR LINK SLAB BRIDGE (LSB)

```
/BATCH
/input,start100,ans,'C:\Program Files\Ansys
Inc\v100\ANSYS\apdl\',,,,,,,,,,,,,,,,,1
/PREP7

ET,1,SOLID65
MPTEMP,,,,,,,,
MPTEMP,1,0
MPDATA,EX,1,,4.42e6
MPDATA,PRXY,1,,0.16

K,1,0,0,0,
K,2,22,0,0,
K,3,0,7,0,
K,4,22,7,0,
K,5,7.5,14.5,0,
K,6,14.5,14.5,0,
K,7,7.5,33.5,0,
K,8,14.5,33.5,0,
K,9,14.5,38,0,
KDELE,          9
K,9,3,38,0,
K,10,19,38,0,
K,11,3,45,0,
K,12,19,45,0,
LSTR,           1,          2
LSTR,           2,          4
LSTR,           3,          1
LSTR,           5,          6
LDELE,          4
LSTR,           3,          5
LSTR,           5,          7
LSTR,           9,          7
LSTR,          11,          9
LSTR,          12,         11
LSTR,          12,         10
LSTR,          10,          8
LSTR,           8,          6
LSTR,           6,          4
LSTR,          11,         19
LDELE,         25
LSTR,          11,         20
LSTR,          12,         21
LSTR,          10,         21
LDELE,         27
GPLOT
FLST,2,4,4
FITEM,2,8
```

```
FITEM,2,26
FITEM,2,20
FITEM,2,25
AL,P51X

FLST,2,14,5,ORDE,2
FITEM,2,1
FITEM,2,-14
VA,P51X

FLST,3,1,6,ORDE,1
FITEM,3,1
VGEN,2,P51X, , ,104, , , ,0

FLST,2,12,5,ORDE,2
FITEM,2,29
FITEM,2,-40
VA,P51X

FLST,3,1,6,ORDE,1
FITEM,3,3
VGEN,2,P51X, , , , ,-357, ,0
FLST,3,1,6,ORDE,1
FITEM,3,3
VGEN,2,P51X, , , , ,-714, ,0

FLST,3,13,6,ORDE,2
FITEM,3,1
FITEM,3,-13
VGEN,2,P51X, , , , ,-726, ,0

FLST,3,13,6,ORDE,2
FITEM,3,1
FITEM,3,-13
VGEN,2,P51X, , , , ,-1452, ,0

FLST,2,5,6,ORDE,4
FITEM,2,28
FITEM,2,42
FITEM,2,46
FITEM,2,-48
VOVLAP,P51X

FLST,2,3,6,ORDE,3
FITEM,2,53
FITEM,2,-54
FITEM,2,57
VADD,P51X
FLST,2,3,6,ORDE,3
FITEM,2,51
FITEM,2,-52
FITEM,2,56
VADD,P51X
FLST,2,3,6,ORDE,3
```

```
FITEM,2,49
FITEM,2,-50
FITEM,2,55
VADD,P51X

FLST,2,50,6,ORDE,16
FITEM,2,3
FITEM,2,-5
FITEM,2,7
FITEM,2,-9
FITEM,2,11
FITEM,2,-14
FITEM,2,17
FITEM,2,28
FITEM,2,42
FITEM,2,-44
FITEM,2,47
FITEM,2,-48
FITEM,2,51
FITEM,2,-57
FITEM,2,60
FITEM,2,-85
VGLUE,P51X

VOFFST,751,-6, ,

FLST,2,2,6,ORDE,2
FITEM,2,1
FITEM,2,-2
VGLUE,P51X

MPTEMP,,,,,,,
MPTEMP,1,0
MPDATA,EX,3,,3.605e6
MPDATA,PRXY,3,,0.16
MPTEMP,,,,,,,
MPTEMP,1,0
MPDE,EX,3
MPDE,PRXY,3
MPDATA,EX,3,,3.605E+006
MPDATA,PRXY,3,,0.16
MPTEMP,,,,,,,
MPTEMP,1,0
MPDE,EX,1
MPDE,PRXY,1
MPDATA,EX,1,,4.42E+006
MPDATA,PRXY,1,,0.16
MPTEMP,,,,,,,
MPTEMP,1,0
MPDE,EX,3
MPDE,PRXY,3
MPDATA,EX,3,,3.605E+006
MPDATA,PRXY,3,,0.16
ET,2,SOLID46
```

```
KEYOPT,2,2,0
KEYOPT,2,1,0
KEYOPT,2,3,0
KEYOPT,2,4,0
KEYOPT,2,5,0
KEYOPT,2,6,0
KEYOPT,2,8,0
KEYOPT,2,9,0
KEYOPT,2,10,0

MPTEMP,,,,,,,,
MPTEMP,1,0
MPDATA,EX,2,,2.8e6
MPDATA,PRXY,2,,0.22
MPTEMP,,,,,,,,
MPTEMP,1,0
MPDE,EX,2
MPDE,PRXY,2
MPDATA,EX,2,,2.8E+006
MPDATA,PRXY,2,,0.22

TYPE,    1
MAT,         1
REAL,        1
ESYS,        0
SECNUM,
MSHAPE,1,3D
MSHKEY,0
CM,_Y,VOLU
VSEL, , , ,          1
CM,_Y1,VOLU
CHKMSH,'VOLU'
CMSEL,S,_Y
VMESH,_Y1
CMDELE,_Y
CMDELE,_Y1
CMDELE,_Y2

SMRT,6
SMRT,10
CM,_Y,VOLU
VSEL, , , ,          1
CM,_Y1,VOLU
CHKMSH,'VOLU'
CMSEL,S,_Y

VCLEAR,_Y1
VMESH,_Y1
CMDELE,_Y
CMDELE,_Y1
CMDELE,_Y2

FINISH
/SOL
```

```
FLST,2,41,1,ORDE,25
FITEM,2,14
FITEM,2,-15
FITEM,2,34
FITEM,2,64
FITEM,2,76
FITEM,2,100
FITEM,2,-101
FITEM,2,161
FITEM,2,185
FITEM,2,696
FITEM,2,852
FITEM,2,-853
FITEM,2,4898
FITEM,2,-4900
FITEM,2,4956
FITEM,2,-4958
FITEM,2,5013
FITEM,2,-5015
FITEM,2,5715
FITEM,2,5746
FITEM,2,5840
FITEM,2,5873
FITEM,2,-5887
FITEM,2,6396
FITEM,2,-6397
/GO
D,P51X, ,0, , , ,UX,UY,UZ, , ,

FLST,2,41,1,ORDE,22
FITEM,2,250
FITEM,2,308
FITEM,2,625
FITEM,2,-626
FITEM,2,663
FITEM,2,-664
FITEM,2,685
FITEM,2,-686
FITEM,2,738
FITEM,2,830
FITEM,2,843
FITEM,2,849
FITEM,2,5058
FITEM,2,-5060
FITEM,2,5317
FITEM,2,-5319
FITEM,2,5345
FITEM,2,-5347
FITEM,2,6773
FITEM,2,6804
FITEM,2,6837
FITEM,2,-6854
/GO
D,P51X, ,0, , , ,UX,UY,UZ, , ,
```

```
FINISH
/SOL
FLST,2,8,1,ORDE,8
FITEM,2,191
FITEM,2,-192
FITEM,2,202
FITEM,2,-203
FITEM,2,712
FITEM,2,-713
FITEM,2,715
FITEM,2,-716
/GO
D,P51X, ,0, , , ,UX,UY, , , ,

FLST,2,10,1,ORDE,10
FITEM,2,157
FITEM,2,-158
FITEM,2,174
FITEM,2,180
FITEM,2,707
FITEM,2,-708
FITEM,2,710
FITEM,2,-711
FITEM,2,1396
FITEM,2,-1397
/GO
D,P51X, ,0, , , ,UX,UY, , , ,

FLST,2,2,1,ORDE,2
FITEM,2,1371
FITEM,2,-1372
/GO
D,P51X, ,0, , , ,UX,UY, , , ,

FLST,2,9,1,ORDE,9
FITEM,2,120
FITEM,2,122
FITEM,2,144
FITEM,2,-145
FITEM,2,700
FITEM,2,-701
FITEM,2,705
FITEM,2,-706
FITEM,2,870
/GO
D,P51X, ,0, , , ,UX,UY, , , ,

FITEM,2,8
FITEM,2,-9
FITEM,2,21
FITEM,2,-22
FITEM,2,28
FITEM,2,-29
```

```
FITEM,2,32
FITEM,2,-33
FITEM,2,53
FITEM,2,-54
/GO
D,P51X, ,0, , , ,UX,UY, , , ,

FLST,2,10,1,ORDE,10
FITEM,2,681
FITEM,2,-682
FITEM,2,692
FITEM,2,-693
FITEM,2,847
FITEM,2,-848
FITEM,2,850
FITEM,2,-851
FITEM,2,1296
FITEM,2,-1297
/GO
D,P51X, ,0, , , ,UX,UY, , , ,

FLST,2,10,1,ORDE,10
FITEM,2,659
FITEM,2,-660
FITEM,2,670
FITEM,2,-671
FITEM,2,841
FITEM,2,-842
FITEM,2,844
FITEM,2,-845
FITEM,2,1271
FITEM,2,-1272
/GO
D,P51X, ,0, , , ,UX,UY, , , ,

FLST,2,10,1,ORDE,8
FITEM,2,644
FITEM,2,-645
FITEM,2,649
FITEM,2,-650
FITEM,2,836
FITEM,2,-839
FITEM,2,1421
FITEM,2,-1422
/GO
D,P51X, ,0, , , ,UX,UY, , , ,

FLST,2,10,1,ORDE,10
FITEM,2,619
FITEM,2,-620
FITEM,2,632
FITEM,2,-633
FITEM,2,826
FITEM,2,-827
```

```
FITEM,2,831
FITEM,2,-832
FITEM,2,1246
FITEM,2,-1247
/GO
D,P51X, ,0, , , ,UX,UY, , , ,

FLST,2,20,1,ORDE,20
FITEM,2,505
FITEM,2,-506
FITEM,2,516
FITEM,2,-517
FITEM,2,597
FITEM,2,-598
FITEM,2,608
FITEM,2,-609
FITEM,2,792
FITEM,2,-793
FITEM,2,795
FITEM,2,-796
FITEM,2,820
FITEM,2,-821
FITEM,2,823
FITEM,2,-824
FITEM,2,1121
FITEM,2,-1122
FITEM,2,1221
FITEM,2,-1222
/GO
D,P51X, ,0, , , ,UX,UY, , , ,

FLST,2,18,1,ORDE,18
FITEM,2,483
FITEM,2,-484
FITEM,2,494
FITEM,2,-495
FITEM,2,575
FITEM,2,-576
FITEM,2,586
FITEM,2,-587
FITEM,2,786
FITEM,2,-787
FITEM,2,789
FITEM,2,-790
FITEM,2,814
FITEM,2,-815
FITEM,2,817
FITEM,2,-818
FITEM,2,1196
FITEM,2,-1197
/GO
D,P51X, ,0, , , ,UX,UY, , , ,

FLST,2,20,1,ORDE,20
```

```
FITEM,2,461
FITEM,2,-462
FITEM,2,472
FITEM,2,-473
FITEM,2,553
FITEM,2,-554
FITEM,2,564
FITEM,2,-565
FITEM,2,780
FITEM,2,-781
FITEM,2,783
FITEM,2,-784
FITEM,2,808
FITEM,2,-809
FITEM,2,811
FITEM,2,-812
FITEM,2,1146
FITEM,2,-1147
FITEM,2,1346
FITEM,2,-1347
/GO
D,P51X, ,0, , , ,UX,UY, , , ,

FLST,2,20,1,ORDE,20
FITEM,2,435
FITEM,2,-436
FITEM,2,448
FITEM,2,-449
FITEM,2,527
FITEM,2,-528
FITEM,2,540
FITEM,2,-541
FITEM,2,770
FITEM,2,-771
FITEM,2,775
FITEM,2,-776
FITEM,2,798
FITEM,2,-799
FITEM,2,803
FITEM,2,-804
FITEM,2,1071
FITEM,2,-1072
FITEM,2,1171
FITEM,2,-1172
/GO
D,P51X, ,0, , , ,UX,UY, , , ,

FLST,2,2,1,ORDE,2
FITEM,2,1096
FITEM,2,-1097
/GO
D,P51X, ,0, , , ,UX,UY, , , ,
FLST,2,20,1,ORDE,20
FITEM,2,298
```

```
FITEM,2,304
FITEM,2,323
FITEM,2,325
FITEM,2,413
FITEM,2,-414
FITEM,2,424
FITEM,2,-425
FITEM,2,735
FITEM,2,-736
FITEM,2,739
FITEM,2,-740
FITEM,2,764
FITEM,2,-765
FITEM,2,767
FITEM,2,-768
FITEM,2,946
FITEM,2,-947
FITEM,2,1046
FITEM,2,-1047
/GO
D,P51X, ,0, , , ,UX,UY, , , ,

FLST,2,2,5,ORDE,2
FITEM,2,1227
FITEM,2,1267
/GO
SFA,P51X,1,PRES,23.33

FLST,2,4,5,ORDE,4
FITEM,2,1239
FITEM,2,1245
FITEM,2,1251
FITEM,2,1257
/GO
SFA,P51X,1,PRES,93.33

FLST,2,1,5,ORDE,1
FITEM,2,818
/GO
SFA,P51X,1,PRES,0.284

FLST,2,1,5,ORDE,1
FITEM,2,953
/GO
SFA,P51X,1,PRES,0.284

FLST,2,1,5,ORDE,1
FITEM,2,1290
/GO
SFA,P51X,1,PRES,0.284

FLST,2,4,5,ORDE,4
FITEM,2,1227
FITEM,2,1233
```

```
FITEM,2,1239
FITEM,2,1245
/GO
SFA,P51X,1,PRES,0.284

FLST,2,2,5,ORDE,2
FITEM,2,1251
FITEM,2,1257
/GO
SFA,P51X,1,PRES,0.284

SOLVE
FINISH
/POST1
```

A.2 ANSYS INPUT DATA FOR OPEN JOINT BRIDGE (OJB)

```
/BATCH
/input,start100,ans,'C:\Program Files\Ansys
Inc\v100\ANSYS\apdl\',,,,,,,,,,,,,,,,,1
/PREP7

ET,1,SOLID65

MPTEMP,,,,,,,,
MPTEMP,1,0
MPDATA,EX,1,,4.42e6
MPDATA,PRXY,1,,0.16

K,1,0,0,0,
K,2,22,0,0,
K,3,0,7,0,
K,4,22,7,0,
K,5,7.5,14.5,0,
K,6,14.5,14.5,0,
K,7,7.5,33.5,0,
K,8,14.5,33.5,0,
K,9,3,38,0,
K,10,19,38,0,
K,11,3,45,0,
K,12,19,45,0,

LSTR,         1,        2
LSTR,         2,        4
LSTR,         3,        1
LSTR,         5,        6
LDELE,        4
LSTR,         3,        5
LSTR,         5,        7
LSTR,         9,        7
LSTR,        11,        9
LSTR,        12,       11
LSTR,        12,       10
LSTR,        10,        8
LSTR,         8,        6
LSTR,         6,        4
FLST,3,12,4,ORDE,2
FITEM,3,1
FITEM,3,-12
LGEN,2,P51X, , , , ,-720, ,0
LSTR,        11,       19
LSTR,        11,       20
LSTR,        12,       21
LSTR,        10,       21
GPLOT
FLST,2,4,4
FITEM,2,8
```

```
FITEM,2,26
FITEM,2,20
FITEM,2,25
AL,P51X
LSTR,          9,        19
LSTR,          7,        18
LSTR,          5,        17
FLST,2,4,4
FITEM,2,19
FITEM,2,25
FITEM,2,27
FITEM,2,7
AL,P51X
FLST,2,4,4
FITEM,2,28
FITEM,2,27
FITEM,2,18
FITEM,2,6
AL,P51X
FLST,2,4,3
FITEM,2,2
FITEM,2,1
FITEM,2,13
FITEM,2,14
A,P51X

FLST,2,14,5,ORDE,2
FITEM,2,1
FITEM,2,-14
VA,P51X

FLST,3,1,6,ORDE,1
FITEM,3,1
VGEN,2,P51X, , ,104, , , ,0

FLST,2,12,5,ORDE,2
FITEM,2,29
FITEM,2,-40
VA,P51X

FLST,3,1,6,ORDE,1
FITEM,3,3
VGEN,2,P51X, , , , ,-357, ,0
FLST,3,1,6,ORDE,1
FITEM,3,3
VGEN,2,P51X, , , , ,-714, ,0

FLST,2,3,6,ORDE,3
FITEM,2,49
FITEM,2,-50
FITEM,2,52
VADD,P51X
FLST,2,3,6,ORDE,3
FITEM,2,47
```

```
FITEM,2,-48
FITEM,2,51
VADD,P51X

FLST,2,5,6,ORDE,5
FITEM,2,14
FITEM,2,43
FITEM,2,-44
FITEM,2,53
FITEM,2,-54
VOVLAP,P51X

LSTR,      1011,     1005
LSTR,      1012,     1006
FLST,2,4,4
FITEM,2,407
FITEM,2,809
FITEM,2,1163
FITEM,2,1164
AL,P51X
VOFFST,471,360, ,

FLST,2,2,6,ORDE,2
FITEM,2,1
FITEM,2,72
VPTN,P51X

FLST,2,2,6,ORDE,2
FITEM,2,1
FITEM,2,-2
VGLUE,P51X

FLST,2,74,6,ORDE,12
FITEM,2,1
FITEM,2,-37
FITEM,2,42
FITEM,2,-44
FITEM,2,47
FITEM,2,-48
FITEM,2,51
FITEM,2,-57
FITEM,2,60
FITEM,2,-71
FITEM,2,73
FITEM,2,-85
VGLUE,P51X

MPTEMP,,,,,,,,
MPTEMP,1,0
MPDE,EX,1
MPDE,PRXY,1
MPDATA,EX,1,,4.42E+006
MPDATA,PRXY,1,,0.16
```

```
MPTEMP,,,,,,,,
MPTEMP,1,0
MPDATA,EX,3,,3.605e6
MPDATA,PRXY,3,,0.16
MPTEMP,,,,,,,,
MPTEMP,1,0
MPDE,EX,3
MPDE,PRXY,3
MPDATA,EX,3,,3.605E+006
MPDATA,PRXY,3,,0.16
MPTEMP,,,,,,,,
MPTEMP,1,0
MPDE,EX,1
MPDE,PRXY,1
MPDATA,EX,1,,4.42E+006
MPDATA,PRXY,1,,0.16
MPTEMP,,,,,,,,
MPTEMP,1,0
MPDE,EX,3
MPDE,PRXY,3
MPDATA,EX,3,,3.605E+006
MPDATA,PRXY,3,,0.16

FLST,5,23,6,ORDE,14
FITEM,5,2
FITEM,5,16
FITEM,5,18
FITEM,5,-23
FITEM,5,25
FITEM,5,-27
FITEM,5,29
FITEM,5,-32
FITEM,5,34
FITEM,5,-36
FITEM,5,38
FITEM,5,46
FITEM,5,93
FITEM,5,-95
CM,_Y,VOLU
VSEL, , , ,P51X
CM,_Y1,VOLU
CHKMSH,'VOLU'
CMSEL,S,_Y

VMESH,_Y1

FLST,2,41,1,ORDE,25
FITEM,2,14
FITEM,2,-15
FITEM,2,34
FITEM,2,64
FITEM,2,76
FITEM,2,100
FITEM,2,-101
```

```
FITEM,2,161
FITEM,2,185
FITEM,2,696
FITEM,2,852
FITEM,2,-853
FITEM,2,4898
FITEM,2,-4900
FITEM,2,4956
FITEM,2,-4958
FITEM,2,5013
FITEM,2,-5015
FITEM,2,5715
FITEM,2,5746
FITEM,2,5840
FITEM,2,5873
FITEM,2,-5887
FITEM,2,6396
FITEM,2,-6397
/GO
D,P51X, ,0, , , ,UX,UY,UZ, , ,

FINISH
/PREP7
NDIST,        713,        715
NDIST,        192,        203
NDIST,        712,        716
NDIST,        712,        716
NDIST,        713,        715
FINISH
/SOL
FLST,2,8,1,ORDE,8
FITEM,2,191
FITEM,2,-192
FITEM,2,202
FITEM,2,-203
FITEM,2,712
FITEM,2,-713
FITEM,2,715
FITEM,2,-716
/GO
D,P51X, ,0, , , ,UX,UY, , , ,

FLST,2,10,1,ORDE,10
FITEM,2,157
FITEM,2,-158
FITEM,2,174
FITEM,2,180
FITEM,2,707
FITEM,2,-708
FITEM,2,710
FITEM,2,-711
FITEM,2,1396
FITEM,2,-1397
/GO
```

```
D,P51X, ,0, , , ,UX,UY, , , ,

FLST,2,2,5,ORDE,2
FITEM,2,1227
FITEM,2,1267
/GO
SFA,P51X,1,PRES,23.33

FLST,2,4,5,ORDE,4
FITEM,2,1239
FITEM,2,1245
FITEM,2,1251
FITEM,2,1257
/GO
SFA,P51X,1,PRES,93.33

FLST,2,1,5,ORDE,1
FITEM,2,953
/GO
SFA,P51X,1,PRES,0.284

FLST,2,1,5,ORDE,1
FITEM,2,1290
/GO
SFA,P51X,1,PRES,0.284

FLST,2,4,5,ORDE,4
FITEM,2,1227
FITEM,2,1233
FITEM,2,1239
FITEM,2,1245
/GO

FLST,2,2,5,ORDE,2
FITEM,2,1251
FITEM,2,1257
/GO
SFA,P51X,1,PRES,0.284

SOLVE
FINISH
/POST1
```

APPENDIX B

B.1 STRUCTURAL TESTING OF FRP GRID
REINFORCED DECKS
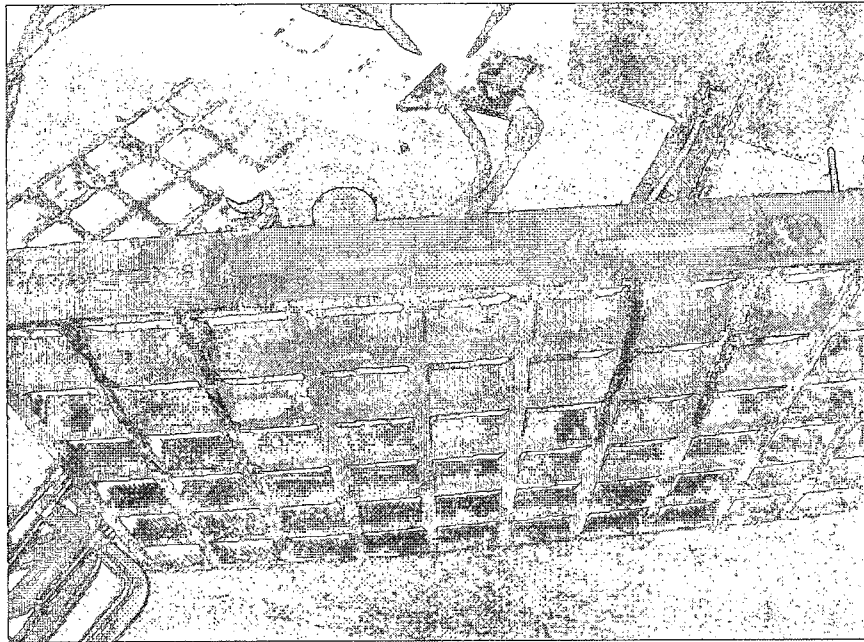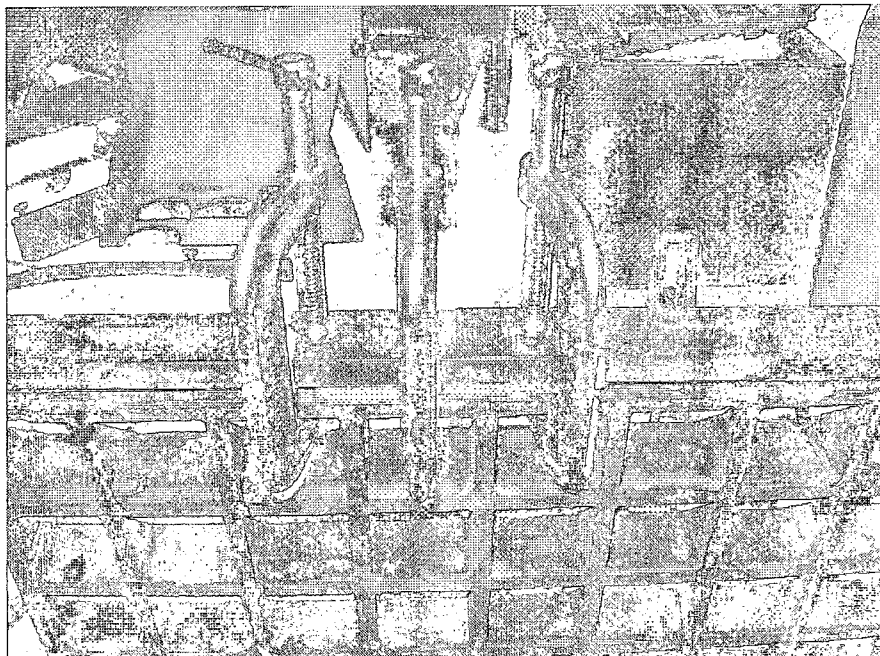

Figure B.1 Strain Gage Installation.

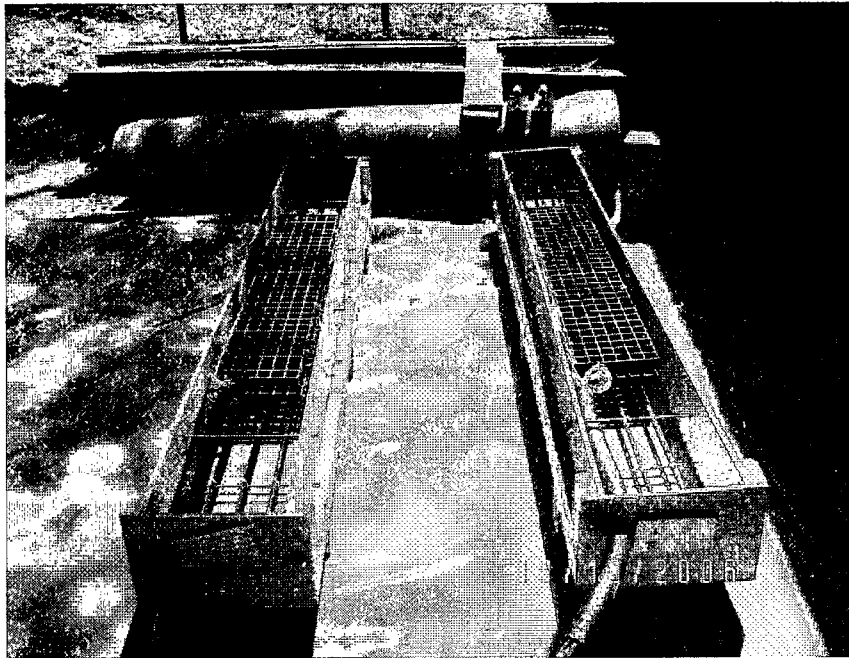Figure B.2 Fixing Strain Gages to the FRP Grid.

Figure B.3 Forms with FRP Grids.

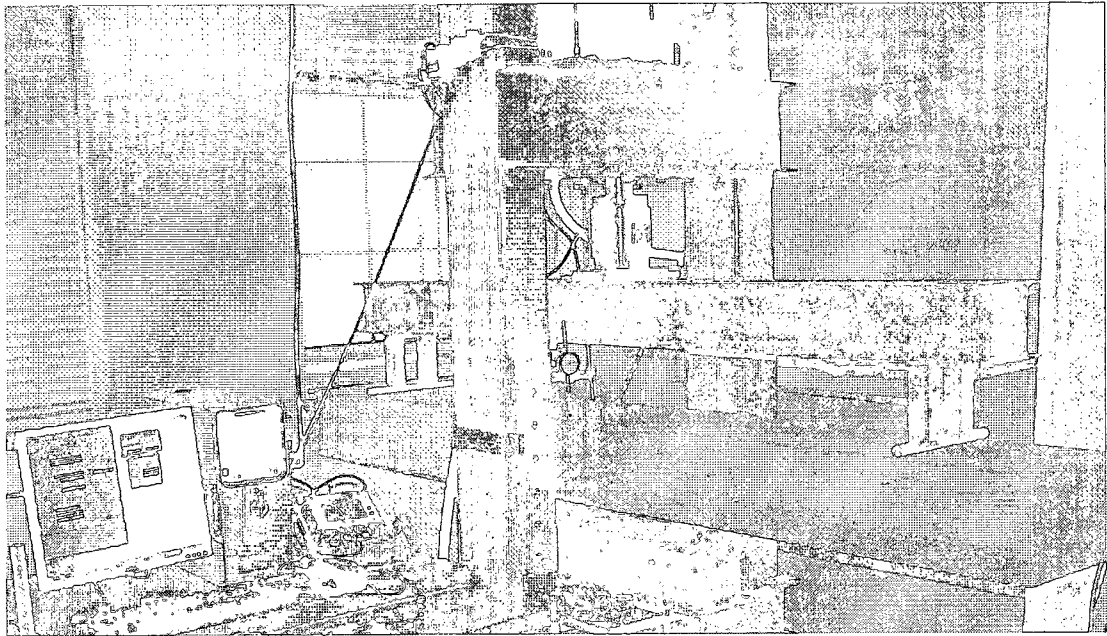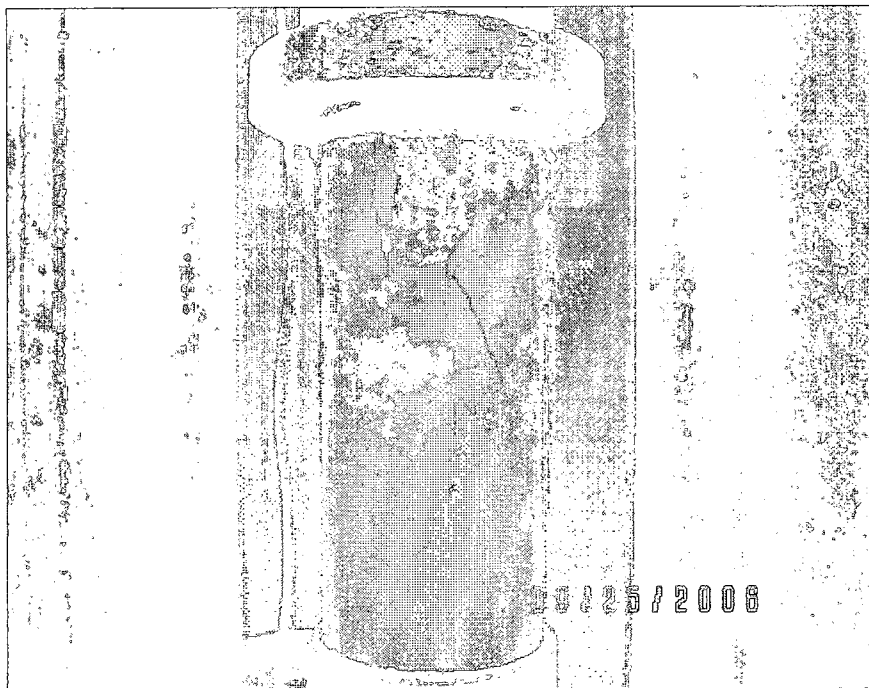Figure B.4 Pouring the Concrete in Beams.

Figure B.5 Beam Testing.

Figure B.6 Cylinder Testing for Compressive Strength.

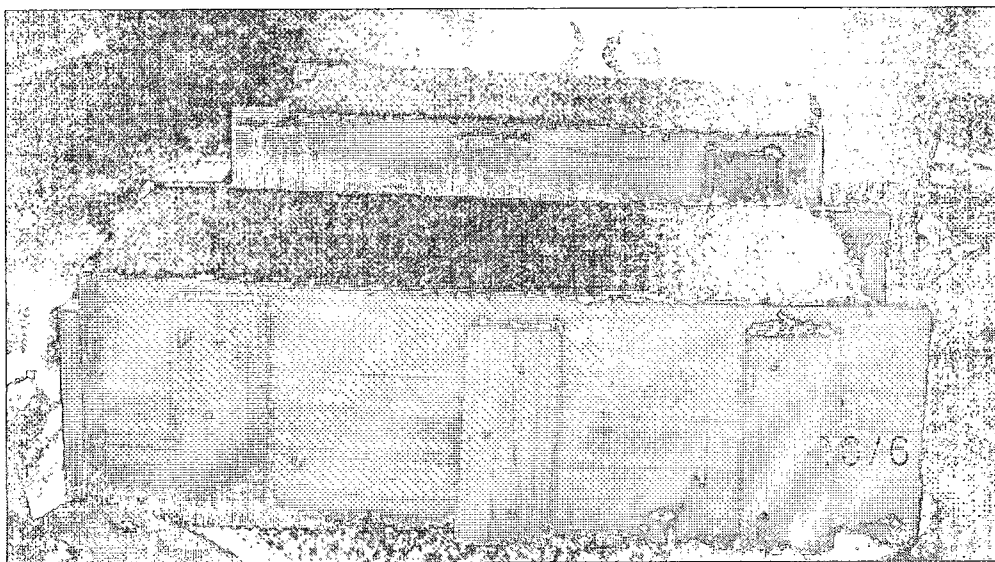## B.2 TEST FOR THE DEVELOPMENT
LENGTH OF FRP GRID

Figure B.7 Beams after Pouring the Concrete.

Figure B.8 Beam Testing.

REFERENCES

AASHTO, 2004, "AASHTO LRFD Bridge Design Specifications," Customary US Units, 3rd Edition.

ACI Committee 318, 2005, "Building Code Requirements for Structural Concrete (ACI 318-05) and Commentary (318R-05)," American Concrete Institute.

ACI 440R, 2002, "Report on Fiber Reinforced Plastic (FRP) Reinforcement for Concrete Structures," American Concrete Institute.

ANSYS Tutorials, www.ansys.com

Ashok, A., and Saber, A., 2010, "Finite Element Analysis of Link Slabs for Jointless Bridge Decks," *The Baltic Journal of Road and Bridge Engineering*.

ASTM C39 / C39M, 2005, "Standard Test Method for Compressive Strength of Cylindrical Concrete Specimens," 2nd Edition, ASTM.

ASTM C78, 2009, "Standard Test Method for Flexural Strength of Concrete (Using Simple Beam with Third-Point Loading)," ASTM.

ASTM C511, 2009, "Standard Specification for Mixing Rooms, Moist Cabinets, Moist Rooms, and Water Storage Tanks Used in the Testing of Hydraulic Cements and Concretes," ASTM.

Bakis, C. E., Bank, L. C., Brown, V. L., Cosenza, E., Davalos, J. F., Lesko, J. J., Machida, A., Rizkilla, S. H., and Triantafillou, T. C., 2002, "Fiber-Reinforced Polymer Composites for Construction - State of the Art Review," *Journal of Composites for Construction*, V. 6, No. 2, pp. 73-87.

Bank, L. C., Xi, Z., and Mosallam, A. S., 1991, "Experimental Study of FRP Grating Reinforced Concrete Slabs," Proceedings of the Advanced Composite Materials in Civil Engineering Structures Specialty Conference, Las Vegas, NV, ASCE, pp. 111-122.

Banthia, N., Al-Asaly, M., and Ma, S., 1995, "Behavior of Concrete Slabs Reinforced with Fiber-Reinforced Plastic Grid," *Journal of Materials in Civil Engineering*, V. 7, No. 4, pp. 252-257.

Berg, A.C., Bank, L.C., Oliva, M.G., and Russell, J.S., 2006, "Construction and Cost Analysis of an FRP Reinforced Concrete Bridge Deck," *Construction and Building Materials*, pp. 515-526.

Dutta, K. P., Bailey, M. D., Tsai, W.S., Jensen, W. D., Hayes Jr, R.J., McDonald, E.W., Smart, W.C., Colwell, T., Earl, S.J., and Chen, H., 1998, "Composite Grids for Reinforcement of Concrete Structures," Construction Productivity Advancement Research Program, *Final Report*, June.

El-Salakawy, E., Benmokrane, B., Amr, E., and Nadeau, D., 2005, "Field Investigation on the First Bridge Deck Slab Reinforced with Glass FRP Bars Constructed in Canada," *Journal of Composites for Construction*, V. 9, No. 6, pp. 470-479.

El-Ghandour, A. W., Pilakoutas, K., and Waldron, P., 2003, "Punching Shear Behavior of Fiber Reinforced Polymers Reinforced Concrete Flat Slabs: Experimental Study," *Journal of Composites for Construction*, V. 7, No. 3, pp. 258-265.

Goodspeed, C.H., Schmeckpeper, E.R., Gross, T., Henry, R., Yost, J., and Zhang, M., 1991, "Cyclical Testing of Concrete Beams Reinforced With Fiber Reinforced Plastic (FRP) Grids," Proceedings of the Advanced Composite Materials in Civil Engineering Structures Specialty Conference, Las Vegas, NV, ASCE, pp. 278-287.

Harris, H. G., Somboonsong, W., and Ko, F. K., 1998, "New Ductile Hybrid FRP Reinforcing Bar for Concrete Structures," *Journal of Composites for Construction*, V. 2, No. 1, pp. 28-37.

Heath, A.C., and Roesler, J.R., 1999, "Shrinkage and Thermal Cracking of Fast Setting Hydraulic Cement Concrete Pavements in Palmdale, California," Preliminary Report Prepared for California Department of Transportation, California, pp. 41-59.

Huang, H., Chajes, M.J., Mertz, D.R., Shenton, H.W., and Kaliakin, V.N., 2002, "Behavior of Open Steel Grid Decks for Bridges," *Journal of Constructional Steel Research*, pp. 819-842.

Karbhari, V. M., Chin, J. W., Hunston, D., Benmokrane, B., Juska, T., Morgan, R., Lesko, J. J., Sorathia, U., and Reynaud, D., 2003, "Durability Gap Analysis for Fiber-Reinforced Polymer Composites in Civil Infrastructure," *Journal of Composites for Construction*, V. 7, No. 3, pp. 238-247.

Kumar, S. V., and GangaRao, H. V. S., 1998, "Fatigue Response of Concrete Decks Reinforced with FRP Rebars," *Journal of Structural Engineering*, V.124, No.1, pp. 11-16.

Larralde, A.M., and Zervai, A., 1991, "Load/Deflection Performance of FRP Grating-Concrete Composites," Proceedings of the Advanced Composite Materials in Civil Engineering Structures Specialty Conference, Las Vegas, NV, ASCE, pp. 271-277.

Lawrence, K.L., "ANSYS Tutorial- Release 8.0," SDC Publications.

Li, G., and Saber, A., 2009, "Elimination of Deck Joints Using a Corrosion Resistant FRP Approach," Louisiana Department of Transportation and Development, Report No.443, September.

Matthys, S., and Taerwe, L., 2000, "Concrete Slabs Reinforced with FRP Grid I: One-Way Bending," *Journal of Composites for Construction*, pp. 145-153.

Matthys, S., and Taerwe, L., 2000, "Concrete Slabs Reinforced with FRP grid II: Punching Resistance," *Journal of Composites for Construction*, V. 4, No. 3, pp. 154-161.

Mothe, R.N., 2006, "Partial Continuity in Prestressed Concrete Girder Brides with Jointless Decks," *Thesis Report*, December.

Paul, Z., Alp. C., and Adel, k., 1995, "Jointless Bridge Decks" North Carolina Department of Transportation, September.

Rahman, H. A., Kingsly, Y. C., and Kobayashi, K., 2000, "Service and Ultimate Load Behavior of Bridge Deck Reinforced with Carbon FRP grid," *Journal of Composites for Construction*, V. 4, No.1, February, pp. 16-23.

Saber, A., 2001, "Failure Behavior of RC T-beams Retrofitted with Carbon FRP Sheets," *In: Creative Systems in Structural and Construction Engineering*, Proceeding of First International Structural Engineering and Construction Conference, Honolulu, Hawaii.

Saber,A., 2000, "Failure of Reinforced Concrete T-Beams Retrofitted with Carbon Fiber Reinforced Plastic (CFRP) Sheets," Louisiana Transportation Research Center, June.

Saber, A., Toups, J., and Alaywan, W., 2005, "Effects of Continuity Diaphragms on Load Transfer in Prestressed Concrete Skewed Bridges," In: Proceedings of the Third International Structural Engineering and Construction Conference, Japan.

Saeed, M., "Finite Element Analysis," Pearson Education, Inc., New Jersey.

Schmeckpeper, E.R., and Goodspeed, C.H., 1994, "Fiber-Reinforced Plastic Grid for Reinforced Concrete Construction," *Journal of Composite Materials*, V. 28, No. 14, pp.1288-1304.

Schmeckpeper, E. R., 1992, "Performance of Concrete Beams and Slabs Reinforced with FRP Grids," *Ph.D. Dissertation*, University of New Hampshire, May.

Smart, C. W., and Jensen, D. W., 1997, "Flexure of Concrete Beams Reinforced with Advanced Composite Orthogrids," *Journal of Aerospace Engineering*, pp.7-15.

Sugita, M., 1993, and Clarke, J.L., "NEFMAC Grid Type Reinforcement," *Alternative Materials for the Reinforcement and prestressing of concrete*, Blackie Academic & Professional, pp. 55-72.

Sugita, M., Nakatsuji, T., Sekijima, K., and Fujisaki, T., 1992, "Applications of FRP Grid Reinforcement to Precast Concrete Panels," *Advanced Composite Materials in Bridges and Structures*, Canadian Society for Civil Engineering.

Tavarez, A. F., Bank, C. L., and Plesha, E. M., 2003, "Analysis of Fiber Reinforced Polymer Composite Grid Reinforced Concrete Beams," *ACI Structural Journal*, V. 100, No. 2, pp. 250-258.

Victor, C., Fischer, G., Kim,Y., Lepech, S., Qian, S., Weimann, M., and Wang, S., 2003, "Durable Link Slabs for Jointless Bridge Decks Based on Strain-Hardening Cementitious Composites," Michigan Department of Transportation, November.

Xiang, Z., 2007, "Structural and Economical Impacts of Heavy Truck Loads on Bridges," *Ph.D. Dissertation*, Louisiana Tech University, November.

Yost, J.R., Goodspeed, C.H., and Schmeckpeper, E.R., 2001, "Flexural Performance of Concrete Beams Reinforced with FRP Grids," *Journal of Composites for Construction*, pp. 18-25.

Zhang, B., Masmoudi, R., and Benmokrane, B., 2004, "Behavior of One-Way Concrete Slabs Reinforced with CFRP Grid Reinforcements," *Construction and Building Materials*, pp. 625-635.